Thermo-responsive reversible dynamic microenvironments to regulate cellular behavior

Inaugural-Dissertation

to obtain the academic degree

Doctor rerum naturalium (Dr. rer. nat.)

submitted to the Department of Biology, Chemistry and

Pharmacy of Freie Universität Berlin

by

Jianguang Zhang

aus Hebei, China

May 2019

The work presented in this thesis was conducted in the research groups of Prof. Dr. Nan Ma and Prof. Dr. Rainer Haag from September 2015 until March 2019 at the Institut für Chemie und Biochemie of the Freie Universität Berlin.

1st Reviewer: Prof. Dr. Nan Ma, Freie Universität Berlin

2nd Reviewer: Prof. Dr. Rainer Haag, Freie Universität Berlin

Date of Defense: 08.08.2019

Acknowledgements

First and foremost, I would express my sincere gratitude to my two doctoral supervisors Prof. Dr. Nan Ma and Prof. Dr. Rainer Haag for the opportunity to study in their groups. Without their consistent and illuminating instruction, this thesis could not be finished. Moreover, I also appreciate their help in planning my future development.

I also want to thank my colleague Dr. Katharina Achazi and Dr. Falko Neumann for their kind help with basic principles and experimental introductions in the biolab. I also thank Dr. Stefanie Wedepohl, Paul Hillmann, Elisa Quaas, and all the other members in the biolab for their patient explanations to help me solve the problem during my experiments.

I am very grateful to all of my cooperation partners for their kind help, particularly to Prof. Dr. Wei Chen (China Pharmaceutical University), Prof. Dr. Zhenhui Qi (Northwestern Polytechnical University, China), Prof. Dr. Shengyi Dong (Hunan University, China), Prof. Dr. Chong Cheng (Sichuan University, China), Dr. Lingyan Gao, Dr. Wenzhong Li, Dr. Leixiao Yu, Dr. Zhaoxu Tu, Dr. Jose Luis Cuellar-Camacho, Dr. Bilen Emek Abali, Dr. Yinan Zhong, Yong Hou, Mingjun Li, Qingcai Zhao, Wanjun Liang, Yan Li, Hua Yang, Yi Xia, Yuanwei Pan, Suqiong Zhou, and Chuanxiong Nie.

I would like to acknowledge Eike Ziegler, Dr. Wiebke Fischer, and Anja Stöshel for dealing with the financial issues and complicated paperwork as well as chemical ordering. I would like to especially thank Dr. Pamela Winchester for language polishing the manuscripts. Furthermore, I am grateful for the financial support afforded by China Scholarship Council (CSC) during my Ph.D. thesis.

Moreover, I am also very grateful to my parents for their understanding and continuous supports throughout all these years. I especially want to thank my wife Chenlei Cai with her love and encouragement. I hope to go back home soon after the defense and spend more time with our daughter.

Table of Contents

1 Introduction

1.1 Biomaterial Guidance of Cell Behaviors

During the natural tissue regeneration process, the biophysical cues of extracellular matrix (ECM) have a profound influence on the cell behaviors, including adhesion, spreading, migration, proliferation, and differentiation.[1, 2] The complex feedback mechanism between cell-cell and cell-ECM interactions, which regulate the ability of cells to generate cell contractility, modulate cell spreading, nuclear mechanics, and ultimately convert into activation of intracellular signaling pathways and gene expression.[3-5] In the last decade, novel synthetic biomaterials with tunable properties have been fabricated to study the effect of ECM on cellular behaviors, such as matrix stiffness, geometrical cues, surface receptors, and mechanical forces, which can provide a single or synergistic effects to regulate cell fate in tissue engineering (**Figure 1**).[6-9] Yet it remains largely unknown, how cells communicate with ECM and how the microenvironment of physicochemical and biochemical cues guide cell fate and organ function. Thus, a better understanding of these issues would greatly advance our knowledge in the role of the ECM remodeling on tumor cell invasion, wound healing, organ aging, and regenerative processes. The development of engineered biomaterials that capture as many aspects of the key features as possible to mimic the nature ECM, which provides indispensable tools for studying cell behavior and cell-based clinical therapy.[10-13]

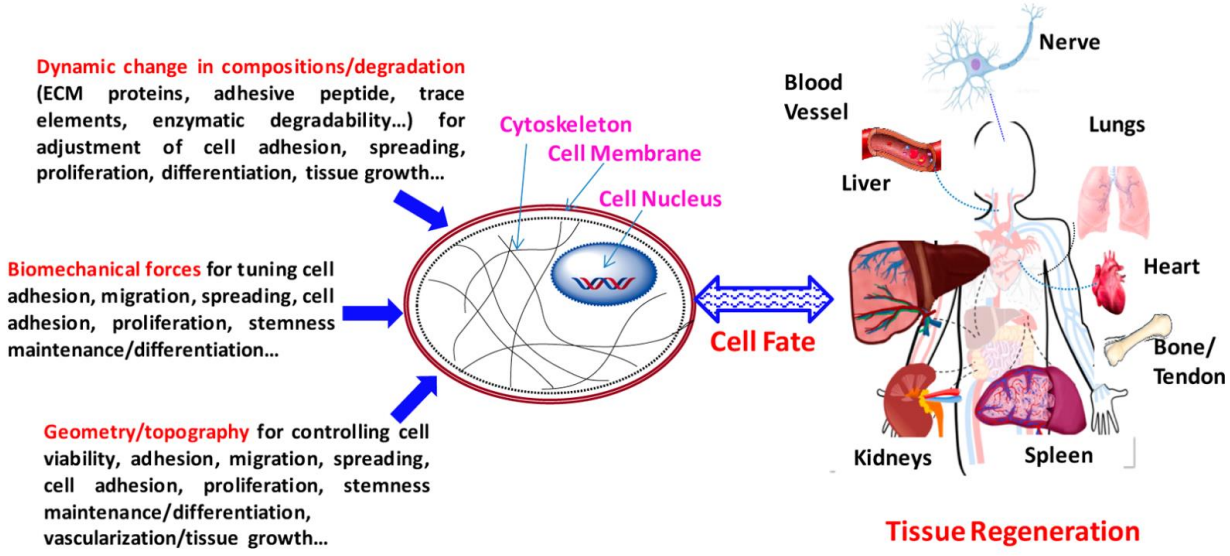

Figure 1. The artificial materials can mediate cell behavior, which ultimately control the tissue regeneration. Reprinted from ref.[6] with the kind permission of The American Chemical Society Copyright 2017.

1.2 Dynamic Interactions Between Cells and ECM

Up to now, many biomaterials with well-defined properties have been applied to elucidate the effects on local microenvironment-mediated cellular behaviors in the static conditions, where both

biochemical and biophysical properties keep constant.[14] However, the native ECM is a highly dynamic microenvironment *in vivo*, which gradually changes its physicochemical cues through local nascent deposition, matrices degradation or remodeling by surrounding cells.[15, 16] On the other hand, the dynamic microenvironment is also present throughout all the body organs, such as the pumping of blood by the heart, compressive stresses from skeletal muscle, and small intestinal peristalsis, which enable us to breathe, move, and digest, respectively.[17, 18] Numerous studies have suggested that cells and their surrounding microenvironment dynamically influence each other, particularly for guiding stem cells to maintain their balance between self-renewal and differentiation, which contribute to tissue regeneration and homeostasis.[19-21]

Therefore, the material with static properties cannot fully represent the native dynamic microenvironment. Owing to the smart capability to regulate molecular interactions under the extra stimuli, bioresponsive materials have been devised to mimic the dynamic properties of the natural ECM, leading to new approach to investigate and precise modulate of the dynamic interaction between cells and ECM, which can be better used to guide cell fate for medical diagnosis and therapies.[22-24] Recently, we have noted that an increasing number of *in vitro* studies have established dynamic manner to regulate cellular behavior with unique optical, electrical, magnetic, thermal, and mechanical properties and applicable forces or switchable topography, as shown in **Figure 2**.[25-27] These highly dynamic tunable cell culture systems enable the manipulation of cells in a controllable way to probe how cells sense and interpret to changes in microenvironments, and the ultimate goal is to gain important implications in recapitulate aspects of native ECM, which have implications for disease diagnosis, stem cell therapy, and organ transplantation.

1.3 Bioresponsive materials

Bioresponsive materials can be fabricated by different strategies, including thin films, functionalized surfaces, and scaffolds, which have been applied to manipulate cell behavior both *in vitro* and *in vivo*. The current dynamic cell culture platforms are classified into five different categories in this thesis, including photo-responsive materials, electro-responsive materials, magnetic-responsive materials, temperature-responsive materials, and mechano-responsive materials.

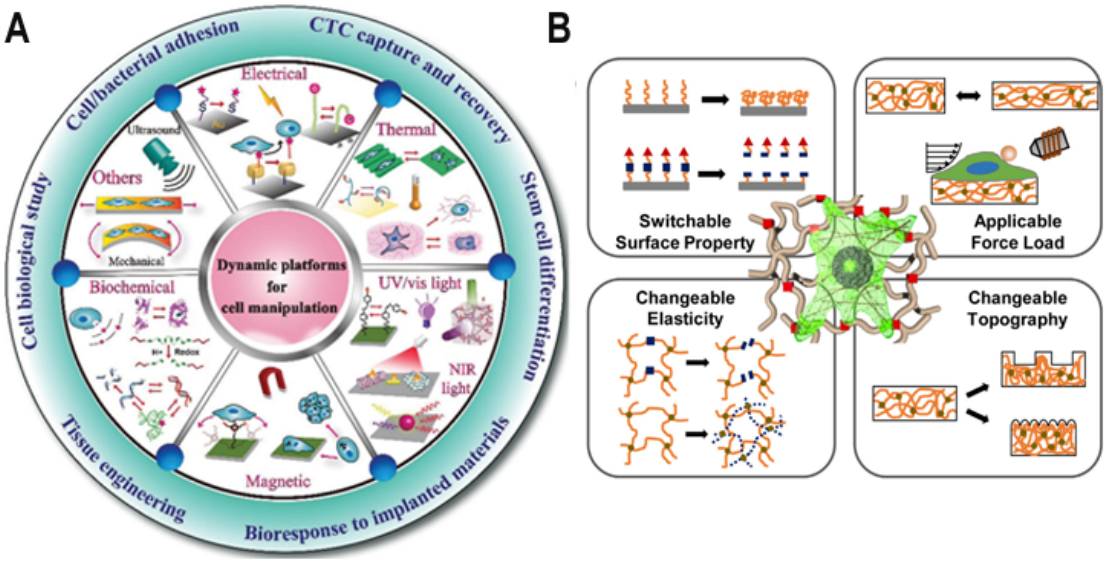

Figure 2. The different stimuli-responsive platforms and their biological and biomedical applications. (A) The dynamic platforms could be designed to respond to different stimulus, such as electrical, thermal, light, magnetic, biological, mechanical, and (B) applicable forces or switchable topography, which can guide cell behavior in dynamic manners. Reprinted from ref.[28] and ref.[29] with the kind permission of The Royal Society of Chemistry Copyright 2018 and Elsevier Copyright 2017, respectively.

1.3.1 Photo-responsive materials

Photo-responsive materials that can be applied to control the cell behavior involve two different mechanisms, including irreversible photocleavage and reversible photoisomerization, which can affect cell functions in a non-invasive fashion.

The irreversible photocleavage functionality was often applied to regulate cell-surface interactions. Aránzazu del Campo and co-workers used this strategy to set up photosensitive cages, which can guide cell adhesion,[30] migration,[31-33] and differentiation (**Figure 3A-B**).[34] The irreversible photocleavage group of 3-(4,5-dimethoxy-2-nitrophenyl)-2-butyl ester (DMNPB) at the amino terminal group of the K residue temporally inhibited the activity of the peptide (e.g., (Arg-Gly-Asp) RGD sequence). The linker was photocleaved, which induced peptide available on the surface at the site of the ultraviolet light (UV) light exposure. Furthermore, they also used this type of substrate to manipulate cell behavior and direct vascularization of implanted materials *in vivo*.[35] This work showed that the control of bioligands presentation can be utilized to mediate reparative response to the implanted materials *in vivo*. Additionally, the protein-patterning approach had been used to modulate cellular function in three-dimensional gels based on the photolytic groups, which could be cleaved by light exposure to induce the protein release.[36] Meanwhile, UV responsive systems have been widely applied for cell regulation. It also opens a new avenue for developing the near-infrared (NIR) light-responsive platform by combining the upconverting nanoparticles (UCNPs), which can emit photons in the UV regions through NIR light

exposure. Qu and co-workers developed a novel technique for dynamic transferring the molecular structure through the UCNPs, which converted NIR light into local UV light and cleaved the linker to guide the cell adhesion. The on-demand cell release can be achieved through NIR light exposure (**Figure 4A**). Recently, their group used a similar strategy to control the release of anti-adhesive effect to modulate cell-matrix interactions and ultimately guide stem cell fate. Their work provided a new way to modulate the multidirectional differentiation of human mesenchymal stem cells (hMSCs) through NIR-based upconversion substrate (**Figure 4B**).[37, 38]

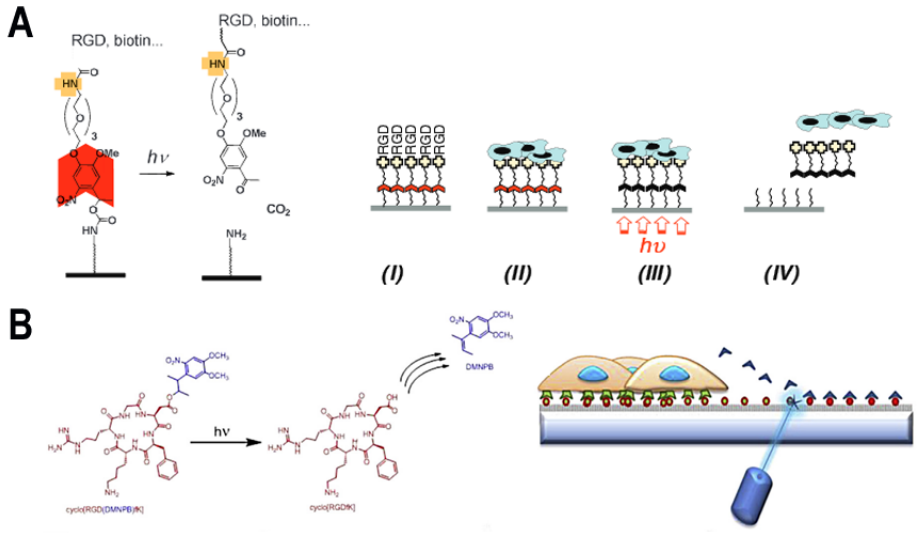

Figure 3. UV light-triggered cell behaviors through the irreversible photocleavage group, which can be applied for cell adhesion (A), migration (B). Reprinted from ref.[30] and ref.[33] with the kind permission of Wiley-VCH Copyright 2011 and Elsevier Copyright 2016, respectively.

Compared with the irreversible photocleavable group, photoisomerization reactions provided a reversible method to construct dynamic cell culture platforms. Reversible photoisomerization is a molecular behavior with the molecular structure changes, when occurred through photo irradiation, such as azobenzene and spiropyran. Azobenzene is a well-known photoisomerization that undergoes reversible conformation from *trans* (E) to *cis* (Z) state under light irradiation and vice versa from Z to E via the visible light exposure.[39] Hence, azobenzene-based switchable materials have been applied to modulate cell adhesion via control of the bioligand (e.g., RGD) availability on the surface. As shown in **Figure 5A-B,** the azobenzene component could be photochemically transformed between the E and Z configurations. When RGD was in their E conformation, which enhanced the cell adhesion, whereas adhesion efficiency decreased with transferring RGD to Z conformation under the UV irradiation.[40-42] Moreover, azobenzene-based liquid crystal polymer networks (LCNs) could change the geometry and roughness of the substrate to *in situ* reversible control the cell migration. This work demonstrated that the topography of the surface can be controlled to switch cell migration in real-time.[43] In an alternative approach,

spiropyran can be also reversibly switched between hydrophilic/zwitterionic. Both hydrophilicity and zwitterions support the hydrated layer formation, which can be used to reversibly control the cell adhesion and detachment through alternative irradiation of visible and UV light or combined UCNPs under NIR light exposure.[44-47] Taken altogether, the utilization of photosensitive groups offers a method to dynamically control cellular behaviors, including cell adhesion, migration, and differentiation.

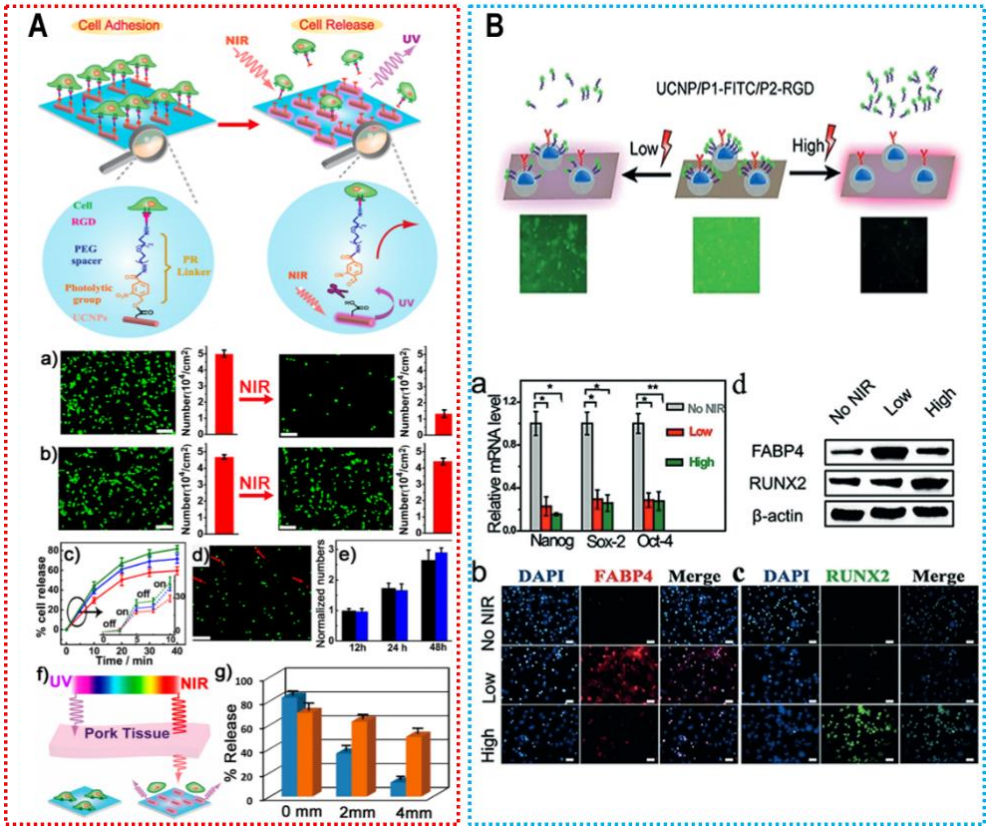

Figure 4. NIR light-triggered cell behavior through the irreversible photocleavage group by combining the upconverting nanoparticles (UCNPs) to guide cell adhesion (A), scale bars are 100 μm; and differentiation (B), scale bars are 50 μm. Adapted from ref.[37] and ref.[38] with the kind permission of The American Chemical Society Copyright 2014 and Wiley-VCH Copyright 2018, respectively.

1.3.2 Electro-responsive materials

Electrochemical responsive materials can directly enable the switchable of ligand activities under the electrical potential. Normally, the electrochemical responsive materials can be used for dynamic regulation of cell behavior involved in three strategies, including charged molecular,[48] conductive polymers,[49, 50] and hydroquinone/quinone redox electroactive groups.[51, 52]

Surface-bound molecules with electrical potential have been widely applied to fabricate rapid and reversible switching substrates. Similar with photoisomerization, the surface was a reversible switch from cell-resistance to cell-adhesive with the dynamic application of the electrical potential, as shown in **Figure 6A**. In this platform, the charged moiety played the role of the active site to

modulate RDG peptide access to cells. The charged moiety was repelled from the electrode to conceal the RGD to cells, when the same potential as the charged moiety was applied. Conversely, the opposite potential with charged moiety resulted in the exposure of RGD, which induced the cell adhesion.[53] Moreover, the wetting behavior also can be regulated via conformational transitions of a self-assembled monolayer (SAM) of charged molecules, which were attracted or repelled from the surface combing the electrical potential.[48, 54]

Due to the good electronic conductivity, conductive polymers have been widely used in biomedical engineering.[55, 56] Conductive polymers, such as poly (3,4-ethylene dioxythiophene) (PEDOT) [57] and polypyrrole (PPy), [26, 58] have been also explored to dynamically control cellular behavior. Unlike small charged molecules reversibly switching the surface wettability, the conductive polymer-based active surface could provide a dynamic change in topography from nanotube to nanotip with the multicycle electrical potential to direct osteogenic differentiation of hMSCs, as shown in **Figure 6B**.

An electrochemically based cell culture platform is another strategy to reversibly regulate cell behaviors by utilizing the redox reactions. The hydroquinone/quinone redox pair can reversibly transferring via oxidative potential. The benzoquinone form can covalently bind to bioligands to guide the cell adhesion and migration.[51, 59] Moreover, the hydroquinone/quinone can also be directly modified to the cell membranes, which guide cell assembly and disassembly in a dynamic manner.

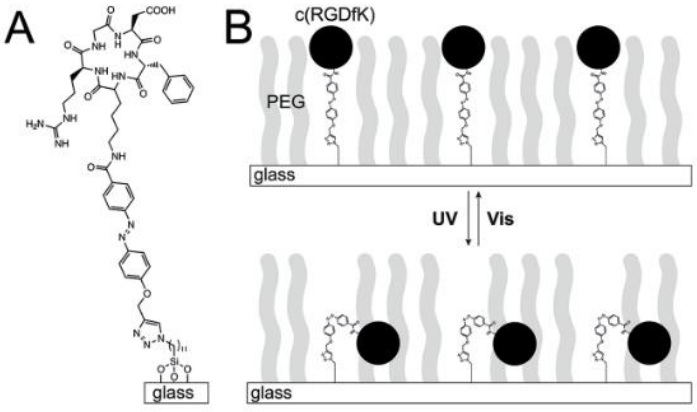

Figure 5. Light-triggered reversibly dynamic cell culture platform to guide cell adhesion. Structure of the c(RGDfK)-azobenzene(A) and polyethylene glycol (PEG) (B) mixed covalent immobilization on the glass. Reprinted from ref.[40] with the kind permission of Wiley-VCH Copyright 2016.

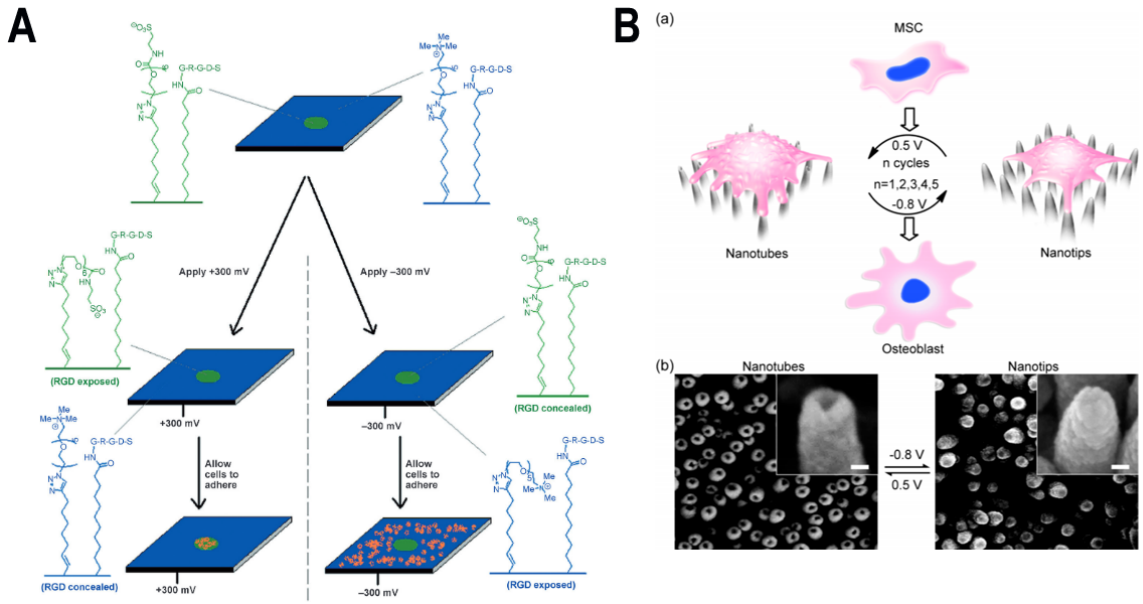

Figure 6. The electro-responsive interface to guide the cellular behavior, including cell adhesion (A) and differentiation (B), scale bars are 20 nm. Reprinted from ref.[53] and ref.[26] with the kind permission of Wiley-VCH Copyright 2012 and The American Chemical Society Copyright 2017, respectively.

1.3.3 Magnetic-responsive materials

Similar to electrical materials mediate cell behavior under the electrical potential, the magnetic stimulus also requires a magnetic material, such as magnetic nanoparticles (MNPs). Normally, cells are aligned in many complex tissues, especially for muscles and nerves.[60, 61] The De Laporte's group developed a novel anisotropic gel (Anisogel), in where the fibroblasts and nerve cells can grow and extend unidirectionally with the Anisogel based on aligned fibers or microgels by mixing superparamagnetic iron oxide nanoparticles (SPIONs) inside under the magnetic field (**Figure 7**). This strategy created a simple way to fabricate implantable materials to avoid additional damage to sensitive tissue, including spinal cord injury (SCI).[62, 63]

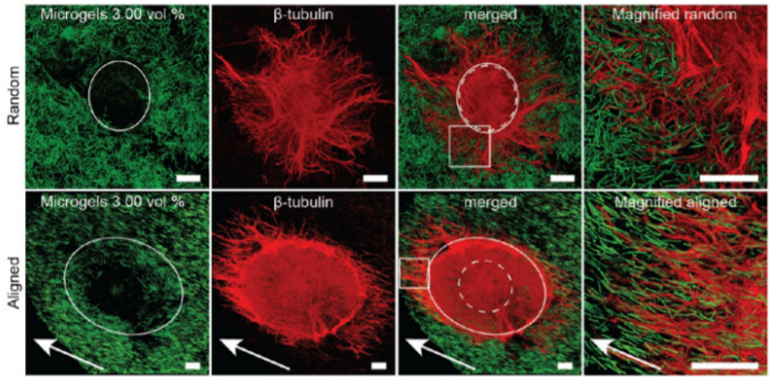

Figure 7. Superparamagnetic iron oxide nanoparticles (SPIONS)-based Anisogel to dynamically control nerve cells (dorsal root ganglia (DRG)) with aligned order. Reprinted from ref.[62] with the kind permission of The American Chemical Society Copyright 2017.

In order to precisely control the cellular behavior, Bian and co-workers developed a novel technique to dynamically control the stem cell behavior. The tether RGD ligands was covalently anchored to the MNPs that were conjugated to the glass substrate through a poly (ethylene glycol, PEG) linker. The tether length and freedom of the RGD peptides could be controlled by the magnetic field as shown in **Figure 8A**. In this study, Bian and co-workers demonstrated that the restricted RGD tether mobility exhibited enhance cell adhesion, spreading, and osteogenic differentiation of hMSCs under the magnetic field.[64] Similar with reversible photoisomerization and electrical potential, they also presented a dynamically controlled movement of nanocages that reversibly uncaged or caged RGD under the magnetic field, which could promote stem cell adhesion and differentiation through magnetic switching between "ON" and "OFF" *in vivo*.[65] Moreover, the blockade of immune checkpoints is an effective way for cancer immunotherapy. The immunotherapy induced immune cells to give an antitumor immune response that relates to macrophages, including the pro-inflammatory M1 phenotype and the pro-healing M2 phenotype.[66] Generally speaking, the M2-like phenotype displays an immune-suppressive that fosters tumor growth and promotes resistance to therapy. Yet, macrophages are highly plastic and can also acquire an anti-tumorigenic M1-like phenotype. The M2 macrophages repolarize to M1 macrophages and are subsequently used to potentiate the anticancer efficiency of immune checkpoint inhibitors, such as programmed death-ligand 1 (PD-L1).[67, 68] Bian's group used the same above-mentioned strategy to dynamically control the reversible RGDs' uncaging to temporally manipulate the adhesion and polarization of M2 macrophages under the magnetic field both *in vitro* and *in vivo*.[69]

Moreover, Du et al. developed 3D cell structures with magnetic forces. The embryonic stem cells (ECSs) were assembled and organized into a 3D embryonic body after being internalized with MNPs under the magnetic forces. The differentiation of the embryonic body can be guided towards the mesodermal cardiac pathway under the magnetic stretcher.[70] In addition, recent studies have reported that transient receptor potential vanilloid 1 (TRPV1) and piezo (stretch-activated) ion channels can be engineered to become sensitive under the magnetic stimulation, which utilized magnetic forces to control the nervous system.[71-74] Andy Tay, et.al described a 3D magnetic hyaluronic acid (HA) hydrogel, which was covalently bound with magnetic microparticles (MMPs) to dynamic control the neuromodulation of primary dorsal root ganglion (DRG) neurons. They demonstrated that the Ca^{2+} influx in primary DRG was enhanced and reduced the expression of piezo 2 channels at the same time by seeding on the 3D magnetic HA hydrogels with chronic magnetomechanical stimulation, which can be useful for modulating pain (**Figure 8B**).[75]

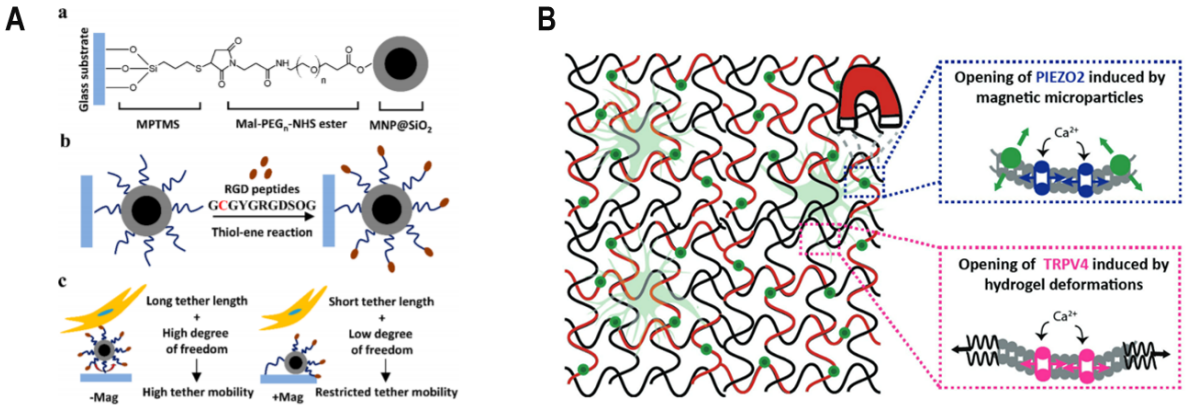

Figure 8. Magnetic fields trigger cell behavior and fate through dynamic adhesion (A) and magnetomechanical stimulation (B). Reprinted from ref.[64] and ref.[75] with the kind permission of The American Chemical Society Copyright 2017 and Wiley-VCH Copyright 2018, respectively.

1.3.4 Temperature-responsive materials

Temperature-responsive materials exhibit reversible changes in response to the temperature. The temperature-responsive materials, including classical poly (N-isopropylacrylamide) (PNIPAM) and its derivatives, gelatin-based natural materials, and poly (ε-caprolactone) (PCL)-based shape memory polymers, have been widely used to design dynamic platforms.[76]

It is well known that PNIPAM exhibits thermo-responsive reversible hydrophobicity changes in aqueous solutions around the lower critical solution temperature (LCST) of 32 ºC.[77, 78] Based on dynamic hydrophilicity/hydrophobicity changes in response to temperature, PNIPAM and its derivatives have been applied for cell sheet technology, which can be transplanted to injured host tissues for regeneration.[79-81] Teruo Okano's group was first reported cell sheet engineering via PNIPAM-based thermo-sensitive substrate. At 37 ºC, the cell can attach and grow on the hydrophobic PNIPAM surface. When the temperature was decreased to the 20 ºC, the surface changed from hydrophobic to hydrophilic; the cells were detached from the surface and the cell sheet formed while maintaining cell-cell junctions and basal ECM. Based on this strategy, more and more dynamic platforms have been developed to improve the cell sheet harvesting by combining PNIPAM-based hydrogels. As shown in **Figure 9**, RGD can be imprinted to the hydrogel, which could re-bind and release RGD at 37 ºC and 20 ºC, respectively, to enhance the cell sheet formation.[79] In addition, Weinhart's group developed a new thermoresponsive technique based on poly(glycidyl ether) for cell sheet engineering. In their studies, they grafted poly(glycidyl ether) based copolymers on different substrates for cell sheet fabrication, such as glass surfaces, gold substrates, and polystyrene (PS) tissue culture substrates.[82, 83]

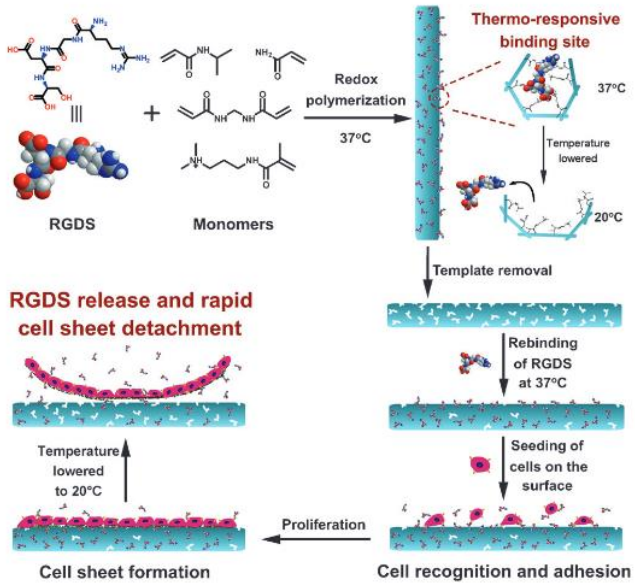

Figure 9. Cell sheet detachment from temperature-responsive culture surfaces. Reprinted from ref. [79] with the kind permission of Wiley-VCH Copyright 2013.

Due to the dynamic hydrophilicity/hydrophobicity changes, Wang's group developed a novel method to reversibly capture and release circulating tumor cells (CTCs).[84] Anti-EpCAM-modified bovine serum albumin (BSA) molecules were anchored on the PNIPAM-based surface through the hydrophobic interactions. At 37 ºC, the EpCAM-positive cells could be recognized on the surface; the anti-EpCAM cells detached from the surface when the temperature decreased to 20 ºC. Based on this strategy, the temperature-triggered device for reversible capture and release of the CTCs can be achieved to effectively isolate the CTCs from the peripheral blood of patients, which is essential for the early stage of cancer diagnostics.[85, 86]

In addition, the PNIPAM-based responsive material can also respond to alternations of external temperature, including swelling/shrinking, mechanical strength, and porosity, which can be used for on-demand cell capture, encapsulation and release.[87] Moreover, graphene and gold nanoparticles that exhibit a photothermal effect under the NIR light irradiation, can generate the heat to induce the transition of the PNIPAM-based material with the highly localized and reversible deformation to further manipulate cell capture, release and migration (**Figure 10A-B**).[88, 89]

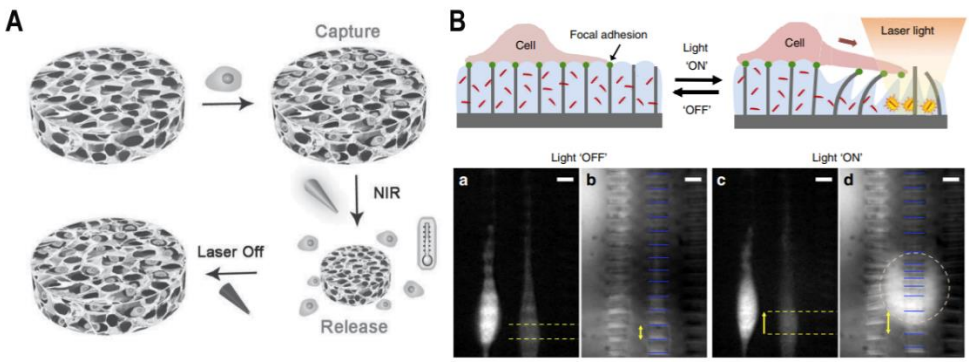

Figure 10. PNIPAM-based thermo-triggered dynamic platforms for cell capture, release (A) and migration (B), scale bars are 10 μm. Reprinted and adapted from ref.[88] and ref.[89] with the kind permission of Wiley-VCH Copyright 2013 and Nature Publishing Group Copyright 2017, respectively.

Besides PNIPAM and its derivatives, gelatin-based hydrogels have been also applied to dynamically guide cell behavior, including CTCs isolation and recognition. Lv et al. reported a CTC-imprinted hydrogel for an effective capture and release cells. The hydrogel was fabricated though gold nanorods (AuNRs) embedded with gelatin, which could release the cells via temperature increase to 37 ºC or site-specific release of a single CTC triggered by NIR light-mediated photothermal activation of AuNRs.[90] Using a similar strategy, Reátegui et al. also developed a gelatin-based layer-by-layer (LBL) nanocoating on polydimethylsiloxane (PDMS) for CTC capture. The effective and precise release cells could be achieved by increasing temperature or a frequency-controlled microtip, as shown in **Figure 11A**.[91] In addition, PCL-based shape memory polymers are other classes of temperature-responsive materials to study cell-geometry interactions. In general, PCL-based shape memory polymers have a capability to change from a temporary shape to a memorized permanent shape upon application of external temperature.[92-94] The topography of the surface can be dynamically changed through temperature. The dynamic cell-orienting study demonstrated that surface topographical changes play a dominant role in cell alignment (**Figure 11B**). Hence, the PCL-based shape-memory surfaces could be applied for spatiotemporal control for probing the dynamic topographical changes in cell behavior.

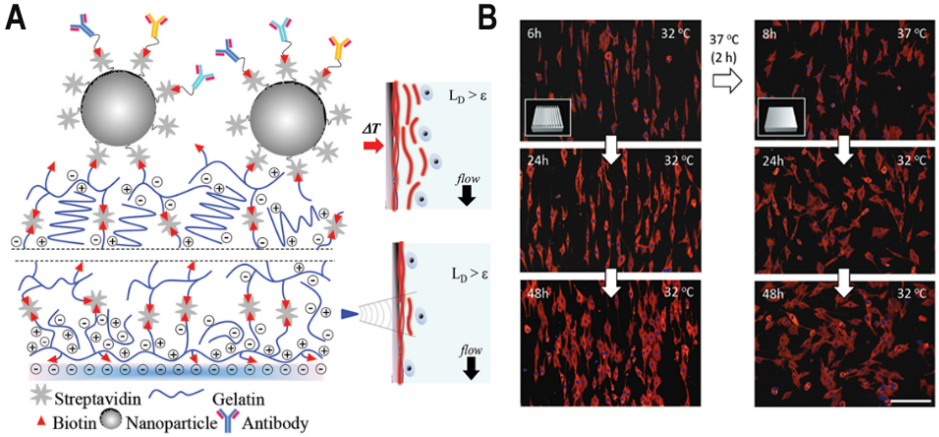

Figure 11. Different classes of thermo-triggered materials to guide cell regulation. (A) Gelatin- based materials for cell release. Reprinted from ref. [91] with the kind permission of Wiley-VCH Copyright 2015. (B) PCL-based shape-memory surfaces for cell alignment. Reprinted from ref.[92] with the kind permission of Wiley-VCH Copyright 2012.

1.3.5 Mechano-responsive materials

Mechanobiology is an emerging field of science between biology and engineering, which was mainly to probe the cell behavior in response to the biophysical cues within the native cellular microenvironments. Understanding how mechanical factors are converted into cell signaling with interaction between cell and ECM is become more important for cellular mechanotransduction,

and biomaterials could be used to study cellular behavior and help us to understand how cells sense and interpret these cues. [5, 95-97] Recently, mechano-responsive materials have been developed to capture matrix dynamics. Some of the mechanisms can be attributed into irreversible or reversible strategies, as shown in **Figure 12,** which can be softened, stiffened, or reversibly stiffened and softened with many of the aforementioned external stimuli.[98, 99]

To elucidate the complex dynamic interaction between the cell and matrices, previous work from Anseth and co-workers developed photodegradable PEG-based hydrogels through photolabile nitrobenzyl ether-derived acrylate moieties, which could be *in situ* degraded via external photoirradiation stimuli.[100] Based on this strategy, they applied this dynamic hydrogel to study the mechanical memory of stem cells, which could be softened with light irradiation during cell culture (**Figure 13A**). They found that activation of the Yes-associated protein (YAP) and transcriptional coactivator with PDZ-binding domain (TAZ) as well as the pre-osteogenic runt-related transcription factor 2 (RUNX2) hMSCs on soft matrix were shown to be involved mechanical memory, which depended on previous culture time on initially stiff (E ~ 10 kPa).[101] Moreover, their group also fabricated different stiffness patterns based on this photodegradable hydrogel with regular or random models. The important results of this study were that hMSCs' fate can be modulated by stiffness pattern organization and stiff-to-soft ratios.[102]

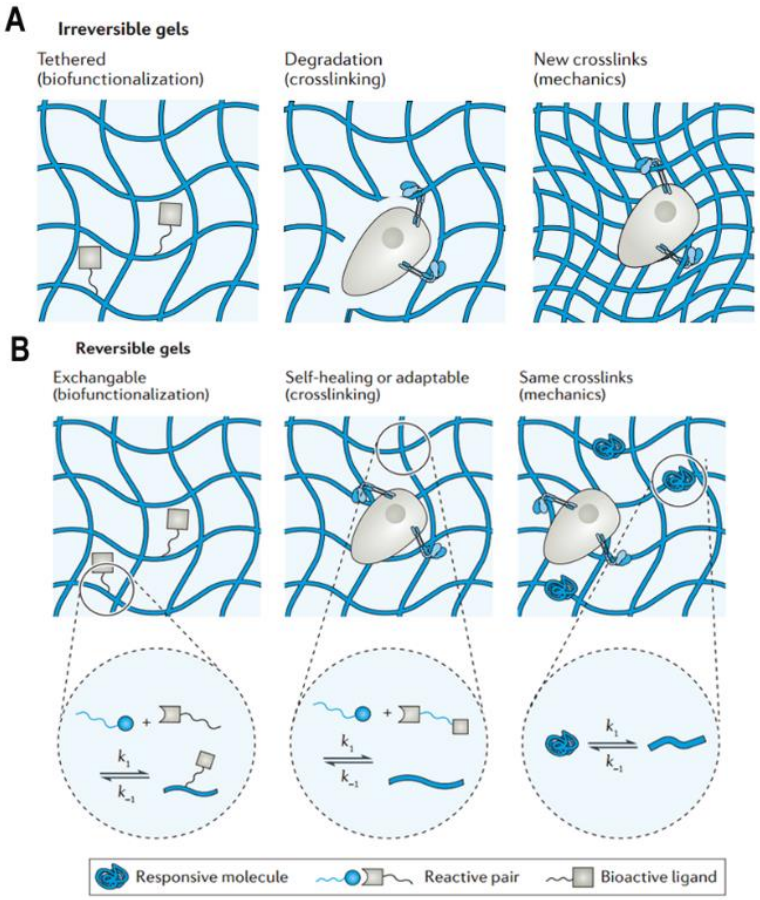

Figure 12. Irreversible (A) and reversible (B) chemistries for hydrogels. Reprinted from ref.[98] with the kind permission of Nature Publishing Group Copyright 2016.

Compared with light-based softening strategies, matrix degradation is an alternative way to mimic mechanical softening process, which can break the crosslinks via cell-mediated enzymatic cleavage or passive hydrolysis. For instance, Burdick and colleagues modified HA with enzymatically degradable peptide (matrix metalloproteinase, MMP) to mediate hydrogel stiffness by tuning the degradability. The degradability of hydrogel can regulate cell morphology and ultimately guide the differentiation of hMSCs in the 3D microenvironment. [103, 104] In addition, the hydrogel stiffness can also be decreased through the addition of hydrolysis component. Mooney and co-workers developed alginate dialdehyde-based microspheres, which were treated as hydrolyzable porogens and incorporated into bulk alginate hydrogel. More impotently, this void-forming hydrogel could mediate better the osteogenesis of encapsulated hMSCs to enhance the bone formation.[105] Furthermore, temperature-responsive polymers, such as PCL, can also be used to softening substrate above their melting temperature (T_m) and investigate how dynamic changes in guiding cell function and fate, such as the sensitivity for dynamic changes in the surrounding microenvironment, were different for each cell type. The YAP/TAZ nuclear translation of cardiac progenitor cells also decreased with stiffness softening. [106, 107]

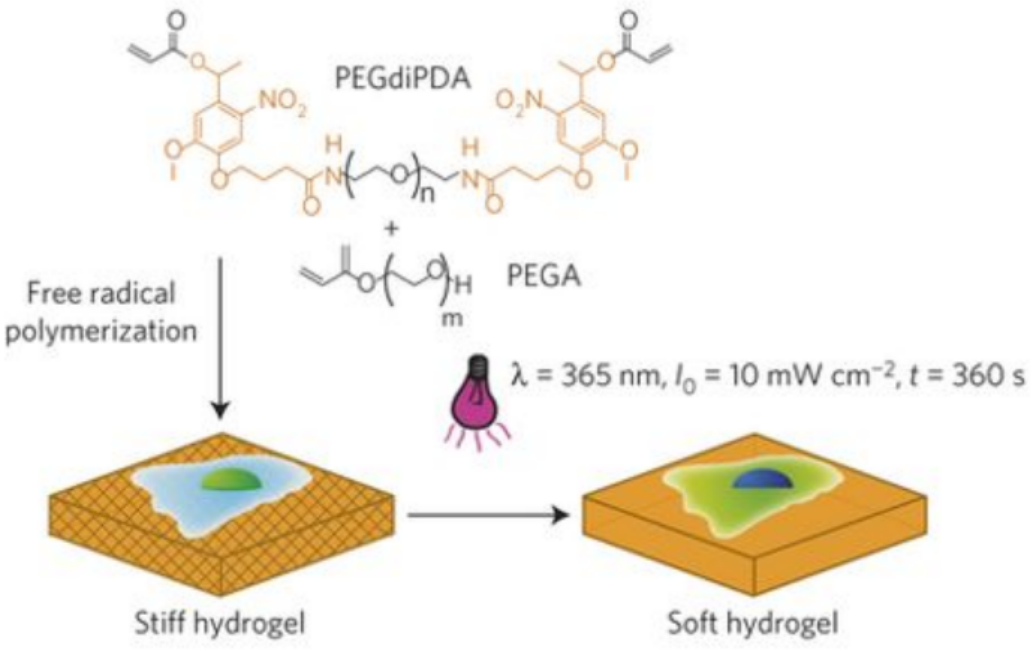

Figure 13. Representative strategy for dynamic control of the stiffness with softening substrates. Reprinted from ref.[101] with the kind permission of Nature Publishing Group Copyright 2014.

Moreover, matrix stiffening is a natural phenomenon for the human body, such as wound healing, tissue fibrosis, and cancer progression.[108-111] To better understand and manipulate the biological process, a variety of novel strategies have been applied to mimic the ECM stiffening. Building on similar light-based strategies for substrates softening, the on-demand stiffening of the hydrogel can also be achieved by light-induced crosslinking. Burdick and colleagues functionalized HA with methacrylate, which can be first crosslinked with dithiothreitol (DTT) and can switch from soft to stiff through light-mediated further crosslinking. In a similar strategy, the team developed a two-step crosslinking with PDMS, which can be crosslinked through platinum-catalyzed crosslinking, and then to increased crosslinking via thiol-ene click reaction. With substrates stiffening, cells displayed increased spreading area in both studies.[112, 113] In addition, Anseth's group reported a strain-promoted azide-alkyne cycloaddition (SPAAC) method to study the dynamically tunable properties through orthogonal photoconjugation and photocleavage reactions.[114] Recently, they fabricated on-demand stiffening of 3D cell scaffolds based on this method to encapsulate muscle cells in these networks (**Figure 14**). This work illustrated the myoblasts decreased cell spreading and nuclear localization of YAP in respond to increased matrix stiffness and cell spreading. The YAP nuclear localization increased when delayed the photocrosslinking reaction.[115] Besides light-triggered mechanical stiffening, Lin's group also reported a tyrosine-mediated stiffness stiffening strategy, which could be oxidated into dihydroxyphenylalanine (DOPA) in the presence of tyrosinase, whereby the DOPA can be further crosslinked.[116-118]

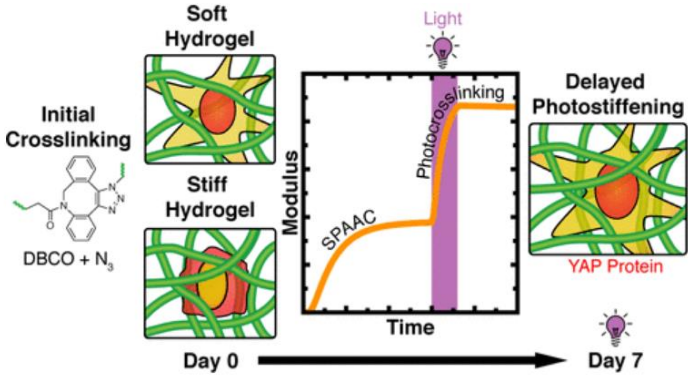

Figure 14. Representative strategy for dynamic control of the stiffness with stiffening substrates. Reprinted from ref.[115] with the kind permission of The American Chemical Society Copyright 2018.

However, the cyclical changes in native ECM remodeling cannot be captured with one-directional softening or stiffening. To address this issue, the reversibly tunable stiffness for dynamic cell culture platform were needed. Addition of chemical reagents was one of the strategies to achieve mechanically reversible microenvironments. Gillette et al. reported alginate-based hydrogels, which could be reversibly mediated for stiffness via the addition of Ca^{2+} or sodium

citrate (**Figure 15**). In addition, Yoshikawa et al. developed a pH-responsive ABA triblock copolymer hydrogel, where the Youngs' modules could be reversibly altered through addition acid or base with a modest pH change between 7.0 to 8.0. The morphology of C2C12 mouse myoblasts exhibited reversible transformation between rounded and spread in response to soft (pH 7.0) and stiff (pH 8.0), respectively.[119] Moreover, the reversible stiffness could also be achieved by adding DNA hybridization-mediated crosslinkers or host-gust-based crosslinkers.[120, 121] As mentioned above, the AuNRs exhibited the photothermal effect under the NIR light irradiation. Another promising work was reported, in which the stiffness of alginate hydrogels that were incorporated with temperature-sensitive liposomes could be meditated by NIR light irradiation. The AuNRs were encapsulated in the liposomes, which acted as a depot for calcium ions' or calcium chelators' (diethylenetriaminepentaacetic acid, DTPA) release in response to NIR light. Importantly, this study demonstrated that the matrix stiffness can be spatially and temporally controlled both *in vitro* and *in vivo*.[122] With a similar strategy as mentioned above for light-based strategies, Anseth's group developed a photo-responsive HA hydrogel to explain the effort for YAP/TAZ signaling with reversible modulus, which could soften and then stiffen with orthogonal wavelengths of light. The cell area and nuclear YAP/TAZ ratio of hMSCs were shown dynamic changes in respond to dynamic substrate mechanics.[25] Recently, they also reported a SPAAC-based protein-polymer hydrogel to study the role of cyclic mechanical loading to cells based on light stimuli, which enhanced fibroblast transdifferentiation into myofibroblasts.[123] Furthermore, the matrix stiffness of azobenzene-based hydrogel could also be reversibly modulated as mentioned above.[124, 125] Taken altogether, these platforms with dynamic stiffness have provided newfound avenues to probe and direct cellular fates in cell outcomes for cell-based therapies.

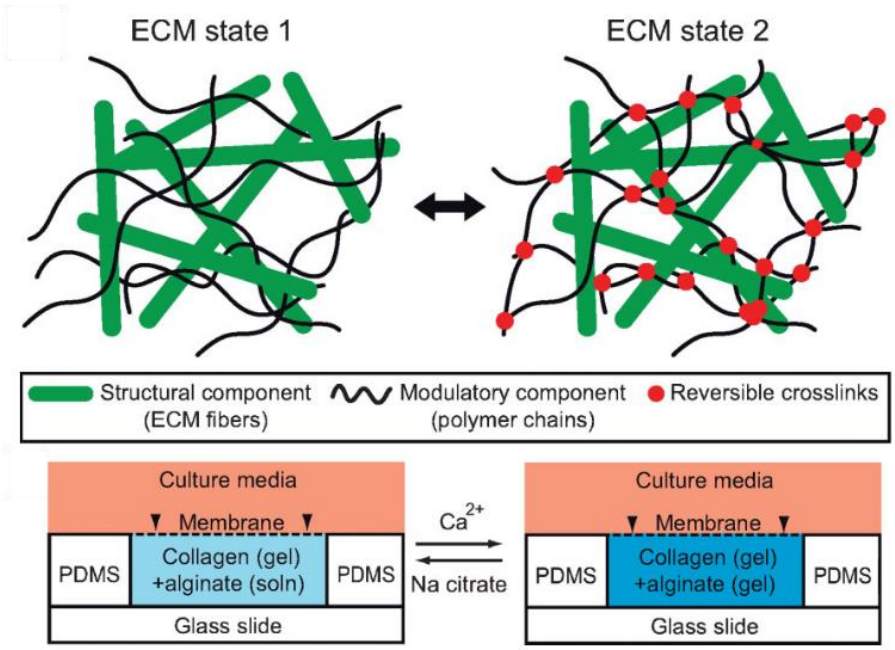

Figure 15. Representative strategy for mechanically reversible microenvironments. Reprinted from ref.[126] with the kind permission of Wiley-VCH Copyright 2010.

1.4 The design of reversibly dynamic scaffolds to study the complexity of native cellular microenvironment

In addition to the dynamic stiffness of ECM, the cells in our bodies are also subjected to cyclic mechanical loading, especially for those from a blood vessel, heart and muscular tissues. Among various types of dynamic cues, stress/strain play a crucial role in heart beating and muscle contraction. Dynamically controlled stress/strain has therefore been applied to mimic such microenvironment. Recently, Yoon et al. reported a thermosensitive, stretchable, and piezoelectric substrate (TSPS) to generate cyclic mechanical strain to hMSCs, as shown in **Figure 16.** It was found that the hMSCs enhanced myogenic differentiation and improved injured skeletal muscle regeneration in this dynamic culture system.[127] This work showed that this dynamic culture system may serve as a tool for research on stem cell-based therapies. Furthermore, the cyclic stress/strain stimuli not only influenced cytoskeleton structure, but also enhanced the signaling pathway. Kaunas et al. demonstrated that both the direction and extent of stretch-induced stress fiber orientation in bovine aortic endothelial cells can be guided via the activity of the Rho signaling pathway.[128] On the other hand, cells in different locations of the embryo also subjected stress/strain forces during embryonic development.[129] Fu's group developed *in vitro* platforms that could exploit self-organize of stem cells under the dynamic stress/strain forces. More importantly, their study highlighted that the cell shape of human pluripotent stem cells (hPS) can be modulated by mechanical stretching or geometrical confinement, which can ultimately mediate (bone morphogenetic protein) BMP signaling to regulate neuroectoderm patterning.[2] Moreover, substrate stretching-induced mechanical stress also can trigger the formation of lamin A/C, which play a central role in nuclear mechanotransduction.[130]

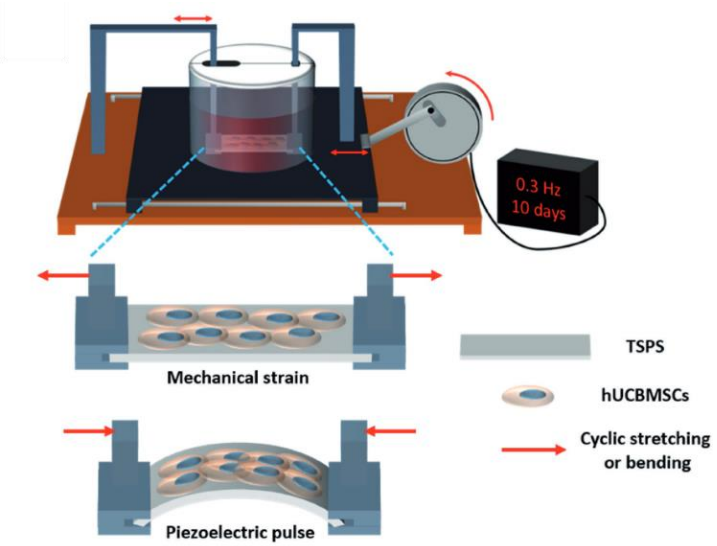

Figure 16. Dynamically controlled stress/strain for cell regulation. Reprinted from ref.[127] with the kind permission of Wiley-VCH Copyright 2017.

Furthermore, most native tissues exhibited dynamic stress relaxation behavior with viscoelastic properties and viscoelasticity can also substantially impact cellular responses.[131-135] However, they were typically almost purely elastic in the reconstituted native ECM. To impart viscoelastic features, pioneering work from Mooney and co-workers developed an alginate-based hydrogel, which can be dynamically cross-linked by calcium with controlled stress relaxation rate.[136] The rate of stress relaxation can be altered by lowering the molecular weight and coupling of PEG spacers to control the chain mobility and connectivity of a polymer network. This study illustrated the matrix with faster stress relaxation enhanced actomyosin's contractability and nuclear translocation of YAP through the integrin recruitment and clustering. Moreover, cell spreading, proliferation, and osteogenic differentiation of hMSCs were all enhanced with faster stress relaxation in these viscoelastic microenvironments.[137] A time scale of the viscoelasticity can be changed within the recent development of reversible covalent interaction, which would leverage cross-linking mechanisms via dynamic covalent chemistries, such as hydrazone bonds,[138-140] boronate bonds,[141, 142] and allyl sulfide-based chain transfer.[143-145] For example, Anseth' group reported a covalently adaptable network with PEG-based dynamic boronate bonds, which could be formed into boronic esters with fast stress relaxation between boronic acids and cis-1,2-diols (**Figure 17**). This work observed that these fast-relaxing hydrogels can increase the cell spreading area and YAP/TAZ nuclear localization of hMSCs.[146] In addition, this research team incorporated allyl sulfide‐containing molecules to establish hydrogel network, which could be degraded via a radical addition–fragmentation chain transfer (AFCT) process to allow for a radical-initiated thiol-ene exchange reaction. The connectivity and viscoelastic properties of networks could be controlled by light exposure.[145]

In summary, cells reside in a complex dynamic 3D microenvironment *in vivo* with both biochemical and physical cues that change over time. It has long been recognized that the microenvironment can guide cell fate. However, there are remain few successes that truly demonstrate how external stimuli regulate cell fate with time regulation. As the field of tissue engineering and regenerative progress, there is a need to develop novel scaffolds approaches and *in vitro* models to mimic key aspects of the native ECM and fully capture cell dynamics.

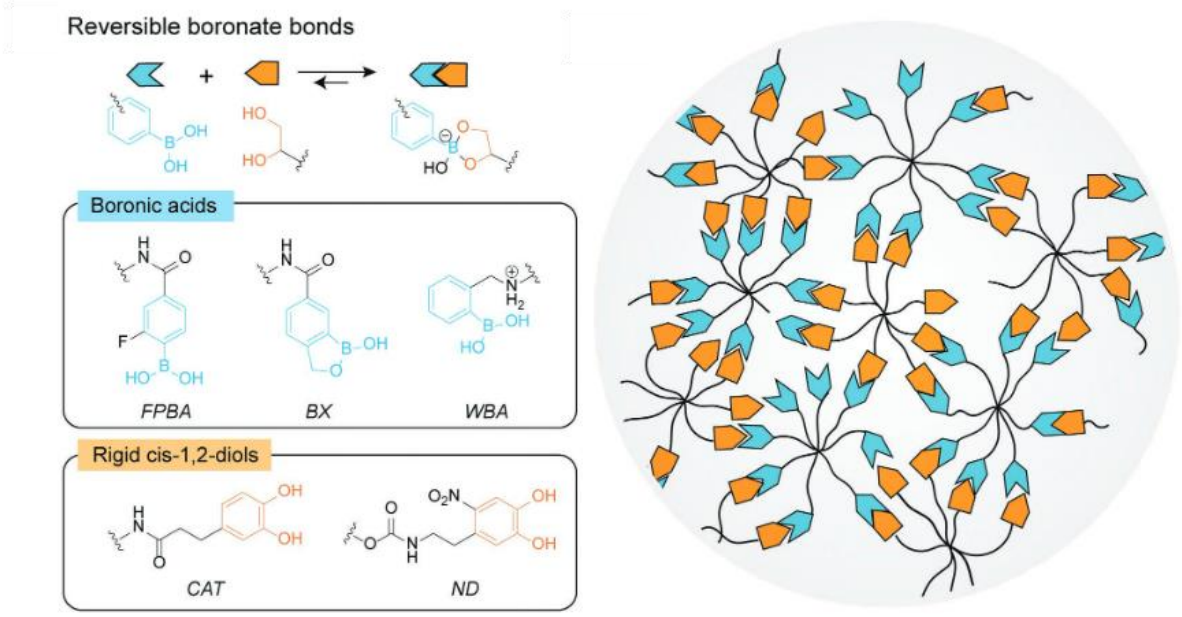

Figure 17. Engineering 3D dynamic viscoelastic microenvironments through reversible bonds. Adapted from ref.[146] with the kind permission of Wiley-VCH Copyright 2018.

2. Scientific Goals

The endothelial cells (ECs) are major component of blood vessel walls, which play a crucial role in vascular homeostasis and remodeling.[147] ECs adhesion onto scaffolds is a preliminary and crucial step for long-term vascular repair in the dynamic microenvironment of blood vessel. To better understand dynamic cell recruitment for endothelialization and vascularization of the polymer substrate, we tried to design a smart scaffold with "switchable surfaces" to achieve the cell recruitment within a dynamic manner. In the first project, we will use PNIPAM-based thermo-triggered dynamic microfiber substrates to modulate the endothelial cells adhesion and release. The aim of this work is to establish a method to achieve endothelial cell recruitment and overcome the endothelialization of polymer substrates.

Most dynamic mechanobiology studies focused on 2D substrates with linear elastic mechanics. However, the native ECM usually exhibit nonlinear elasticity. Moreover, such a nonlinear mechanical behavior, which has been confirmed to have a great effect on cell migration,[148, 149] stem cell differentiation,[150] and wound healing process.[151] Therefore, the second challenge was to understand how cyclic dynamic nonlinear elasticity guide cell behavior in the 3D microenvironment, especially for the stem cells. hMSCs have high sensitivity to mechanical stimuli in many reported studies. Although many strategies have been guided hMSCs' fate in a dynamic manner, the cells reside in natural 3D ECM consist of fibrous microenvironment.[152] In the second project, we will fabricate PNIPAM-based electrospun 3D microfiber network, which could exhibit reversibly swollen and de-swollen transition around LCST. We expect that this design could provide a platform to understand how cyclic mechanical stimuli guide stem cell fate in the reconstituted native ECM.

Although the complex feedback mechanisms of cell-material interaction are increasingly understood, it is still unknown how soft stiffness mediate cell behavior. For instance, hMSCs can attach and spread on soft PDMS, while they tend to not spread on similarly soft substrates such as polyacrylamide.[153, 154] Recently, surface energy and phosphatidylinositol-mediated signals have been verified to promote cell spreading and focal adhesion on 2D soft substrates.[155, 156] In the third project, we plan to generate a new type of PNIPAM-based nanogel-actuated-integrated responsive soft hydrogels, whose moduli can be *in situ* reversibly stiffened and softened through covalent crosslinking coordinated reversibly physical network. This design could explain how dynamic soft niches regulate hMSCs spheroids' fate via multicyclic changing temperatures from 25 to 37 ºC in 3D microenvironment.

Overall, the ECM directs cell function through a complex feedback mechanism. In this thesis, we will try to elucidate how cells sense and interpret microenvironment in a dynamic manner based on surface modification, fibrillar fabrication, and smart hydrogels (**Figure 18**).

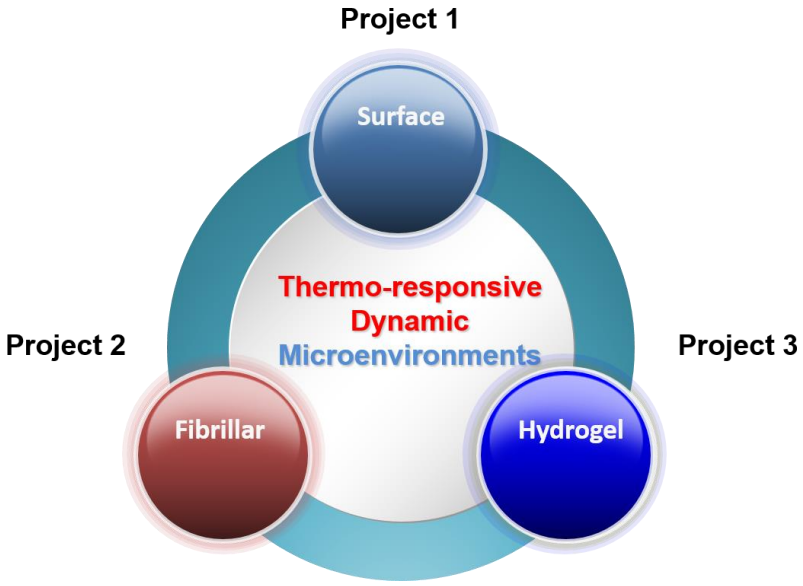

Figure 18. Thermo-responsive dynamic microenvironments to guide cellular behavior on surfaces, on fibers, and in hydrogels, respectively.

3. Publications

3.1 Selective Endothelial Cell Adhesion via Mussel-Inspired Hybrid Microfibrous Scaffold

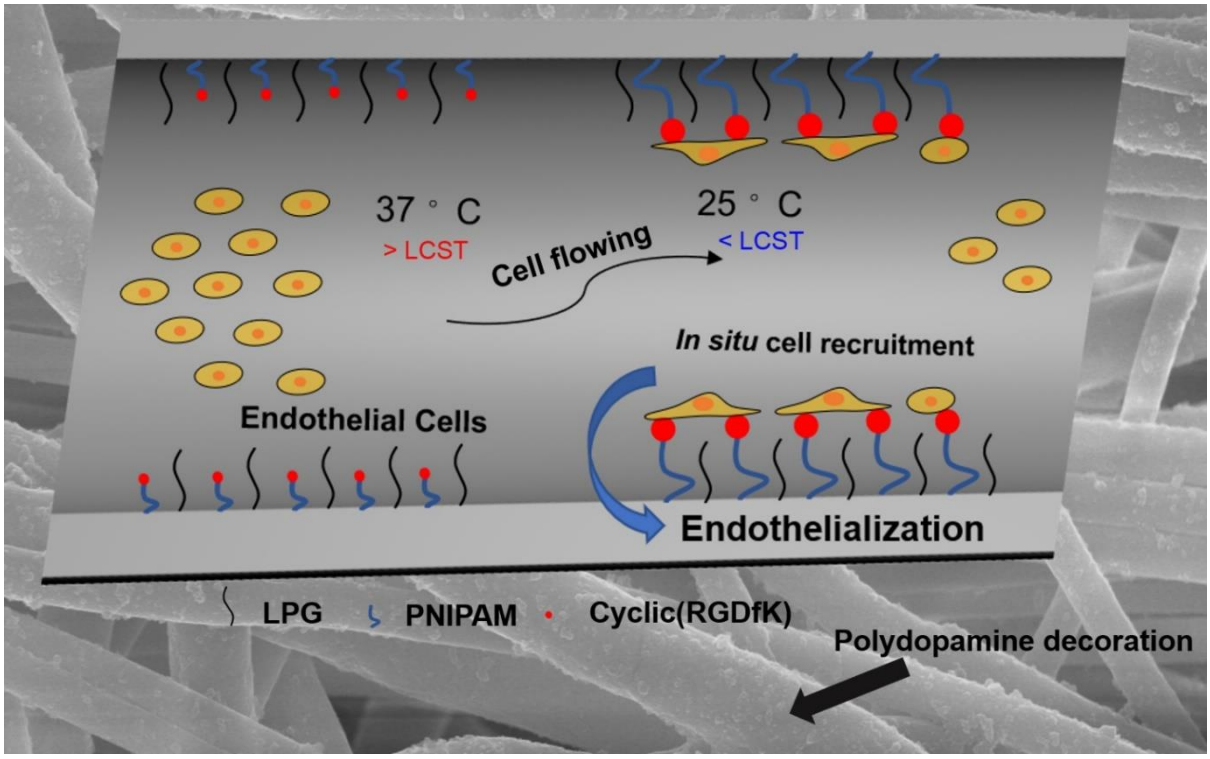

Jianguang Zhang, [‡,#] Wei Chen, [‡,§,#] Leixiao Yu, [‡] Mingjun Li, [‡] Falko Neumann, [‡] Wenzhong Li, [‡] and Rainer Haag [*‡]

ACS Appl. Nano Mater. 2018, 1, 4, 1513-1521

https://doi.org/10.1021/acsanm.8b00017

Author contributions

J. Zhang and Wei Chen designed the research. **J. Zhang** performed most experiments and analyzed the data, wrote the manuscript.

Dr. L. Yu synthesized linear polyglycerol (LPG). M. Li enabled and supported the cell culture experiments. Dr. W. Li and Falko Neumann contributed to discussion part. Prof. Rainer Haag conceived and supervised the project, as well as corrected the manuscript.

3.2 Thermally Responsive Microfibers Mediated Stem Cell Fate via Reversibly Dynamic Mechanical Stimulation

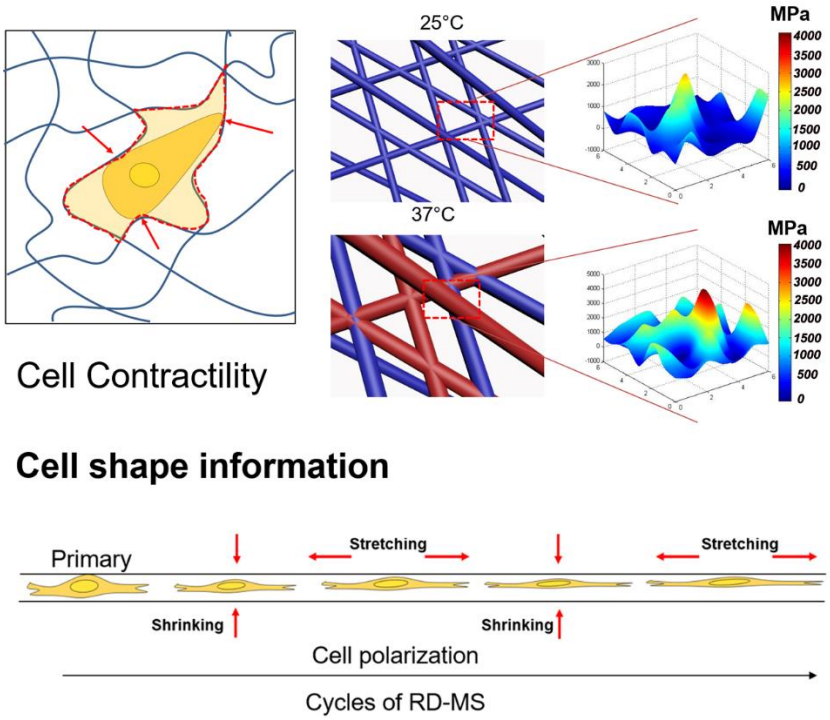

Jianguang Zhang, Chong Cheng, Jose Luis Cuellar-Camacho, Mingjun Li, Yi Xia, Wenzhong Li*, and Rainer Haag*

Adv. Funct. Mater. 2018, 28, 47, 1804773

https://doi.org/10.1002/adfm.201804773

Author contributions

J. Zhang designed and performed the research and wrote the manuscript.

Dr. C. Chong analyzed the XPS data, Dr. Luis performed the AFM images and analyzed the data, M. Li, Y. Xia Dr. W. Li contributed to discussion part. Prof. Rainer Haag conceived and supervised the project as well as corrected the manuscript.

3.3 Dynamic Mechanics-modulated Hydrogels to Regulate the Differentiation of Stem-cell Spheroids in Soft Microniches and Modeling of the Nonlinear Behavior

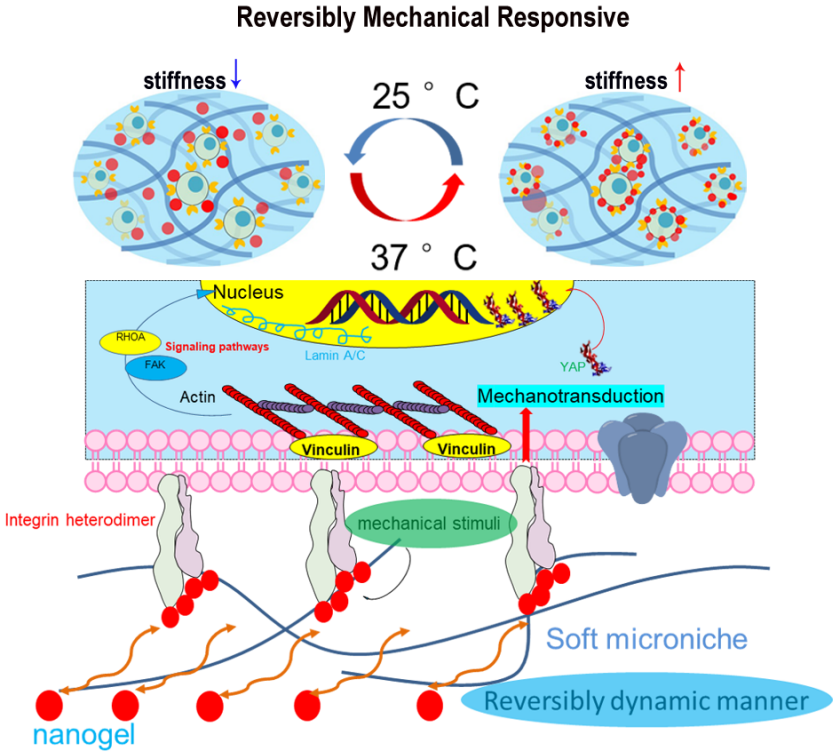

Jianguang Zhang, [†]* Hua Yang, [‡] Bilen Emek Abali,[‡] Mingjun Li,[†] Yi Xia,[†] and Rainer Haag[†]*

2019. Submitted

Author contributions

J. Zhang designed, performed the research, and wrote the manuscript;

Hua Yang and Dr. Bilen Emek Abali analyzed the MATLAB results and set up the modeling of the nonlinear behavior. Mingjun Li and Yi Xia analyzed cell images. Prof. Rainer Haag conceived and supervised the project as well as corrected the manuscript.

Small

Dynamic Mechanics-modulated Hydrogels to Regulate the Differentiation of Stem-cell Spheroids in Soft Microniches and Modeling of the Nonlinear Behavior

--Manuscript Draft--

Manuscript Number:	smll.201901920
Full Title:	Dynamic Mechanics-modulated Hydrogels to Regulate the Differentiation of Stem-cell Spheroids in Soft Microniches and Modeling of the Nonlinear Behavior
Article Type:	Full Paper
Section/Category:	
Keywords:	soft microniches; stiffness-cyclable hydrogels; stem cell spheroids; FAK signaling; lamin A/C
Corresponding Author:	Rainer Haag, Prof. Freie Universitat Berlin Berlin, GERMANY
Additional Information:	
Question	**Response**
Please submit a plain text version of your cover letter here.	Dear Dr. José Oliveira, Please find attached our manuscript entitled: “Dynamic Mechanics-modulated Hydrogels to Regulate the Differentiation of Stem-cell Spheroids in Soft Microniches and Modeling of the Nonlinear Behavior” by Jianguang Zhang, Hua Yang, Bilen Emek Abali, Mingjun Li, Yi Xia, and Rainer Haag, which we would like to submit as a full paper to “Small”. Stem cells in vivo reside in a complex and specialized microenvironment. It is well known that the mechanical stiffness of the extracellular matrix (ECM) or microniche offers a powerful tool to control human mesenchymal stem cells (hMSCs) proliferation, migration and differentiation. The mechanical interactions between the ECM and cell-cell junctions play a key part in transmitting forces to cells. However, the natural ECM in vivo is a dynamic changing fibrous system, especially during callus proliferation and tissue development. Up to now, mechanisms of how physical forces convert into biochemical signals are increasingly understood, it is still unknown how soft cues guide cell behavior. Recently, surface energy and phosphatidylinositol -mediated signals have been verified to promote cell spreading and focal adhesion on 2D soft substrates (Pro. Natl. Acad. Sci. U. S. A. 2018, 115 (18), 4631-4636; ACS Nano 2019.13(1), 203-214). In this manuscript, we show that the commitment and differentiation of encapsulating hMSC spheroids in thermosensitive three-dimensional (3D) hydrogels are simply altered by interpenetrating a nanogel network. This nanogel-actuated-integrated responsive hydrogel provides dynamic mechanics with covalent crosslinking coordinated reversibly physical network, which can regulate hMSCs in situ by reversible stiffening soft niches via multicyclic temperature changes from 25 to 37 ºC. We revealed how dynamic mechanics guide cell morphology, nuclear mechanotransduction and differentiation, which ultimately favors hMSCs undergoing osteogenesis (but not adipogenesis) in soft microniche. In addition, we also apply computational tools to elucidate the in-situ relationship between nonlinear viscoelastic properties and different temperatures with cycles. Our findings highlight the central roles of the dynamic relationship between the biomechanical signals and mechanosensitive transcriptional regulators in the cellular mechanosensing that occur in human bodies. I would like to confirm that this article has not previously been published and is not under consideration for publication in another journal at the time of submission.

	Thank you for considering our manuscript for publication in “Small”. Rainer Haag (on behalf of the authors) As requested from the author guidelines, the data of the corresponding authors are: J. Zhang (jgz720@zedat.fu-berlin.de) R. Haag (haag@chemie.fu-berlin.de) Department of Chemistry and Biochemistry, Freie Universität Berlin, 14195 Berlin, Germany.
Do you or any of your co-authors have a conflict of interest to declare?	No. The authors declare no conflict of interest.
Corresponding Author Secondary Information:	
Corresponding Author's Institution:	Freie Universitat Berlin
Corresponding Author's Secondary Institution:	
First Author:	Jianguang Zhang
First Author Secondary Information:	
Order of Authors:	Jianguang Zhang
	Hua Yang
	Bilen Emek Abali, Dr.
	Mingjun Li, limingjun0000@126.com
	Yi Xia
	Rainer Haag, Prof.
Order of Authors Secondary Information:	
Abstract:	Although mechanisms of how physical forces convert into biochemical signals are increasingly understood, it is still unknown how soft cues guide cell behavior. Herein, we show that the commitment and differentiation of encapsulating hMSC spheroids in thermosensitive three-dimensional (3D) hydrogels are simply altered by interpenetrating poly (NIPAM-HEMA) nanogel to gelatin methacryloyl (GelMA) network. This cell-laden hydrogel provides dynamic mechanics with covalent crosslinking coordinated reversibly physical network, which can regulate hMSCs in situ by reversible stiffening soft niches via multicyclic temperature changes from 25 to 37 ºC. The spreading of hMSC spheroids in the hydrogel is strongly dependent on myosin-dependent traction stress with dynamic mechanical stimuli through focal adhesion kinase (FAK) signaling. Notably, the dynamic microenvironment gradually influences the expression and the distribution from the basal to apical side of nuclear lamin A/C and increases the Yes-associated protein (YAP) nuclear localization with cycles, which ultimately favors hMSCs undergoing osteogenesis (but not adipogenesis) in soft microniche. Moreover, we also demonstrate that the viscoelastic behavior of soft microniche can be guided by temperature through a nonlinear model. These findings highlight the central roles of the dynamic relationship between the biomechanical signals and mechanosensitive transcriptional regulators in the cellular mechanosensing.

DOI: 10.1002/ ((please add manuscript number))
Article type: Full Paper

Dynamic Mechanics-modulated Hydrogels to Regulate the Differentiation of Stem-cell Spheroids in Soft Microniches and Modeling of the Nonlinear Behavior

*Jianguang Zhang *, Hua Yang, Bilen Emek Abali, Mingjun Li, Yi Xia, and Rainer Haag **

J.G.Zhang, M. Li, Y. Xia, Prof. R. Haag

Institut für Chemie und Biochemie, Freie Universität Berlin, Takustr. 3, 14195 Berlin, Germany

H. Yang, Dr. B E. Abali

Institute of Mechanics, Chair of Continuum Mechanics and Constitutive Theory, Technische Universität Berlin, Einsteinufer 5, 10587, Berlin, Germany

E-Mail: jgz720@zedat.fu-berlin.de, haag@chemie.fu-berlin.de

Keywords
soft microniches, stiffness-cyclable hydrogels, stem cell spheroids, FAK signaling, lamin A/C

ABSTRACT: Although mechanisms of how physical forces convert into biochemical signals are increasingly understood, it is still unknown how soft cues guide cell behavior. Herein, we show that the commitment and differentiation of encapsulating hMSC spheroids in thermosensitive three-dimensional (3D) hydrogels are simply altered by interpenetrating poly (NIPAM-HEMA) nanogel to gelatin methacryloyl (GelMA) network. This cell-laden hydrogel provides dynamic mechanics with covalent crosslinking coordinated reversibly physical network, which can regulate hMSCs *in situ* by reversible stiffening soft niches via multicyclic temperature changes from 25 to 37 ºC. The spreading of hMSC spheroids in the hydrogel is strongly dependent on myosin-dependent traction stress with dynamic mechanical stimuli through focal adhesion kinase

(FAK) signaling. Notably, the dynamic microenvironment gradually influences the expression and the distribution from the basal to apical side of nuclear lamin A/C and increases the Yes-associated protein (YAP) nuclear localization with cycles, which ultimately favors hMSCs undergoing osteogenesis (but not adipogenesis) in soft microniche. Moreover, we also demonstrate that the viscoelastic behavior of soft microniche can be guided by temperature through a nonlinear model. These findings highlight the central roles of the dynamic relationship between the biomechanical signals and mechanosensitive transcriptional regulators in the cellular mechanosensing.

1. Introduction

Although only a few stem cell-based therapies are currently available to patients, stem cells possess tremendous properties to form mature cell types and even miniature organoids in the laboratory.[1] Human mesenchymal stem cells (hMSCs) are attractive candidates for tissue engineering, which can be potentially applied for bone, cartilage, fat, and tendon regeneration.[2] *In vivo*, most cells are organized in tissues where they are interconnected with other cells and continuously subjected to mechanical forces including shear, compressive, and extensional forces.[3] The homeostasis of tissues is ensured by the ability of cells to exploit traction forces to sense the physical characteristics of their microenvironment.[4] Stem cells reside *in vivo* in a complex and specialized microenvironment. It is well established that the behavior of hMSCs is strongly affected by the mechanics of the extracellular matrix (ECM), such as cell adhesion, migration, polarization, and differentiation, as well as organelle organization and trafficking inside the cytoplasm.[5, 6] The mechanical interactions between the ECM-cell and cell-cell junctions play a key role in transmitting forces to cells in *in vivo* microenvironment, which can further regulate intracellular signaling pathways.[7-10] At the cellular scale, the pericellular response can be viscoelastic, roughness, or surface energy as well as stiffness.[11-14] Most of the known cues on

cell physiology have been almost exclusively using static biomaterials. However, natural ECM also exhibits dynamic interactions between the ECM mechanics and cell behavior, i.e., the ECM remodeling during disease, aging, and regeneration, which exhibit sequential stiffening or softening over time and the cell niches also impart dynamic cues to regulate organ function.[15-17] Thus, to probe the effects of dynamic manners on stem cell fate is becoming particularly important in cell biology and the tissue-engineering field.

Recently, we have noted that an increasing number of *in vitro* studies have established dynamic cues to regulate stem cells on two-dimensional (2D) systems.[18-20] However, the 2D nature of the culture system limits its further application to mimic a 3D physiological condition. hMSCs cultured as 3D multicellular spheroids were known to maintain cell-cell contacts and increase differentiation into various cells.[21] Furthermore, hMSC spheroids can be stimulated to transmigrate from the microniche in response to injury and to differentiate on engraftment.[22] Studies of cell behaviors on soft substrates have employed 2D systems coated with ECM components, which can act as adhesive anchors.[23, 24] Surface energy and phosphatidylinositol-mediated signals have been demonstrated to promote cell spreading and focal adhesion on 2D soft substrates.[25, 26] Yet it remains largely unknown what the effect of dynamic cues on stem-cell spheroids fate is within 3D soft microniches.

Stimuli-responsive polymer materials are powerful tools to establish dynamic microenvironment. Poly(N-isopropylacrylamide) (PNIPAM) is one of the most widely studied temperature-sensitive polymers with a reversible volume that change around the lower critical solution temperature (LCST) of 32 ºC.[27, 28] GelMA is a biocompatible gelatin-based polymer that has been widely used to fabricate cell-laden 3D tissue analogs, due to the natural cell binding motifs, such as RGD, and tunable physical characteristics.[29, 30] Here, we report on a new type of PNIPAM based

nanogel-actuated-integrated responsive hydrogels, whose moduli can be *in situ* reversibly stiffened and softened. To generate stiffness-cyclable hydrogels, we perform a hybrid material system composed of photocrosslinkable gelatin methacryloyl (GelMA) hydrogels, which have been embedded in stimuli-responsive poly(N-isopropylacrylamide-*co*-2hydroxyethyl methacrylate) (P-NIPAM-HEMA) nanogels that can convert temperature into reversible mechanical deformations using dynamic cell culture systems for multicyclic changing the temperature from 25 to 37 ºC (**Figure 1**F). The nanogel-actuated hydrogels with a dynamically tunable mechanical stimulation are similar to the compressive stresses from native skeletal muscle contraction because the muscle cells mechanically contract under the influence of action potentials from motor neurons.[31] We adapt this platform to achieve soft microniche (elastic modulus < 0.5 kPa) to investigate the role of reversible dynamic mechanics on hMSC spheroids mechanosensitivity. We reveal how dynamic mechanics guide cell morphology, nuclear mechanotransduction and differentiation. We also apply computational tools to elucidate the *in-situ* relationship between nonlinear viscoelastic properties and different temperatures with cycles. The present work offers a platform to probe the complex mechanisms underlying the mechanics within soft microniche and interactions between cells and reversibly mechanical cues that occur in human bodies.

2. Results and Discussion

2.1 Preparation and characterization of gelatin methacryloyl (GelMA) and poly(NIPAM-HEMA) nanogels

The photocrosslinkable (GelMA) prepolymers can be obtained by reacting methacrylic anhydride with gelatin. ^{1}H NMR analysis confirmed that the synthesized GelMA had 70% methacryloyl modification, which was calculated from the peaks at 7.4 ppm for the aromatic amino acid residues of gelatin and the peaks at 5.3 ppm and 5.5 ppm for the double bonds of the

methacrylate groups (Figure 1A, B).[32] The poly(NIPAM-HEMA) nanogels were synthesized by emulsion polymerization (Figure 1C). Dynamic light scattering was employed to determine the size of the nanogel dispersions in PBS at 4 °C, 25 °C, and 37 °C, respectively. The hydrodynamic diameters of nanogels dramatically increased from 4 to 25 °C and decreased from 25 to 37 °C, which related to the volume phase transition temperature (VPTT) of the nanogels with approximately 27 °C (Figure 1D).[33-35] The sol-gel phase change of the nanogels was also observed, which was a solution at room temperature but changed into a soft gel at 37 °C as shown in Figure 1E. The hydrophobic interactions and electrostatic repulsions between the nanogels resulted in the formation of the hydrogel.[36] Fourier transform infrared (FTIR) spectroscopy analysis was used to identify the functional groups of the nanogel. The spectrum of the nanogels exhibited main peaks at 1645 and 1540 cm^{-1}, which represented the chemical bond for amide I and amide II of NIPAM, respectively.[35] The band around 1713 cm^{-1} was assigned to the carbonyl group of HEMA,[37] which indicated that the poly (NIPAM-HEMA) nanogels successfully formed (Figure S1, Supporting Information). The modulus-cyclable hydrogel was fabricated by introducing the thermoreversible nanogel into the GelMA to form interpenetrating networks throughout UV irradiation (10 mW cm^{-2}, 365 nm, 80 s) in the presence of lithium acylphosphinate (LAP) as a photoinitiator,[38] as shown in Table 1. The dynamic mechanics can be generated using dynamic cell culture systems for multicyclic changing temperature from 25 to 37 °C to probe stem cell spheroids respond to cyclic moduli alteration (Figure 1F).

Table 1. The composition of nanogel and GelMA in the hydrogel.

Samples	Nanogel (w/v %)	GelMA (w/v %)	Storage modulus (Pa, 25 to 40 °C)
Low stiffness (LS)	2.5	1.5	80-120
Medium stiffness (MS)	2.5	2.5	500-2500
High stiffness (HS)	2.5	3.5	800-4000

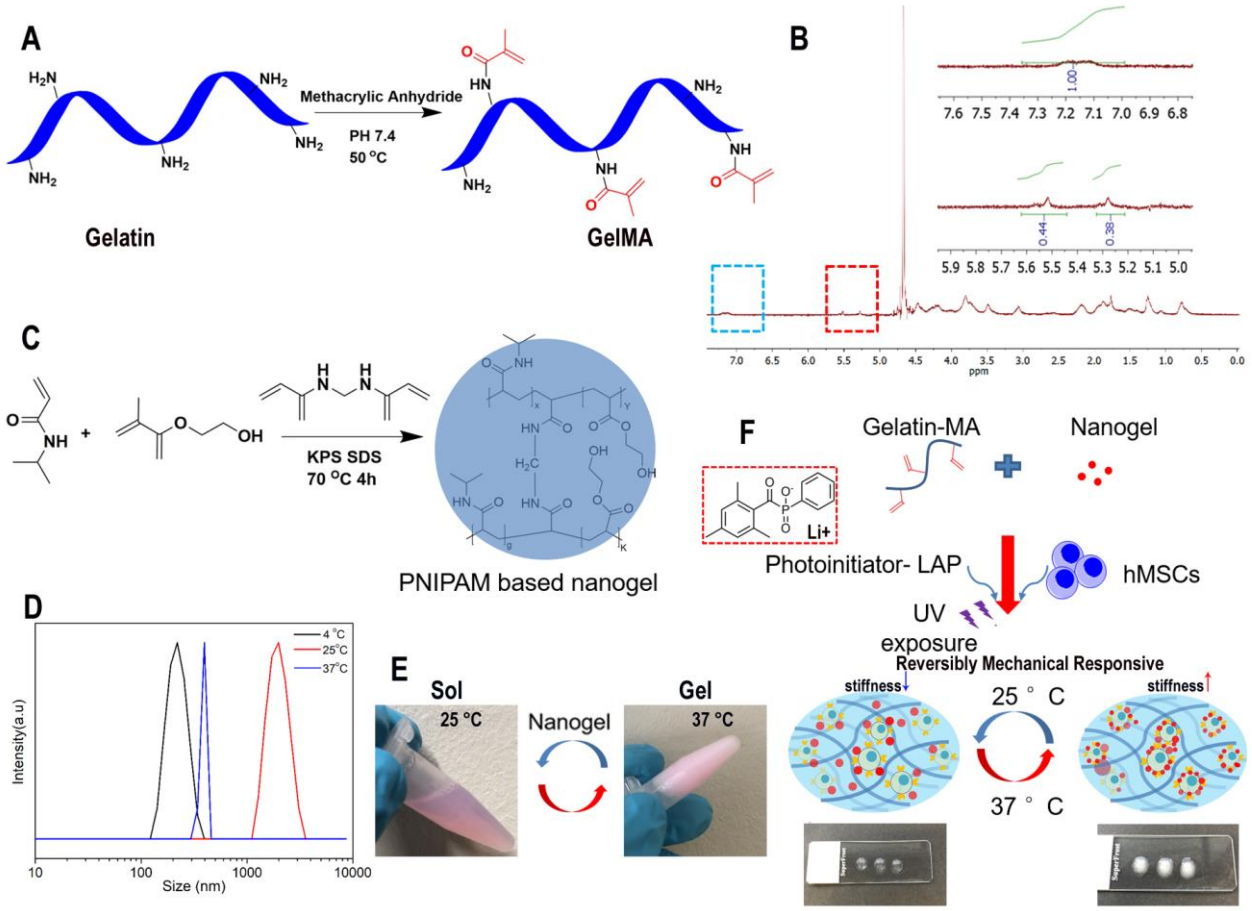

Figure 1. Synthesis and characterization of gelatin methacryloyl (GelMA) and poly (NIPAM-HEMA) nanogels. (A) Synthesis of GelMA with the binding of methacrylate groups to the primary amine groups of gelatin. (B) The ^{1}H NMR spectrum of synthesized GelMA, which can form crosslinked networks upon light exposure (400 MHz, D_2O). (C) Synthesis of poly (NIPAM-HEMA) nanogels by emulsion polymerization. (D) Temperature-dependent hydrodynamic diameter for 0.5 mg/mL poly(NIPAM-HEMA) nanogels in PBS at 4 °C, 25 °C, and 37 °C, respectively. (E) The 50 mg/mL of poly (NIPAM-HEMA) nanogels in 10× PBS reversible transfer from sol state (25 °C) to gel state (37 °C). (F) Schematic of dynamic mechanics with the covalent crosslinking-coordinated reversible physical network using light illumination (10 mW cm^{-2}, 365 nm, 80 s) with a photoinitiator (LAP, 0.5 w/v) crosslinks, and subsequent through dynamic cell culture systems for multicyclic changing temperature from 25 to 37 °C within stem cell spheroids.

The geometries of the dynamic hydrogels at different temperatures were examined by scanning electron microscopy (SEM). As shown in **Figure 2**A, the dynamic hydrogels exhibited typical microporous structures with dense walls, whereby the pore sizes decreased with the higher

concentration of the GelMA at 25 °C. The whole porous structure shrank together when the temperature was increased to 37 °C in contrast to the geometry without changes under the different temperatures for the pure GelMA (Figure S2, Supporting Information). The results revealed that the porous structure of responsive hydrogels can be triggered by VPTT. The oscillatory rheology was further conducted to characterize the nonlinear mechanical response of the dynamic hydrogels from 20 to 40 °C (Figure 2B-D and Supplementary Video S1). The storage modulus (G') revealed thermoreversible changes and the thermoresponsive stiffening effect was enhanced from 80 Pa to 120 Pa, 500 Pa to 2500 Pa, and 800 Pa to 4000 Pa for LS, MS and HS hydrogels, respectively. In contrast, there was no stiffening effect for the pure GelMA (Figure S3, Supporting Information). The moduli cyclability can be achieved by multicyclic changing temperature from 25 to 37 ºC. Furthermore, frequency sweep tests showed that G' at 37 °C was always larger than that at 25 °C under the measured frequency range (0.1-1 Hz), which indicated a more rigid behavior for the hydrogels at 37 °C (Figure 2E-G). The structural changes observed in the SEM images were consistent with the temperature-induced stiffness changes. Taken together, our data reflected the dynamic changes including morphologies and network moduli, which could provide a 3D dynamically intercellular elements for studying hMSC spheroids behavior.

We further investigated live/dead assays to examine cytocompatibility of the encapsulated hMSCs in the hydrogels under the dynamic culture system (multicyclic changing temperature from 25 to 37 ºC) and static culture (constant at 37 ºC). The live/dead assay (calcein AM/ethidium homodimer-1) was performed after 1 day and 7 days in growth media for all the gels. After 1 day, the stem cell spheroids in different stiffness hydrogels showed excellent viability post-encapsulation under both static and dynamic culture conditions, respectively. After 7 days, the cells remained more than 90% viable in LS hydrogels, and a significant fraction of the

cells had spread with the dynamic culture condition. In contrast, cell viability decreased to 81.6% ± 1.3% and 80.9% ± 1.2% for MS and HS hydrogels, and most cells remained rounded under the static culture conditions, respectively, confirming the cytocompatibility of the photocrosslinking reaction as determined by the CCK-8 assay (**Figure 3**). Moreover, low-dose 365 nm light exposure and dynamic culture condition have a lower influence on cell proliferation (Figure S4, Supporting Information). Our results demonstrated that cells cultured between "stiff" and "soft" material for MS and HS hydrogels were better maintained cell viability and permitted cell spreading, respectively.

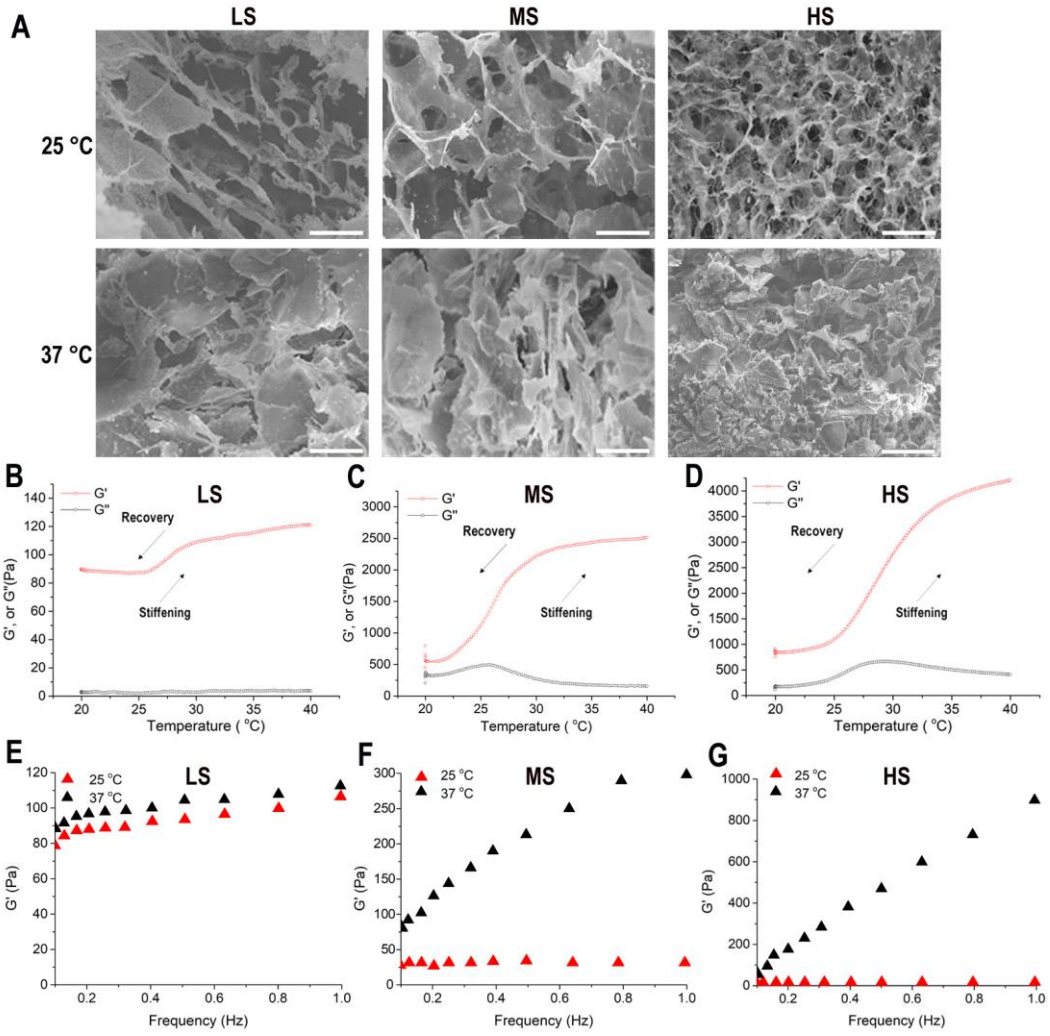

Figure 2. Temperature-dependent geometry and mechanical properties of poly(NIPAM-HEMA) nanogels interpenetrating with GelMA networks. (A) Typical SEM images of the lyophilized hydrogel network at 25 and 37 °C, respectively. Scale bar: 25 μm. (B-D) Storage modulus (G′) and loss modulus (G″) as a function of temperature for dynamic changes for LS, MS and HS hydrogels from 20 and 40 °C, respectively (1 Hz, 0.1% strain). (E-G) The representative frequency sweep spectrum after equilibrium of G′ for LS, MS and HS hydrogels at 25 and 37 °C, respectively.

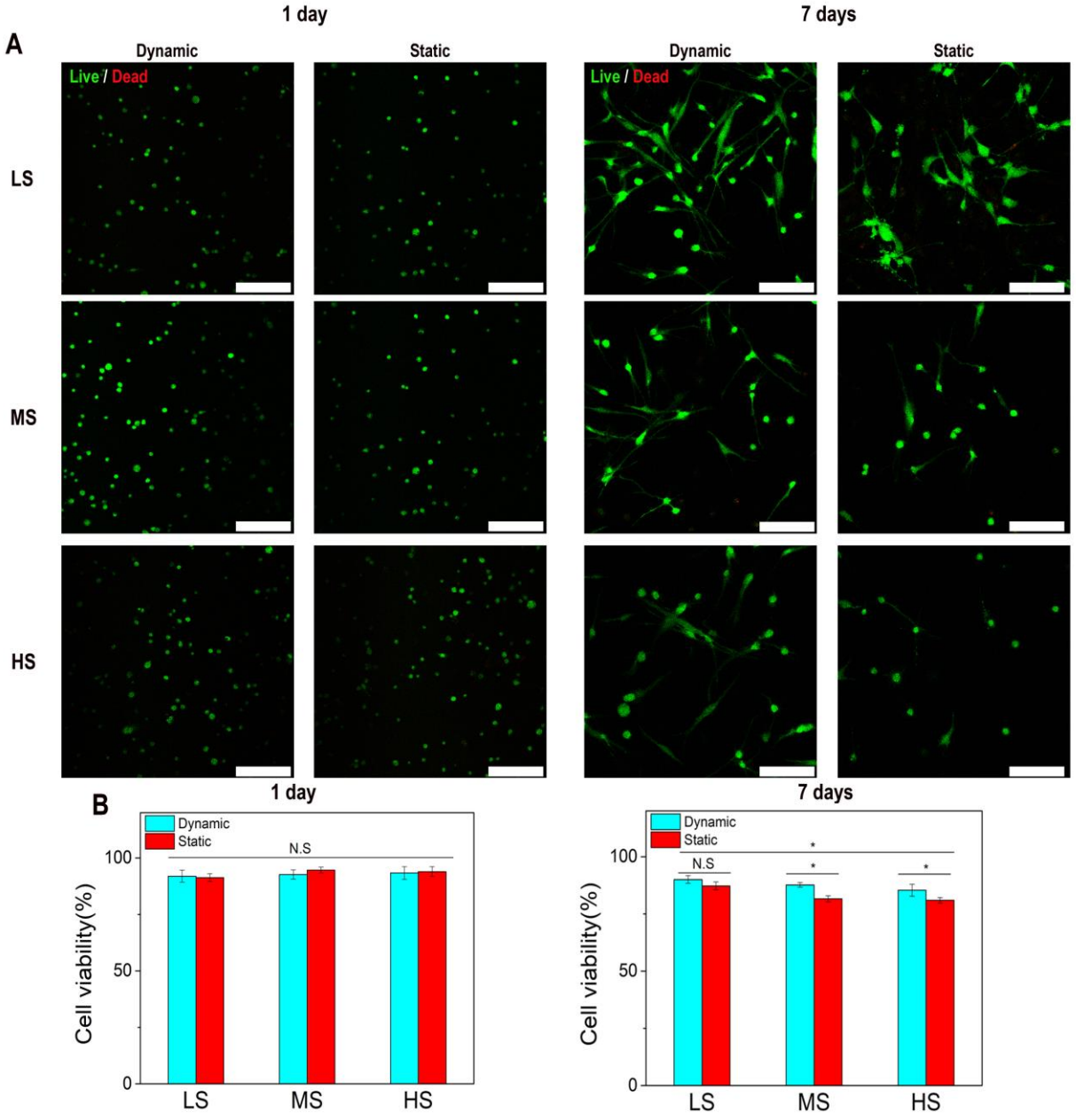

Figure 3. Viability and metabolic activity of hMSCs encapsulated in the dynamic hydrogels. (A) Live/dead staining of hMSC spheroids in the dynamic hydrogels after 1 day and 7 days under the

static and dynamic culture conditions. Calcein-AM/ethidium homodimer staining for living (green) and dead (red) cells, respectively. Scale bar: 250 μm. (B) CCK-8 assay of hMSC spheroids viability after 1 day and 7 days in the dynamic hydrogels under the static and dynamic culture conditions. N.S, not significant; * $p < 0.05$.

2.2 Focal adhesion mechanosensing for interaction with hMSC spheroids in dynamic hydrogels

Extracellular matrix stiffness sensing of the cells activates a cascade of biochemical signals, which can regulate cytoskeleton rearrangements and focal adhesion formation.[39, 40] Focal adhesions (FAs) at the cell-ECM interface play a crucial role in cell spreading, motility, and differentiation through the focal adhesion kinase (FAK) signaling pathway.[41-43] To further evaluate cell spheroids-ECM interactions during the response to cyclic mechanical stimuli, hMSCs were encapsulated in the dynamic hydrogels for 3 days under the static and dynamic culture conditions, respectively (Supplementary Video S2). Representative immunofluorescence of FAs protein vinculin showed that the FAs' size markedly increased in dynamic culture conditions. In addition, cell spheroids subjected to the dynamic culture condition exhibited a gradual change of shape with highly spread and elongated morphologies compared with those in static conditions (**Figure 4**A and Figure S5 Supporting Information). Furthermore, correlative analysis of the total FA area per cell spheroids showed that the FAs in the dynamic culture conditions were larger than those in the static conditions (Figure 4B), suggesting that the dynamic matrix could provide more anchoring opportunities for FAs to facilitate cell motility and adhesion, especially in soft matrices. The shape and the size of the cell during the cycle are not only dependent on its growth but also on cell-cell and cell-matrix forces.[9, 42] Thus, we used fractal analysis to quantify cytoskeletal density changes under the dynamic culture condition.[44] The cytoskeleton arrangement was assigned a fractal dimension (D_f), as shown in Figure 4A. By looking into the cytoskeleton distribution of whole cell spheroids, the D_f values under the

dynamic culture conditions were significantly higher than those under the static conditions (Figure 4C). Inhibition of FAK phosphorylation, which was a robust regulator to regulate the response to mechanical signals,[45] we treated cells with FAK inhibitor-14. The cells displayed a rounded phenotype on both soft and stiff hydrogels under the dynamic culture conditions (Figure S6A, Supporting Information). Furthermore, no significant differences were observed in total FA per cell spheroids and fractal dimension (Figure S6B-C Supporting Information). Altogether, our data supported that the cell spheroids in the soft matrix could easily favor the formation of mature FAs and cytoskeleton rearrangement, which enhanced the cell-ECM adhesion and cell spreading under dynamic culture conditions. The cyclic mechanical stimuli may act as a potential direct signaling role for FAK in cell-matrix interactions.

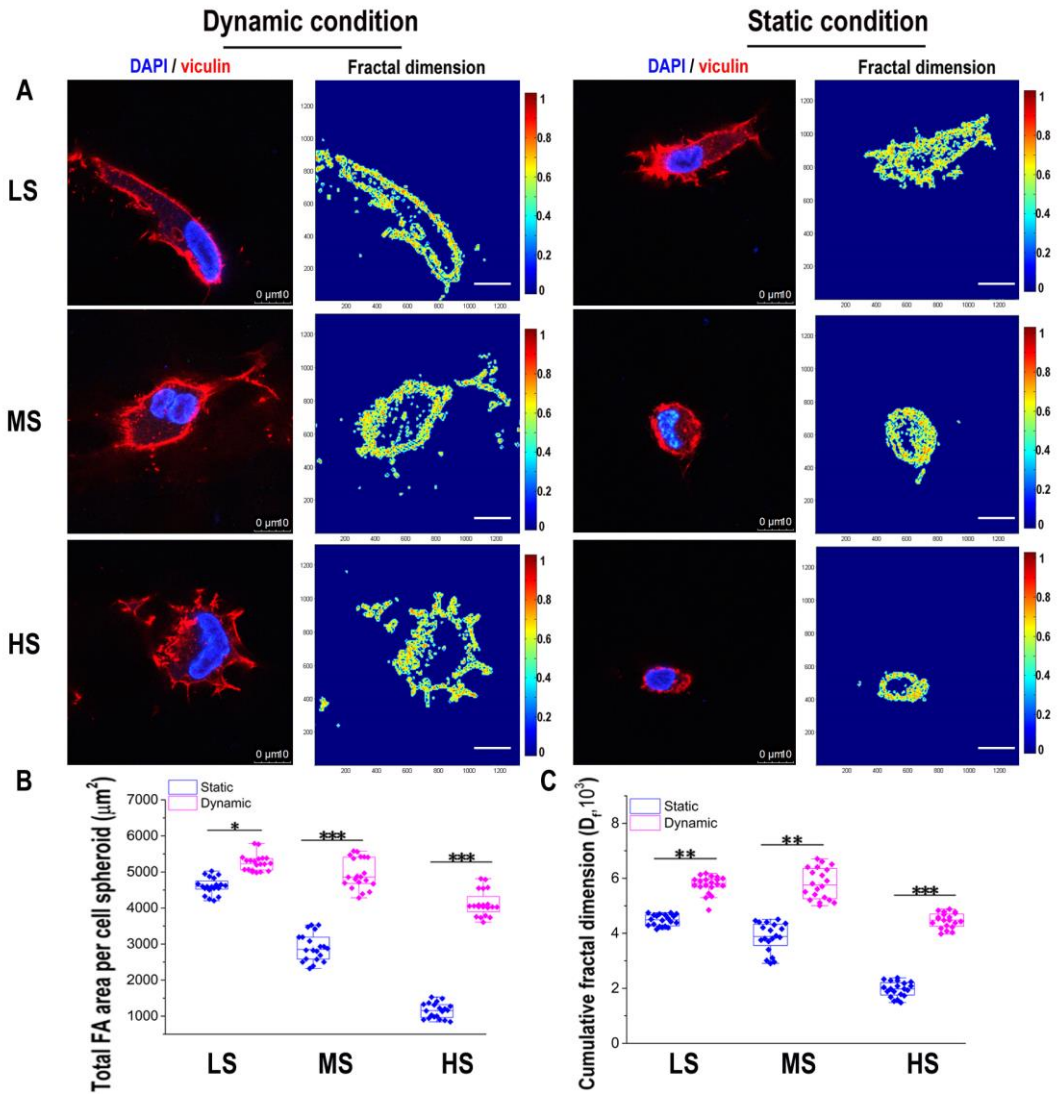

Figure 4. Dynamic hydrogels regulate integrin-mediated cell spheroids adhesion. (A) Representative immunofluorescence images of the hMSC spheroids DAPI (blue), vinculin (red) and the results of corresponding 2D fractal dimension (D_f) under the static and dynamic culture conditions for 3 days, respectively. Scale bar: 10 μm. (B and C) Quantitative analysis of the total FA area per cell spheroids and D_f value in each spheroid region of interest (n= 20 spheroids per each condition from 3 independent experiments). * $p < 0.05$, ** $p < 0.01$ and *** for $p < 0.001$.

2.3 Soft microniches influence intracellular biological signals, and differentiation of hMSC spheroids under the dynamic culture conditions

According to previous studies,[18, 19] the cytoskeletal tension would lead to activation of the subcellular transcriptional coactivator Yes-associated protein (YAP), which can gauge

mechanical stimulation into the genetic signaling pathway and eventually guide the hMSCs' differentiation.[46, 47] Using our dynamic hydrogels, we hypothesized that the cellular activation in response to the dynamic mechanical microenvironment may also exist for cell spheroids in the 3D microenvironment. Thus, we investigated the role of the YAP location during static and dynamic culture conditions. The immunofluorescence staining of YAP in hMSC spheroids revealed distinct intracellular localization; YAP was located in the cytoplasm (deactivated state) of hMSC spheroids with 4 days of static culture in LS hydrogels. In contrast, YAP was primarily in the cytoplasm and gradually changed into the nucleus (activated state) as the number of cycles (from 5 to 20) under the dynamic culture conditions (**Figure 5**A). Moreover, the YAP nuclear translocation was faster and persisted in the nuclei after 10 cycles than that under the static condition for MS and HS hydrogels, respectively **(**Figure 5B, C). In control experiments, YAP was located in the nucleus of the hMSCs when cultured on the tissue culture plates (TCPS) under both culture conditions (Figure S7, Supporting Information). To further understand the mechanism by cyclic mechanical stimuli to stem cell spheroids, the cell encapsulated in LS hydrogels under the dynamic culture condition were treated with (10μM) Y27632, an inhibitor of the RhoA-associated protein kinase (ROCK), which induced non-muscle myosin II-mediated contractility and actin filament levels.[48, 49] As previously shown,[50] YAP translocation was also inhibited upon Y27632 daily during the 20 cycles within growth-media incubation for both hydrogels under the dynamic culture condition (Figure 5A, D and Figure S8, Supporting Information). Correspondingly, the expression of YAP under the dynamic culture conditions was significantly higher than that cultured under the static conditions for 4 days (Figure 5E). Furthermore, we visualized the confocal images of cell cytoskeleton by immunostaining. In the static condition, the hMSCs retained a rounded shape with higher circularity. However, the hMSC spheroids' shape exhibited visible trailing migrating with elongated phenotypes for LS,

MS and HS hydrogels, respectively, and the cell spreading area also dramatically increased under the dynamic culture conditions as opposed to rounded cells under the static conditions (Figure 5F and Figure S9, Supporting Information). Together, these data supported the positive correlation between the extent of YAP activation and dynamic hydrogels with cycles. The dynamic mechanical stimuli can mediate hMSC spheroids' behavior by enhancing myosin activity.

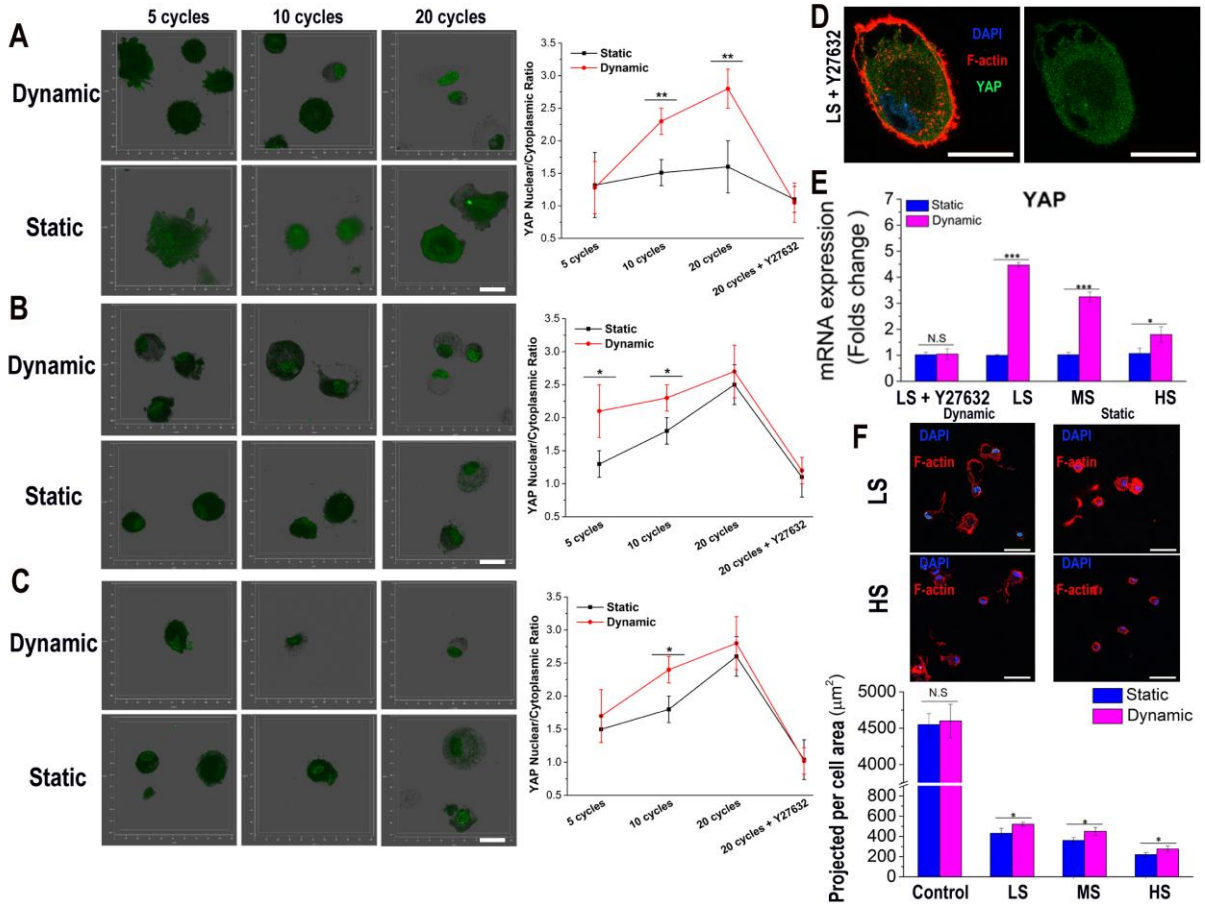

Figure 5. The role of cyclic mechanical loading on YAP activation. (A-C) Confocal 3D reconstructions and quantification of YAP nuclear: cytoplasmic intensity ratio after 5, 10, 20 cycles for LS, MS and HS hydrogel in the presence of a ROCK inhibitor, Y-27632, respectively. YAP (green); Scale bars: 20 μm. n= 100 spheroids per each condition. (D) Immunostaining of hMSC spheroids for F-actin (red), YAP (green) and cell nucleus (DAPI, blue) within LS hydrogels following 20 cycles dynamic culture in growth media with 10 μM Y27632 treatment. Scale bars: 25 μm. (E) Quantitative analysis of the YAP nucleus localization and gene expression level for 4 days under both culture conditions. The expression of target gene normalized by GAPDH and static culture conditions. (F) Immunostaining and quantitative analysis of hMSC spheroids per cell spreading area within LS and HS hydrogels following 4 d growth-media under the static and dynamic incubation. F-actin, red; DAPI, blue. Scale bars: 50 μm. n= 200 spheroids

per each condition. The cells seeded on the TCPS were used as controls. N.S, not significant; * $p < 0.05$, ** $p < 0.01$ and *** $p < 0.001$ for significant difference.

Furthermore, nuclear lamin A/C played central roles at the intersection between cytoplasmic signaling and nuclear events, which was located under the inner nuclear envelope and linked to numerous human diseases.[51, 52] Emerging evidence indicated that external mechanical forces also trigger changes in nuclear envelope structure and gene expression.[53, 54] To address how multicyclic mechanical stimuli altered the structural organization of the nuclear envelope, we encapsulated stem cell to LS hydrogels with defined reversibly mechanical loading to manipulate the compressive forces under the dynamic culture conditions. We found that the lamin A/C-dependent distinct evolution of nuclear morphology in response to the multicyclic mechanical loading, as shown in **Figure 6**A and Figure S10. 3D-reconstructed yz-confocal cross-sections of the lamin A/C immunostained nuclei clearly showed that the basal-to-apical intensity ratios gradually decreased with the cycles during cell spreading. In contrast, the lamin A/C stained both sides equally well under the static conditions (Figure 6B, C), which was consistent with previous studies performed using a 2D cell culture.[55, 56] As nuclear morphology projected to the xy-confocal cross-sections showed an elongated nuclear shape and an enlarged nuclear area (Figure 6D, E). Moreover, the expression levels of lamin A/C also increased within LS hydrogels by cyclic mechanical loading under the dynamic culture system (Figure 6F). Together, these results demonstrated that the cyclic mechanical stimuli modulated not only the global cell orientation by FAK signaling, but also elucidated the 3D-nuclear deformation by suggesting an important role of the lamin A/C in response to cellular mechanotransduction with cycles in soft microniches.

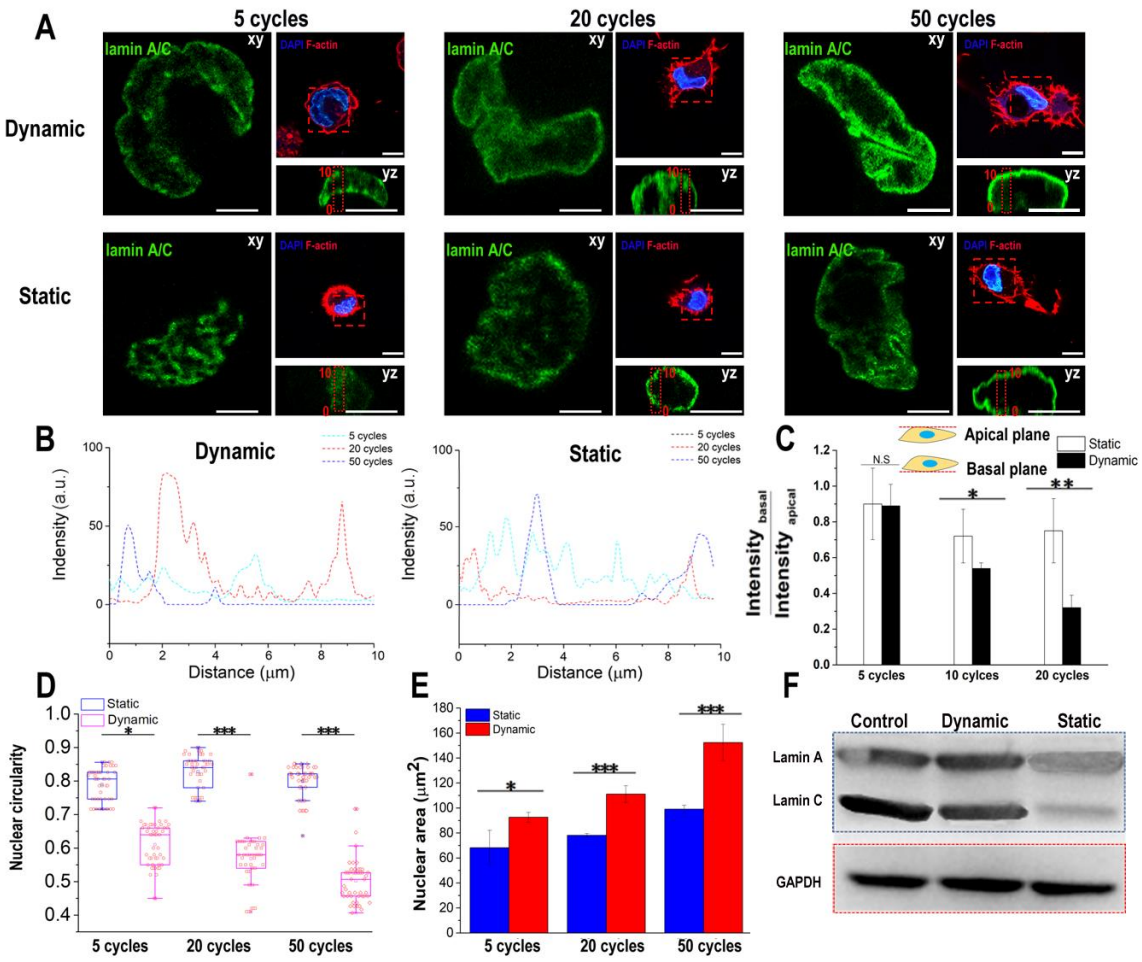

Figure 6. Lamin A/C-dependent differential formation of nuclear deformation in response to cyclic mechanical loading on stem-cell spheroids in the 3D microenvironment. (A) Representative immunofluorescence staining for nuclear morphology of lamin A/C. Insets display details of F-actin and nucleus in the apical region. Nuclear yz-confocal cross-sections (bottom right) and (B) respective intensity distribution profiles along the z-axis from the boxed-in nuclear region (red rectangle) for stem-cell spheroids (C) Average basal-to-apical peak intensity ratios of lamin A/C as a function of cycles for spheroids in LS hydrogels. (D-E) Quantification of nuclear circularity and nuclear area after 5, 20, 50 cycles in LS hydrogels under the static and dynamic culture conditions, respectively. (F) Lamin A/C expression level of hMSC spheroids under static and dynamic culture conditions (50 cycles) within LS hydrogels by Western blots. The cells seeded on the TCPS were used as controls. Experiments were performed in six replicates per condition, and $n > 30$ spheroids were examined per condition from 3 independent experiments. N.S, not significant; * $p < 0.05$, ** $p < 0.01$ and *** $p < 0.001$ for significant difference.

It was reported that hMSCs on the stiff surface favored osteogenesis but on the soft surface they favored adipogenesis with static matrices.[57, 58] Furthermore, there was a systematic relationship between the nuclear lamin A/C and differentiation of hMSCs.[59] To test the functional role of dynamic mechanics' changes in controlling cell differentiation, we further investigated the encapsulated hMSC spheroids after 7 days of culture in the bipotential differentiation medium (1:1 v/v osteogenic and adipogenic media) under static and dynamic culture conditions. Consistent with previous studies,[60] the predominant adipogenesis for cells in the soft gels, which were observed in LS hydrogels under the static condition. Immunofluorescent staining of the osteogenesis biomarker RUNX2 and adipogenic biomarker PPARɣ demonstrated that osteogenesis was progressively favored over adipogenesis under dynamic culture conditions for LS and MS hydrogels, respectively (**Figure 7**A, B). Differentiation became increasingly biased towards osteogenesis within HS hydrogels under the dynamic culture conditions as well as hMSCs cultured on the TCPS under both culture conditions (Figure 7C and Figure S11, Supporting Information). The hMSC spheroids were also stained with alkaline phosphatase (ALP), a standard marker for differentiated osteoblasts and Oil Red O for lipid droplets, an indicator of the degree of adipogenesis, respectively. A substantial amount of lipid droplets formed in LS hydrogels under the static conditions. Compared to this observation, the lipid droplets decreased and a positive staining area for ALP exhibited for LS hydrogels under the dynamic culture conditions. The similar trends were also observed for MS and HS hydrogels under both culture conditions, respectively, as well as determined from the mean percentages of the osteogenic and adipogenic commitments (Figure 7A-C). Finally, the hMSC spheroids' osteogenic commitments were verified by analyzing the expression of the RUNX2 and PPARɣ via RT-qPCR, respectively. As shown in Figure 7D-E, it observed an increase in the RUNX2 gene expression under the dynamic culture conditions in agreement with the immunofluorescence,

ALP staining, and further confirmed by the decrease in PPARɣ gene expression. Furthermore, hMSC spheroids are very important for target-injured tissues with transmigration and stimulated local angiogenesis by secretion of cytokines.[22] Vascular endothelial growth factor (VEGF) and fibroblast growth factor (FGF) played a major role for endothelial cell proliferation.[61] The mRNA expression of an angiogenic biomarker of VEGF and FGF was also significantly enhanced under the dynamic culture conditions (Figure 7F-G). Collectively, these data demonstrated that dynamic mechanically modulated hydrogels are an effective strategy to guide the fate and enhance the angiogenesis potential of hMSC spheroids. Furthermore, we also highlighted the complex relationship between the YAP and lamin A/C for osteogenic differentiation in soft microniches with multiple mechanoresponsive elements simultaneously.

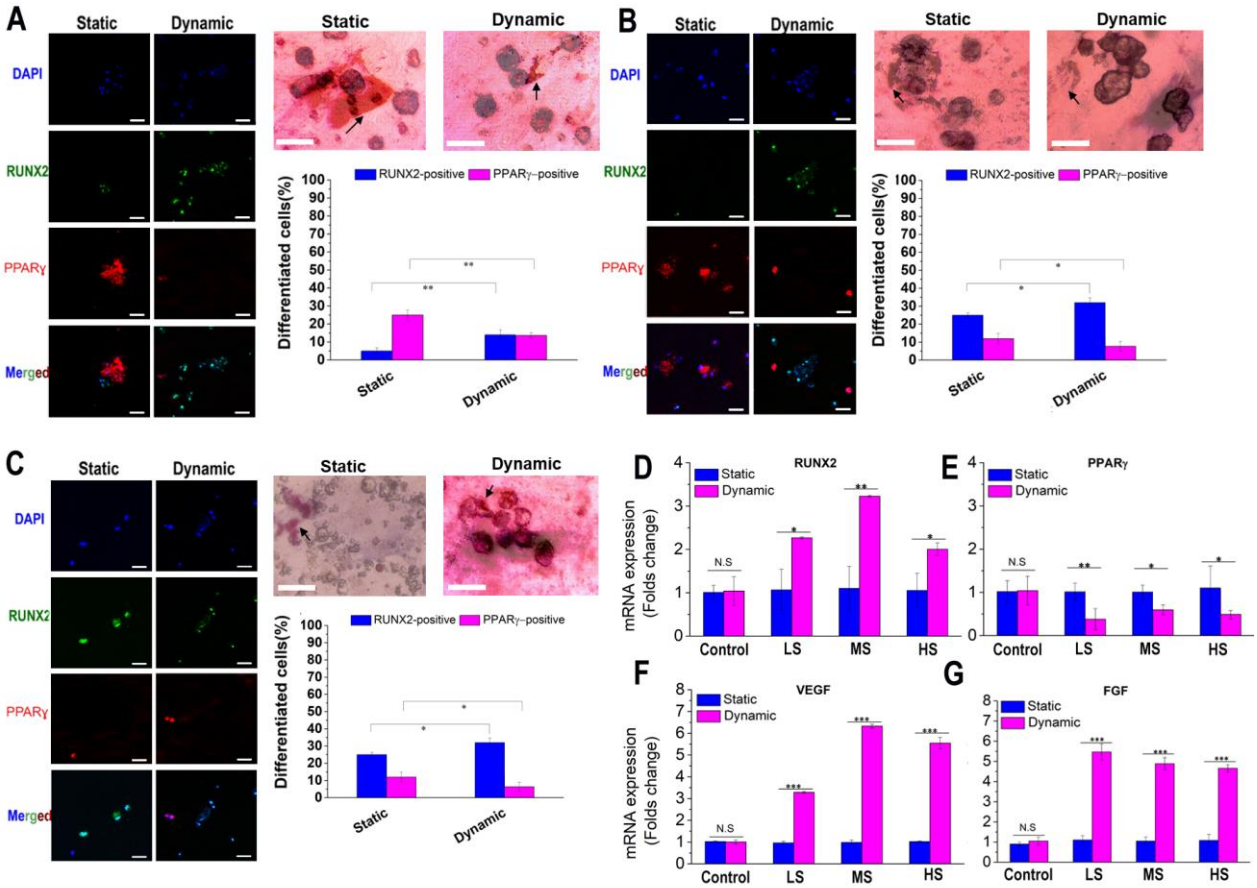

Figure 7. Influence of dynamic modulus on the differentiation of hMSC spheroids during the 3D culture after 7 d. (A-C) Representative immunofluorescence images of the hMSC spheroids in the bipotential differentiation medium for the osteogenesis biomarker RUNX2 (green) and adipogenic biomarker PPARɣ (red) DAPI, blue (left); representative images of alkaline phosphatase (osteogenesis) and oil-droplet (blank arrows) staining of hMSC spheroids (right top); quantification of the percentage of the RUNX2-positive and PPARɣ-positive cells under the static and dynamic culture conditions (right below) for LS, MS, and HS hydrogels, respectively. Scale bars: 50 μm. (D) Expression of osteogenesis biomarker RUNX2, (E) adipogenic biomarker PPARɣ and the angiogenic biomarkers of VEGF (F) and FGF (G) for hMSC spheroids under the static and dynamic culture conditions. The expression of target genes normalized by GAPDH and static culture conditions. Experiments were performed in three replicates per condition and n = 40 cells were examined per condition from 3 independent experiments. The cells seeded on TCPS were used as controls. N.S, not significant; * $p < 0.05$, ** $p < 0.01$ and *** for $p < 0.001$.

2.4 Modeling the nonlinear viscoelastic material response of soft microniches

Recent studies have shown that substrate viscoelasticity can significantly affect the behavior and function of cells.[5, 12, 62] In order to mimic the mechanical response of the created soft microniche, we have determined the nonlinear viscoelastic characteristics based on oscillatory rheometer experiments of LS hydrogels for a range of temperatures between 25-40 °C by using the energy-based method.[63, 64] For a better understanding of the capability of this nonlinear viscoelastic material model, we solved two cases, where a harmonic (sinusoidal) strain with amplitudes of 1% and 10% caused stresses computed from the material model with the obtained parameters as shown in Table 2. As shown in **Figure 8**A, the response was exhibited in Lissajous-Bowditch curves for two different amplitudes of 1% (left) and 10% (right), respectively. The effect of the temperature was obvious in twofold: first, the slope changed that signalizes a stiffening of the material; second, the dissipation measured as the area within the hysteresis curve, which increased denoting a more viscous response in higher temperatures. Both changes were seen from the parameters affecting the equation linearly, c_1 was responsible for the stiffening effect, whereas c_3 directly influenced the viscosity. In order to observe the consequences of nonlinear parameters, we introduced the significant response changes of c_2 and c_4 in different amplitudes.

The viscous character in large displacements was significant different with that in relatively small displacement, especially for T = 40 °C (Figure 8A).

Table 2: Material parameters obtained by the energy-based method for the model. The relation between stress, strain, and strain rate is $\boldsymbol{\sigma} = (c_1 + c_2 II_{\varepsilon})\boldsymbol{\varepsilon} + (c_3 + c_4 II_{\dot{\varepsilon}})\dot{\boldsymbol{\varepsilon}}$

T in °C	c_1 in Pa	c_2 in Pa	c_3 in Pa s	c_4 in Pa s^3
25	202	-224	1.95	0.21
30	279	-1174	1.25	-0.08
35	359	-1165	3.25	-0.57
37	382	446	3.98	2.31
40	395	-1790	2.40	3.85

We emphasized that the nonlinear viscous effect was of paramount importance in case of investigating the dynamics at the cell level leading to an effective change in transport or diffusion phenomena. With increased temperature, viscosity changes altered the overall reaction force that hMSC spheroids can sense and manipulate the spreading area for soft microniches under dynamic culture conditions. In comparison, the viscosity was a negligible effect on the hMSC spheroids' spreading for a higher stiffness matrix under the static culture conditions as the viscous character was mostly suppressed for very slow processes. Herein, we demonstrated that the nonlinear mechanical response induced a significant change in viscous behavior even in 1 Hz cyclic loading, which may help the FAs extend their lifetime as the hMSC spheroids can gradually sense the relaxation in mechanical response. Figure 8B briefly summarize our previous key finding illustrated by a schematic diagram when hMSC spheroids grow in the dynamic hydrogels. The cell spheroids in the soft microniches can enhance the maturation of FA complexes and the rate of F-actin polymerization under the dynamic culture conditions. Moreover, cellular response to the stiffness led to downstream up-regulation of the biochemical signal YAP into the nucleus,

increased the expression of lamin A/C, and ultimately switched from adipogenesis to osteogenesis simply by dynamic culturing. Altogether, our results demonstrated the local stiffness and viscosity could exert a synergistic effect for hMSC spheroids differentiation in soft microniches under dynamic culture conditions.

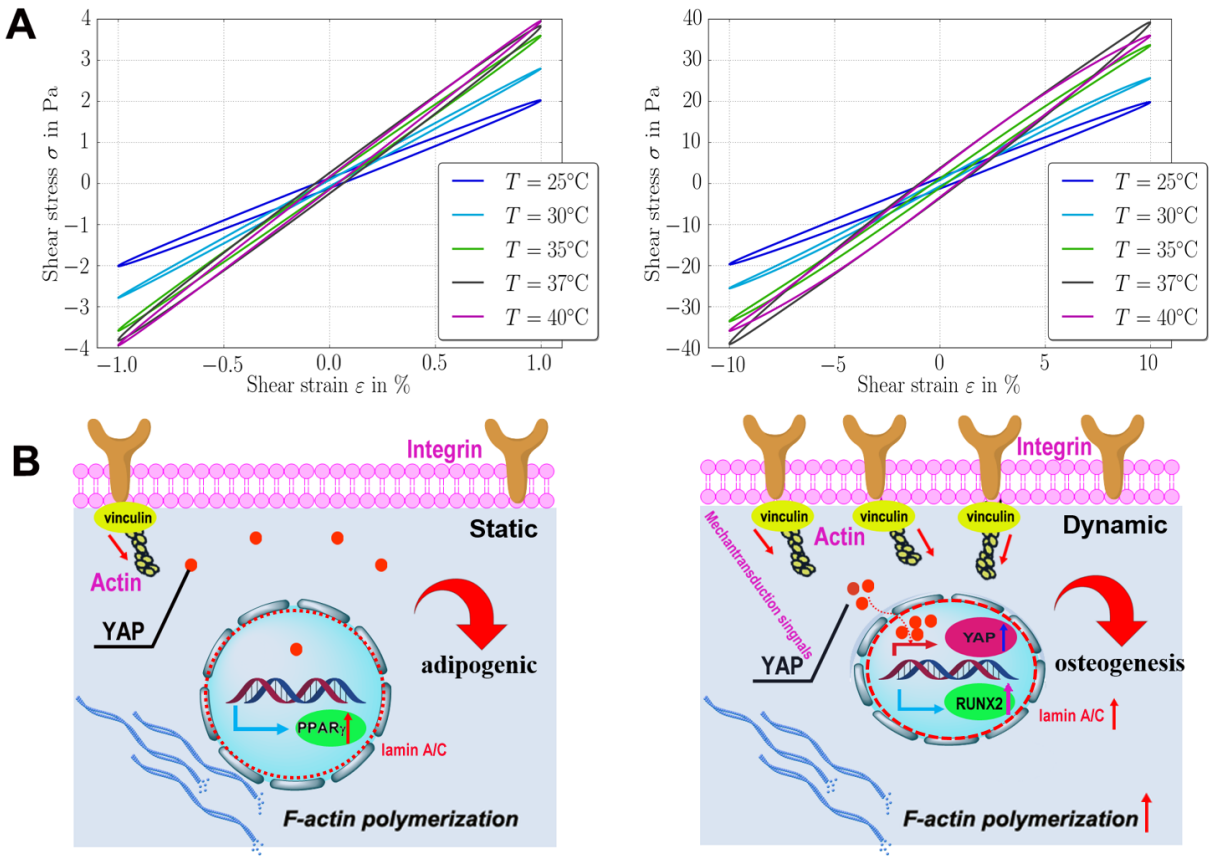

Figure 8. Influence of dynamic local stiffness and viscosity of soft microniches to direct stem cell fate (A) Stress-strain response of the proposed material model at two large strain amplitudes. (B) Schematic illustration of the potential mechanism underlying the synergistic effect of the local stiffness and viscosity to guide the differentiation of stem cell spheroids under the dynamic culture conditions.

3. Conclusion

In summary, we present a new tool for studying how reversible dynamic mechanics direct the hMSC spheroids' shape and FAs via a covalent crosslink-coordinated, physically reversible multicyclic network from 25 °C to 37 °C. The dynamic hydrogel provides an effective means to

drive the hMSC spheroids' spreading and downstream signaling-related cell fate under the dynamic culture conditions. Our study also shows how soft microniches can dramatically affect the osteogenic phenotype of the cell, which cannot be attributed to the well-known stiffness effect. Furthermore, the present study also reveals new insight into the synergistic effect of local stiffness and viscosity that regulate the response of hMSC spheroids to the surrounding microniche. This strategy for a mechanics-modulated hydrogel in a multicycle-dependent manner can be potentially to improve our understanding the role of dynamically mechanoresponsive elements in guiding stem cell fate for cell therapeutics and regenerative medicine.

4. Experimental Section

Materials: N-isopropylacrylamide (NIPAM, Sigma-Aldrich, 99%) was recrystallized three times from n-hexane and dried under vacuum before use. Potassium persulfate (KPS, Sigma-Aldrich, 99%), sodium dodecyl sulfate (SDS, Sigma-Aldrich, 98.5%), N, N-methylene bis(acrylamide) (MBA, Sigma-Aldrich, 98%), and 2-hydroxyethyl methacrylate (HEMA, Alfa Aesar, 97%) were also used.

Synthesis of poly (NIPAM-HEMA) nanogels: Poly(NIPAM-HEMA) nanogels were synthesized via free radical emulsion polymerization. Briefly, NIPAM (1.1203 g, 9.9 mmol), HEMA (50 µL, 0.1 mmol), MBA (31 mg, 0.2 mmol), and SDS (57.9 mg, 0.2mmol) were mixed together in 47 mL of DI-water in a 100 mL Schlenk flask with continuous stirring, and the system was degassed for 30 min. After degassing, the reaction system was injected 3 mL of KPS aqueous solution (27 mg, 0.1 mmol) and sealed to start the polymerization at 70 °C under the argon protection for 4 h with mechanical stirring. The product of poly (NIPAM-HEMA) nanogels was dialyzed against Milli-Q water using 12-14 kDa molecular weight cutoff tubing for 7 days with a daily water change. After purification, the nanogels were concentrated by heating at 60 °C, and 200 µL of nanogels dispersion was dried to calculate the concentration.

Encapsulation of human mesenchymal stem cells (hMSCs): hMSCs (purchased from Lonza) were cultured in basal media (high-glucose Dulbecco's Modified Eagles Medium (DMEM) containing 10% fetal bovine serum (FBS) and 1% penicillin/streptomycin) and expanded to in between passage 3 and 5 before use. For the encapsulation of cells in the gels, the cell pellets were obtained by centrifugation. The 4×10^6 cells/mL in culture media were then mixed with the cold (~10 °C) GelMA (dissolved in 10 × PBS with LAP 0.3% (w/v)) and poly (NIPAM-HEMA) nanogels (50 mg/mL) liquid in a ratio of 1:1:2 (Table 1). 1×10^5 hMSCs were cultured in 100 µL of hydrogels or on the TCPS on the 96-well plate. The solution was exposed to 365 nm UV (10 mW cm^{-1}) for 80 s. Afterward, it was transferred to the 37 °C incubator containing 5% CO_2 for gelation to occur. After 6 h culture, the experimental system multiple cycles started from 37 °C to 25 °C for the dynamic culture. Briefly, the cells were incubated at 37 °C for 20 min and switched to 25 °C for 20 min in a labeled 1 cycle using variable temperature incubator with mK2000 series high precision temperature controller (INSTEC, USA). The rate of increase and decrease temperature was 1 °C/min. The cells were 3D cultured by using high-glucose DMEM media supplemented with 10% FBS, 1.0% penicillin/streptomycin (Gibco), and 1.0% antimitotic antimycotic (Gibco) for immunocytochemistry, viability and proliferation analysis. mRNA expression of angiogenic genes was evaluated after 7 days of cell culture. The differentiation of the gel-encapsulated hMSC spheroids was investigated after 7 days of dynamic culture conditioning with a co-induction differentiation medium (1:1 v/v osteogenic and adipogenic media, Gibco). The medium was changed every 3~4 days during the differentiation. For all the experiments, static culture conditions at 37 °C and 5% CO_2 served as a control.

Cell viability and proliferation assays: Cell viability was determined using a viability/cytotoxicity kit (Thermo Fisher) according to the manufacturer’s instructions. After 96 h of dynamic and static cultures, the culture medium was replaced with fresh medium containing 0.5 µM calcein

AM and 4.0 μM ethidium homodimer-1 for 20 min incubation. The fluorescence images were recorded using the Carl Zeiss microimaging fluorescence microscope. A cell counting kit-8 (CCK-8, Thermo Fisher) was used to measure cell proliferation according to the manufacturer's instructions. Briefly, after 24 h and 96 h dynamic and static culture, 10 μL of the CCK-8 solution was added to each well of 96-well plates, and cells were incubated at 37 °C for 4 h. The absorbance intensity of each sample was determined at a wavelength of 450 nm using a microplate reader (infinite M200PRO, TECAN, Switzerland). All experiments were repeated three times and six parallel replicates were read for each sample.

Immunocytochemistry: The samples were washed with PBS three times and fixed with 1% (v/v) paraformaldehyde at room temperature for 30 min. Subsequently, the fixation solution was removed, and the samples were washed thrice with PBS before permeabilization with 0.1% Triton-100 in PBS for 1 h. The non-specific binding epitopes were blocked with 5% (w/v) BSA (bovine serum albumin) for 1 h after permeabilization with a quick rinse three times with PBS. The primary antibodies were prepared in 5% (w/v) BSA, including anti-YAP IgG (1:400, rabbit; Cell Signaling); anti-lamin A/C IgG (1:400, mouse; Cell Signaling); anti-RUNX2 IgG (1:400, mouse; Cell Signaling) for osteogenic differentiation analysis; anti-PPARɣ IgG (1:400, rabbit; Cell Signaling) for adipogenic differentiation analysis; anti-Vinculin IgG (1:400, mouse; Cell Signaling) for focal adhesion analysis. The samples were incubated with the primary antibodies at 4 °C overnight. After that, the primary antibodies were removed and washed with 0.5 wt% Tween-20 in PBS for 3 times. After washing, the secondary antibody (1:1000, goat anti-rabbit IgG Alexa Fluor 488, 594 or anti-mouse IgG Alexa Fluor 488, 594; molecular probes) in 1% (w/v) BSA were applied to samples for 1 h at room temperature. After incubation, the secondary antibody solution was removed and rinsed 3 times with 0.5 wt% Tween-20 in PBS. Finally, the samples were stained with DAPI (4'-6-diamidino-2-phenylindole) (1:1000, molecular probes)

and Alexa Fluor 647-phalloidin (1:500, molecular probes) in PBS for 10 min at room temperature. Following three additional items of washing with PBS, the samples were observed under an inverted confocal microscope (Leica confocal microscope SP8 with a ×63/1.43 NA oil immersion objective, Germany). All the staining images were taken under the same exposure conditions for analyzing the relative fluorescence intensity. Six parallel replicates were read for each sample. The used drugs and concentrations were: Y27632 (10μM, Sigma-Aldrich) and FAK inhibitor-14 (50μM, Sigma-Aldrich).

Time-lapse imaging: The following laser wavelengths were used to acquire images of cell trace™ CFSE immunolabelled cells 488nm to merge bright field image cells in the hydrogel. During live-cell image acquisition (from 25 to 37 °C and 10% CO_2), each cell was imaged live for 30 to 60 min, with a scanning ratio of 1min per frame.

Image analysis: Cell spreading area, the shape factor and volume were quantified based on F-actin staining and nucleus form z-direction confocal imaging. The focal adhesion analyses were performed based on vinculin staining. The fluorescent intensity and contrast were drawn along the representation morphology of each cell under the 8-bit greyscale images. The area and integrated density were measured by the calibrate function. At least 200 cells were evaluated for each independent sample. For measurements of YAP nucleus localization in scaffolds, the images were thresholded on each color channel to determine the nucleus and cytoskeleton area outside of the nucleus. The YAP nucleus localization ratio was calculated according to Equation 1.[18]

$$\text{Nucleus YAP (nuc / cyt ratio)} = \frac{\frac{Nuclear\ YAP\ intensity}{Area\ of\ nucleus}}{\frac{Cell\ YAP\ intensity - nuclear\ YAP\ intensity}{Area\ of\ cell - area\ of\ nucleus}} \quad (1)$$

All the above-mentioned images were presented as maximum intensity and analyzed by Fiji and we determined the 2D fractal dimension organization with a custom-developed MATLAB

program (MATLAB, Natick, MA) divided images into a series of regions of 100 pixels² spaced at 20 pixels and individually averaged to filter out noise throughout the cell study.

Fitting model of the nonlinear behavior: Cyclic measurements by using the rheometer were optimized for linear rheology with a linear material equation. In the case of nonlinear material behavior, the moduli were fail to be used directly, especially for large amplitude oscillatory strain.[65, 66] As large displacements were expected in such a soft tissue type material, strain amplitude has been varied from 0.01% up to 10% at a fixed frequency of 1 Hz providing a great range of mechanical response incorporated in the inverse analysis (Figure S12, Supporting Information). By using the energy-based method,[63, 64] we generate a linear regression problem out of measurement data even in the case of nonlinear material equations. The solution of a linear regression problem is unique and fast such that several material models can be tried in order to identify a simple but accurate material equation. The following material equation-giving relation between stress, $\boldsymbol{\sigma}$, strain $\boldsymbol{\varepsilon}$, and strain rate $\dot{\boldsymbol{\varepsilon}}$-has been successful for capturing the response for the whole measurement according to Equation 2-4.

$$\boldsymbol{\sigma} = (c_1 + c_2 II_{\varepsilon})\boldsymbol{\varepsilon} + (c_3 + c_4 II_{\dot{\varepsilon}})\dot{\boldsymbol{\varepsilon}} \tag{2}$$

$$II_{\varepsilon} = \mathrm{tr}(\boldsymbol{\varepsilon}^2) = \varepsilon_{ij}\varepsilon_{ij} \tag{3}$$

$$II_{\dot{\varepsilon}} = \mathrm{tr}(\dot{\boldsymbol{\varepsilon}}^2) = \dot{\varepsilon}_{ij}\dot{\varepsilon}_{ij} \tag{4}$$

where we apply summation convention over the repeated indices i,j from 1 to 3. This material model is in 3D space and in the case of the rheometer measurement, only the shear component of the strain remains such that we can gather information solely on the second invariant. In general, all three invariants existing in 3D space are necessary to describe materials response adequately. All determined parameters are compiled in Table 2.

The inverse analysis is based on converting the moduli, G', G", into two energies over the whole and quarter period according to Equation 5-6.

$$e_1 = \int_0^{1/\nu} \sigma_{ij}\dot{\varepsilon}_{ij}dt = 2G''\varepsilon_0^2\pi \tag{5}$$

$$e_2 = \int_0^{1/(4\nu)} \sigma_{ij}\dot{\varepsilon}_{ij}dt = G'\varepsilon_0^2 \tag{6}$$

where the strain amplitude, ε_0, and frequency, ν, are known for one measurement. By having more than 4 measurements, we can obtain four material parameters by using the linear regression by means of minimizing the sum of squared errors between measurement and computation. The outcome with the material model in Equation 2 was presented in Figure S13.

Statistical analysis: All data were expressed as the means ± standard deviations (s.d) with independent experiments (n = 3). The statistical analysis was performed using a one-way or two-way analysis of variance (ANOVA) with the Tukey significant-difference *post hoc* test using Origin 9.0 software. The date is indicated with (*) for $p < 0.05$, (**) for $p < 0.01$ and (***) for $p < 0.001$.

Data availability: All the data generated or analyzed with MATLAB scripts during this study are available from the corresponding author on request.

Supporting Information

Supporting Information is available from the Wiley Online Library or from the author.

Acknowledgements

This work was funded by SFB 1112 and the Focus Area Nanoscale of Freie Universität Berlin. J.Z., H.Y., and M.L. also thank the China Scholarship Council (CSC) from P. R. China. We would like to thank Prof. Nan Ma and Prof. Jeremy Teo for their valuable discussion on the manuscript.

We would like to acknowledge the assistance of the Core Facility BioSupraMol supported by the DFG. We would like to thank Dr. Pamela Winchester for language polishing this manuscript.

Conflict of Interest

The authors declare no competing financial interest.

Received: ((will be filled in by the editorial staff))
Revised: ((will be filled in by the editorial staff))
Published online: ((will be filled in by the editorial staff))

References

[1] C. M. Madl, S. C. Heilshorn, H. M. Blau, *Nature* **2018**, *557*, 335-342.
[2] H. M. Xia, X. Li, W. W. Gao, X. Fu, R. H. Fang, L. F. Zhang, K. Zhang, *Nat. Rev. Mater.* **2018**, *3*, 279-279.
[3] L. Q. Li, J. Eyckmans, C. S. Chen, *Nat. Mater.* **2017**, *16*, 1164-1168.
[4] P. H. Wu, D. R. Aroush, A. Asnacios, W. C. Chen, M. E. Dokukin, B. L. Doss, P. Durand-Smet, A. Ekpenyong, J. Guck, N. V. Guz, P. A. Janmey, J. S. H. Lee, N. M. Moore, A. Ott, Y. C. Poh, R. Ros, M. Sander, I. Sokolov, J. R. Staunton, N. Wang, G. Whyte, D. Wirtz, *Nat.Methods* **2018**, *15*, 491-498.
[5] A. W. Holle, J. L. Young, K. J. Van Vliet, R. D. Kamm, D. Discher, P. Janmey, J. P. Spatz, T. Saif, *Nano Lett.* **2017**, *18*, 1-8.
[6] T. C. von Erlach, S. Bertazzo, M. A. Wozniak, C. M. Horejs, S. A. Maynard, S. Attwood, B. K. Robinson, H. Autefage, C. Kallepitis, A. D. Hernandez, C. S. Chen, S. Goldoni, M. M. Stevens, *Nat. Mater.* **2018**, *17*, 237-242.
[7] J. E. Frith, G. D. Kusuma, J. Carthew, F. Li, N. Cloonan, G. A. Gomez, J. J. Cooper-White, *Nat. Commun.* **2018**, *9*, 257.
[8] E. E. Charrier, K. Pogoda, R. G. Wells, P. A. Janmey, *Nat. Commun.* **2018**, *9*, 449.
[9] X. Xue, Y. Sun, A. M. Resto-Irizarry, Y. Yuan, K. M. Aw Yong, Y. Zheng, S. Weng, Y. Shao, Y. Chai, L. Studer, J. Fu, *Nat. Mater.* **2018**, *17*, 633-641.
[10] M. Uroz, S. Wistorf, X. Serra-Picamal, V. Conte, M. Sales-Pardo, P. Roca-Cusachs, R. Guimerà, X. Trepat, *Nat. Cell Biol.* **2018**, *20*, 646.
[11] K. H. Vining, D. J. Mooney, *Nat. Rev. Mol. Cell Biol.* **2017**, *18*, 728-742;
[12] Z. Gong, S. E. Szczesny, S. R. Caliari, E. E. Charrier, O. Chaudhuri, X. Cao, Y. Lin, R. L. Mauck, P. A. Janmey, J. A. Burdick, V. B. Shenoy, *Pro. Natl. Acad. Sci. U. S. A.* **2018**, *115*, E2686-E2695.
[13] T. Razafiarison, C. N. Holenstein, T. Stauber, M. Jovic, E. Vertudes, M. Loparic, M. Kawecki, L. Bernard, U. Silvan, J. G. Snedeker, *Pro. Natl. Acad. Sci. U. S. A.* **2018**, *115*, 4631-4636.
[14] C. Zhang, B. Xie, Y. Zou, D. Zhu, L. Lei, D. Zhao, H. Nie, *Adv. Drug Deliv. Rev.* **2018**, *132*, 33-56.
[15] R. O. Hynes, *Science* **2009**, *326*, 1216-1219.

[16] I. Malanchi, A. Santamaria-Martínez, E. Susanto, H. Peng, H.-A. Lehr, J.-F. Delaloye, J. Huelsken, *Nature* **2011**, *481*, 85-89.
[17] H. M. Poling, D. Wu, N. Brown, M. Baker, T. A. Hausfeld, N. Huynh, S. Chaffron, J. C. Y. Dunn, S. P. Hogan, J. M. Wells, M. A. Helmrath, M. M. Mahe, *Nat. Biomed. Eng.* **2018**, *2*, 429-442.
[18] A. M. Rosales, S. L. Vega, F. W. DelRio, J. A. Burdick, K. S. Anseth, *Angew.Chem., Int. Ed.* **2017**, *56*, 12132-12136.
[19] Y. Wei, X. J. Mo, P. C. Zhang, Y. Y. Li, J. W. Liao, Y. J. Li, J. X. Zhang, C. Y. Ning, S. T. Wang, X. L. Deng, L. Jiang, *ACS Nano* **2017**, *11*, 5915-5924.
[20] Y. C. Yeh, E. A. Corbin, S. R. Caliari, L. Ouyang, S. L. Vega, R. Truitt, L. Han, K. B. Margulies, J. A. Burdick, *Biomaterials* **2017**, *145*, 23-32.
[21] D. Y. Ko, M. Patel, H. J. Lee, B. Jeong, *Adv. Funct. Mater.* **2018**, *28*, 1706286.
[22] E. E. L. Lewis, H. Wheadon, N. Lewis, J. L. Yang, M. Mulling, A. Hursthouse, D. Stirling, M. J. Dalby, C. C. Berry, *ACS Nano* **2016**, *10*, 8346-8354.
[23] B. Trappmann, J. E. Gautrot, J. T. Connelly, D. G. T. Strange, Y. Li, M. L. Oyen, M. A. C. Stuart, H. Boehm, B. J. Li, V. Vogel, J. P. Spatz, F. M. Watt, W. T. S. Huck, *Nat. Mater.* **2012**, *11*, 742-742.
[24] J. H. Wen, L. G. Vincent, A. Fuhrmann, Y. S. Choi, K. C. Hribar, H. Taylor-Weiner, S. C. Chen, A. J. Engler, *Nat. Mater.* **2014**, *13*, 979-987.
[25] T. Razafiarison, C. N. Holenstein, T. Stauber, M. Jovic, E. Vertudes, M. Loparic, M. Kawecki, L. Bernard, U. Silvan, J. G. Snedeker, *Pro. Natl. Acad. Sci. U. S. A.* **2018**, *115*, 4631-4636.
[26] K. Mandal, D. R.-B. Aroush, Z. T. Graber, B. Wu, C. Y. Park, J. J. Fredberg, W. Guo, T. Baumgart, P. A. Janmey, *ACS Nano* **2018**, *13*, 203-214.
[27] T. L. Sun, G. Y. Qing, *Adv. Mater.* **2011**, *23*, H57-H77.
[28] J. G. Zhang, C. Cheng, J. L. Cuellar-Camacho, M. J. Li, Y. Xia, W. Z. Li, R. Haag, *Adv. Funct. Mater.* **2018**, *28*, 1804773.
[29] G. L. Ying, N. Jiang, S. Maharjan, Y. X. Yin, R. R. Chai, X. Cao, J. Z. Yang, A. K. Miri, S. Hassan, Y. S. Zhang, *Adv. Mater.* **2018**, 1805460.
[30] S. R. Shin, B. Migliori, B. Miccoli, Y. C. Li, P. Mostafalu, J. Seo, S. Mandla, A. Enrico, S. Antona, R. Sabarish, T. Zheng, L. Pirrami, K. Zhang, Y. S. Zhang, K. T. Wan, D. Demarchi, M. R. Dokmeci, A. Khademhosseini, *Adv. Mater.* **2018**, *30*, 1704189.
[31] J. K. Yoon, M. Misra, S. J. Yu, H. Y. Kim, S. H. Bhang, S. Y. Song, J. R. Lee, S. Ryu, Y. W. Choo, G. J. Jeong, S. P. Kwon, S. G. Im, T. I. Tae, B. S. Kim, *Adv. Funct. Mater.* **2017**, *27*, 1703853.
[32] H. Shin, B. D. Olsen, A. Khademhosseini, *Biomaterials* **2012**, *33*, 3143-3152.
[33] X. L. Cui, J. N. Tang, Y. Hartanto, J. B. Zhang, J. X. Bi, S. Dai, S. Z. Qiao, K. Cheng, H. Zhang, *ACS Appl. Mater. Interfaces* **2018**, *10*, 37783-37796.
[34] Y. G. Lei, D. V. Schaffer, *Pro. Natl. Acad. Sci. U. S. A.* **2013**, *110*, E5039-E5048.
[35] J. N. Tang, X. L. Cui, T. G. Caranasos, M. T. Hensley, A. C. Vandergriff, Y. Hartanto, D. L. Shen, H. Zhang, J. Y. Zhang, K. Cheng, *ACS Nano* **2017**, *11*, 9738-9749.
[36] Z. Y. Shen, J. X. Bi, B. Y. Shi, D. Nguyen, C. J. Xian, H. Zhang, S. Dai, *Soft Matter* **2012**, *8*, 7250-7257.
[37] Y. Liu, K. H. Zhang, J. H. Ma, G. J. Vancso, *ACS Appl. Mater. Interfaces* **2017**, *9*, 901-908.
[38] T. E. Brown, J. S. Silver, B. T. Worrell, I. A. Marozas, F. M. Yavitt, K. A. Gunay, C. N. Bowman, K. S. Anseth, *J. Am. Chem. Soc.* **2018**, *140*, 11585-11588.

[39] O. Chaudhuri, S. T. Koshy, C. B. Da Cunha, J.-W. Shin, C. S. Verbeke, K. H. Allison, D. J. Mooney, *Nat. Mater.* **2014**, *13*, 970-978.
[40] M. Guo, A. F. Pegoraro, A. Mao, E. H. Zhou, P. R. Arany, Y. Han, D. T. Burnette, M. H. Jensen, K. E. Kasza, J. R. Moore, F. C. Mackintosh, J. J. Fredberg, D. J. Mooney, J. Lippincott-Schwartz, D. A. Weitz, *Pro. Natl. Acad. Sci. U. S. A.* **2017**, *114*, E8618-E8627.
[41] M. Bao, J. Xie, A. Piruska, W. T. S. Huck, *Nat. Commun.* **2017**, *8*, 1962.
[42] M. Uroz, S. Wistorf, X. Serra-Picamal, V. Conte, M. Sales-Pardo, P. Roca-Cusachs, R. Guimerà, X. Trepat, *Nat. Cell Biol.* **2018**, *20*, 646-654.
[43] C. Grashoff, B. D. Hoffman, M. D. Brenner, R. B. Zhou, M. Parsons, M. T. Yang, M. A. McLean, S. G. Sligar, C. S. Chen, T. Ha, M. A. Schwartz, *Nature* **2010**, *466*, 263-266.
[44] W. Y. Qian, L. Q. Gong, X. Cui, Z. J. Zhang, A. Bajpai, C. Liu, A. B. Castillo, J. C. M. Teo, W. Q. Chen, *ACS Appl. Mater. Interfaces* **2017**, *9*, 41794-41806.
[45] F. J. Sulzmaier, C. Jean, D. D. Schlaepfer, *Nat. Rev. Cancer* **2014**, *14*, 598-610.
[46] S. Dupont, L. Morsut, M. Aragona, E. Enzo, S. Giulitti, M. Cordenonsi, F. Zanconato, J. Le Digabel, M. Forcato, S. Bicciato, *Nature* **2011**, *474*, 179.
[47] G. Brusatin, T. Panciera, A. Gandin, A. Citron, S. Piccolo, *Nat. Mater.* **2018**, *17*, 1063-1075.
[48] J. Y. Shiu, L. Aires, Z. Lin, V. Vogel, *Nat. Cell Biol.* **2018**, *20*, 262-271.
[49] E. Latorre, S. Kale, L. Casares, M. Gómez-González, M. Uroz, L. Valon, R. V. Nair, E. Garreta, N. Montserrat, A. del Campo, B. Ladoux, M. Arroyo, X. Trepat, *Nature* **2018**, *563*, 203-208.
[50] A. Totaro, T. Panciera, S. Piccolo, *Nat. Cell Biol.* **2018**, *20*, 888-899.
[51] A. C. Rowat, D. E. Jaalouk, D. A. Weitz, J. Lammerding, *J. Biol. Chem.* **2013**, *288*, 8610-8618.
[52] D.-H. Kim, J. Hah, D. Wirtz, in *Biomechanics in Oncology*, Springer, **2018**, pp. 41-55.
[53] T. J. Kirby, J. Lammerding, *Nat. Cell Biol.* **2018**, *20*, 373-381.
[54] G. Rosso, I. Liashkovich, V. Shahin, *Adv. Sci.* **2018**, 1801638.
[55] J. K. Kim, A. Louhghalam, G. Lee, B. W. Schafer, D. Wirtz, D. H. Kim, *Nat. Commun.* **2018**, *9*, 1115.
[56] T. O. Ihalainen, L. Aires, F. A. Herzog, R. Schwartlander, J. Moeller, V. Vogel, *Nat. Mater.* **2015**, *14*, 1252-1261.
[57] C. Yang, M. W. Tibbitt, L. Basta, K. S. Anseth, *Nat. Mater.* **2014**, *13*, 645-652.
[58] O. Chaudhuri, L. Gu, D. Klumpers, M. Darnell, S. A. Bencherif, J. C. Weaver, N. Huebsch, H. P. Lee, E. Lippens, G. N. Duda, D. J. Mooney, *Nat. Mater.* **2016**, *15*, 326-+.
[59] J. Swift, I. L. Ivanovska, A. Buxboim, T. Harada, P. C. D. P. Dingal, J. Pinter, J. D. Pajerowski, K. R. Spinler, J. W. Shin, M. Tewari, F. Rehfeldt, D. W. Speicher, D. E. Discher, *Science* **2013**, *341*.
[60] R. K. Das, V. Gocheva, R. Hammink, O. F. Zouani, A. E. Rowan, *Nat. Mater.* **2016**, *15*, 318-325.
[61] J. H. W. Distler, A. Hirth, M. Kurowska-Stolarska, R. E. Gay, S. Gay, O. Distler, *Q. J. Nucl. Med.* **2003**, *47*, 149-161.
[62] M. Bennett, M. Cantini, J. Reboud, J. M. Cooper, P. Roca-Cusachs, M. Salmeron-Sanchez, *Pro. Natl. Acad. Sci. U. S. A.* **2018**, *115*, 1192-1197.
[63] B.E. Abali, *Appl. Sci.* **2018**, *8*, 1354.
[64] B. E. Abali, C. C. Wu, W. H. Wüller, *Continuum Mech. Thermodyn.* **2016**, *28*, 1221-1246.

[65] E. A. Andablo-Reyes, D. Auhl, E. L. de Boer, D. Romano, S. Rastogi, *J. Rheol.* **2017**, *61*, 503-513.
[66] F. Del Giudice, M. Tassieri, C. Oelschlaeger, A. Q. Shen, *Macromolecules* **2017**, *50*, 2951-2963.

The nanogel-actuated-integrated responsive hydrogels are able to modulate the stiffness in soft microniche with covalent crosslinking coordinated reversibly physical network, which can regulate the differentiation of stem-cell spheroids. The central roles of the dynamic relationship between the biomechanical signals and mechanosensitive transcriptional regulators in the cellular mechanosensing are presented.

Keywords: soft microniches, stiffness-cyclable hydrogels, stem cell spheroids, FAK signaling, lamin A/C

*Jianguang Zhang *, Hua Yang, Bilen Emek Abali, Mingjun Li, Yi Xia, and Rainer Haag **

Dynamic Mechanics-modulated Hydrogels to Regulate the Differentiation of Stem-cell Spheroids in Soft Microniches and Modeling of the Nonlinear Behavior

TOC figure

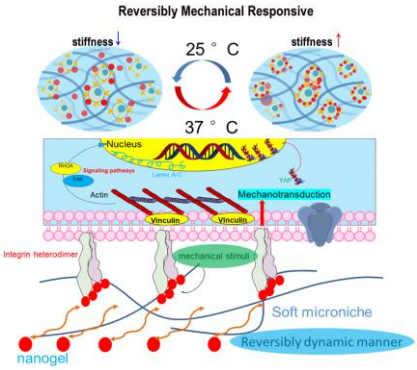

Supporting Information

Dynamic Mechanics-modulated Hydrogels to Regulate the Differentiation of Stem-cell Spheroids in Soft Microniches and Modelling of the Nonlinear Behaviour

*Jianguang Zhang *, Hua Yang, Bilen Emek Abali, Mingjun Li, Yi Xia, and Rainer Haag **

J.G.Zhang, M. Li, Y. Xia, Prof. R. Haag

Institut für Chemie und Biochemie, Freie Universität Berlin, Takustr. 3, 14195 Berlin, Germany

H. Yang, Dr. B E. Abali

Institute of Mechanics, Chair of Continuum Mechanics and Constitutive Theory, Technische Universität Berlin, Einsteinufer 5, 10587, Berlin, Germany

E-Mail: jgz720@zedat.fu-berlin.de, haag@chemie.fu-berlin.de

Gelatin methacryloyl (GelMA)

GelMA was fabricated according to a well-established method.[1] In brief, 10 g porcine skin gelatin (type A, Sigma-Aldrich) was dissolved in 50 mL Dulbecco's phosphate-buffered saline (DPBS, Sigma-Aldrich) at 60 °C under vigorous stirring for 1 h, followed by the dropwise of 8 mL of methacryloyl anhydride (MA, 94%, Sigma-Aldrich) for a 3 h reaction to synthesize gelatin with methacryloyl modification. The resulting mixture was dialyzed against DI water by a dialysis tubing with a molecular weight cut off 12-14 kDa for 7 days at 40 °C to remove salts and unreacted MA. After freeze-drying for 4 d, the GelMA was characterized by ^{1}H NMR (deuterium oxide, Sigma), which was recorded on a Bruker ECX 400 to quantify the degree of acrylation and then stored at -20 °C for further use.

Lithium phenyl-2,4,6-trimethyl-benzoyl-phosphinate (LAP)

The photoinitiator LAP was synthesized as described previously.[2] Briefly, 2,4,6-trimethyl benzoyl chloride (3.2 g, 0.018 mol, Sigma-Aldrich) was added dropwise to an equimolar amount of continuously stirred dimethyl phenyl phosphonate (3.0 g, 0.018 mol, Sigma-Aldrich) via a Michaelis-Arbuzov reaction for 18 h under the argon protection. After that, the four-fold excess of lithium bromide (6.1 g, 0.072 mol) in 100 mL of 2-butanone (both from Sigma–Aldrich) was added to the reaction mixture from the previous step, which was then heated to 50 °C. After 10 min, a solid precipitate formed. The mixture was cooled to ambient temperature, allowed to rest for 4 h, and then filtered. The filtrate was washed and filtered 3 times with 2-butanone to remove unreacted lithium bromide. The excess solvent was removed by vacuum.

Hydrogel morphologies and rheological characterization

All the samples were put into a 37 °C incubator to form the physical gel or double network gel. Once the network formed, all the samples were quenched by liquid nitrogen and then

freeze-dried to observe the hydrogel morphology using a field-emission scanning electron microscopy (FE-SEM, Hitachi S-7400, Japan). A universal stress Malvern rheometer kinexus lab (Germany) with a 20 mm cone-plate geometry was used to characterize the dynamic oscillation experiments for all samples (n = 6) with storage modulus (G′) and loss modulus (G″) after the onset of gel crosslinking and equilibrium. The gap was setup at 0.5 mm with different temperatures from 20 °C to 40 °C at a heating rate of 5 °C min^{-1} at a constant strain of 0.1% and a frequency at 1 Hz. Strain amplitude sweeps were conducted from 0.01 to 10% at 1 Hz, while oscillatory frequency sweeps were carried out from 0.1 to 1 Hz at 0.1% strain, after determining the linear viscoelastic region.

Nanogel characterization

Dynamic light scattering (DLS) measurements were obtained using Malvern Zetasizer Nano ZS (Malvern Instruments GmbH, Herrenberg, Germany) to measure the hydrodynamic diameter of poly(NIPAM-HEMA) nanogels (0.5mg/mL in Phosphate buffered saline (PBS), pH = 7.4) at a different temperature. Attenuated total reflectance Fourier transform infrared (FT-IR/ATR) spectra were collected on a JASCO FT/IR-4100 infrared spectrophotometer equipped with an ATR accessory (JASCO, Japan).

Alkaline phosphatase (ALP) and Oil Red O (ORO) staining

After 7 days of dynamic culturing in co-induction differentiation medium, the samples were fixed with 1% paraformaldehyde for 2 min, followed by quick rinsing with PBS, and then incubated with 4% (v/v) naphthol AS-MS phosphate (Sigma-Aldrich) and 0.1% (w/v) fast blue RR salt (Sigma-Aldrich) in PBS solution for 20 min. Additional samples were stained for Oil Red O (Sigma-Aldrich) by incubation in 60% ORO solution in PBS for 20 min.

Western bolt

The hydrogels were lysed in RIPA lysis buffer with protease and phosphatase inhibitors (Thermo Fisher), and the concentration of protein was measured by using a BCA protein

assay kit (Thermo Fisher). 50 µg of protein was separated by 10 % SDS-PAGE and the protein was then transferred to a PVDF membrane (Bio-Rad). The membrane was blocked in 5 % BSA for 3 h and then incubated with primary antibody GAPDH (rabbit; Cell Signaling), lamin A/C (mouse; Cell Signaling), which were diluted to 1:1,000 (v/v) in blocking buffer for incubation of the membranes overnight at 4 ºC, respectively. Then it was incubated with HRP-labeled secondary antibodies (Abcam) against the species of primary antibodies under a dilution of 1:8,000 (v/v) for 1 h at room temperature, after washing with tris-buffered saline Tween-20, the HRP signals were detected and visualized using ChemiDoc™ MP imaging system (Bio-Rad, USA).

Gene expression analysis

The RT-qPCR analysis was performed for 3D cultures. In brief, RNA was isolated and pooled via TRI reagent from five hydrogel samples under the same conditions. RNA was precipitated in isopropanol, washed by 75 % (vol/vol) ethanol/water, and quantified by spectrophotometry (Thermo Fisher; Nano-Drop). Total RNA was reverse transcribed to cDNA using SuperScript™ IV VILO™ Master Mix (Invitrogen). RT-qPCR was then performed using SYBR Green reagents (Bio-Rad) on the PIKOREAL 96 Real-Time PCR system. Relative mRNA expression levels of RUNX2, PPARɣ, VEGF, and FGF were normalized to the housekeeping gene GAPDH using the delta-delta Ct method. Primer sequences are listed below:

Gene Name	Forward Primers (5’-3’)	Reverse Primers (5’-3’)
GAPDH	GCAAGAGCACAAGAGGAAGAG	AAGGGGTCTACATGGCAACT
YAP	TGTAGTGGCACCTATCACTC	CCATCTCATCCACACTGTTC
RUNX2	GGTATGTCCGCCACCACTC	TGACGAAGTGCCATAGTAGAGATA
PPARɣ	CGGTTTCAGAAGTGCCTTG	GGTTCAGCTGGTCGATATCAC
VEGF	GCT TACTCTCACCTGCTTCTG	CTGTCATGGGCTGCTTCT T

FGF	AAAGGCAAGATGCAGGAGAG	GAGCAGAGCATGTGAGCTAAT

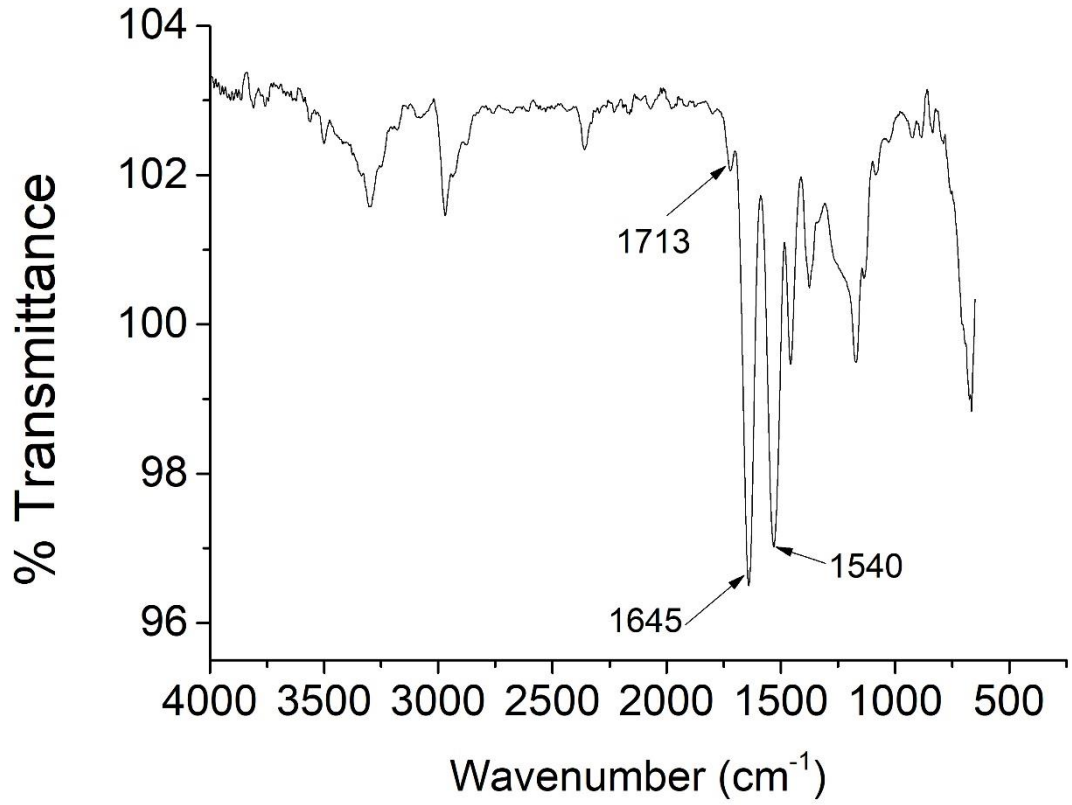

Figure S1. FTIR spectroscopy of poly (NIPAM-HEMA) thermoresponsive nanogel.

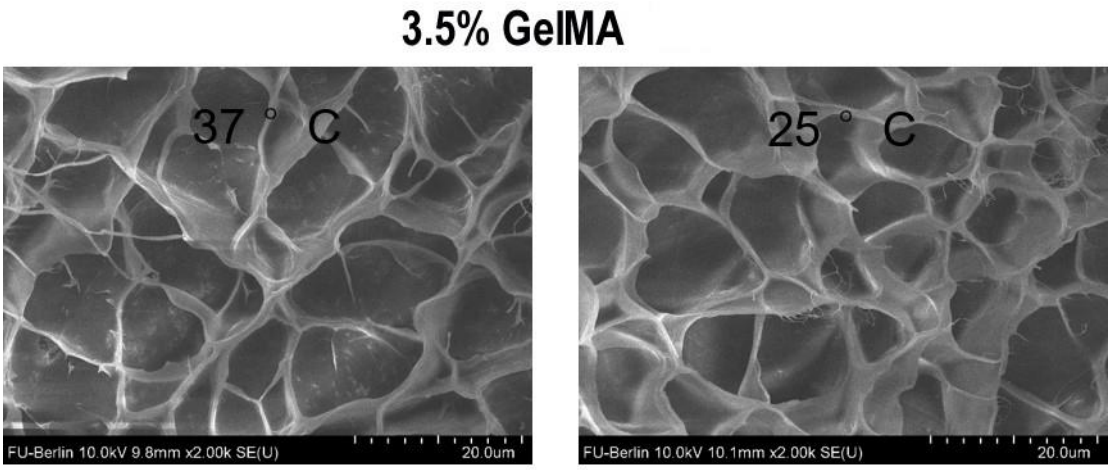

Figure S2. Typical SEM images of the lyophilized hydrogel for 3.5% GelMA at 25 ºC and 37 ºC, respectively. Scale bars: 20 µm.

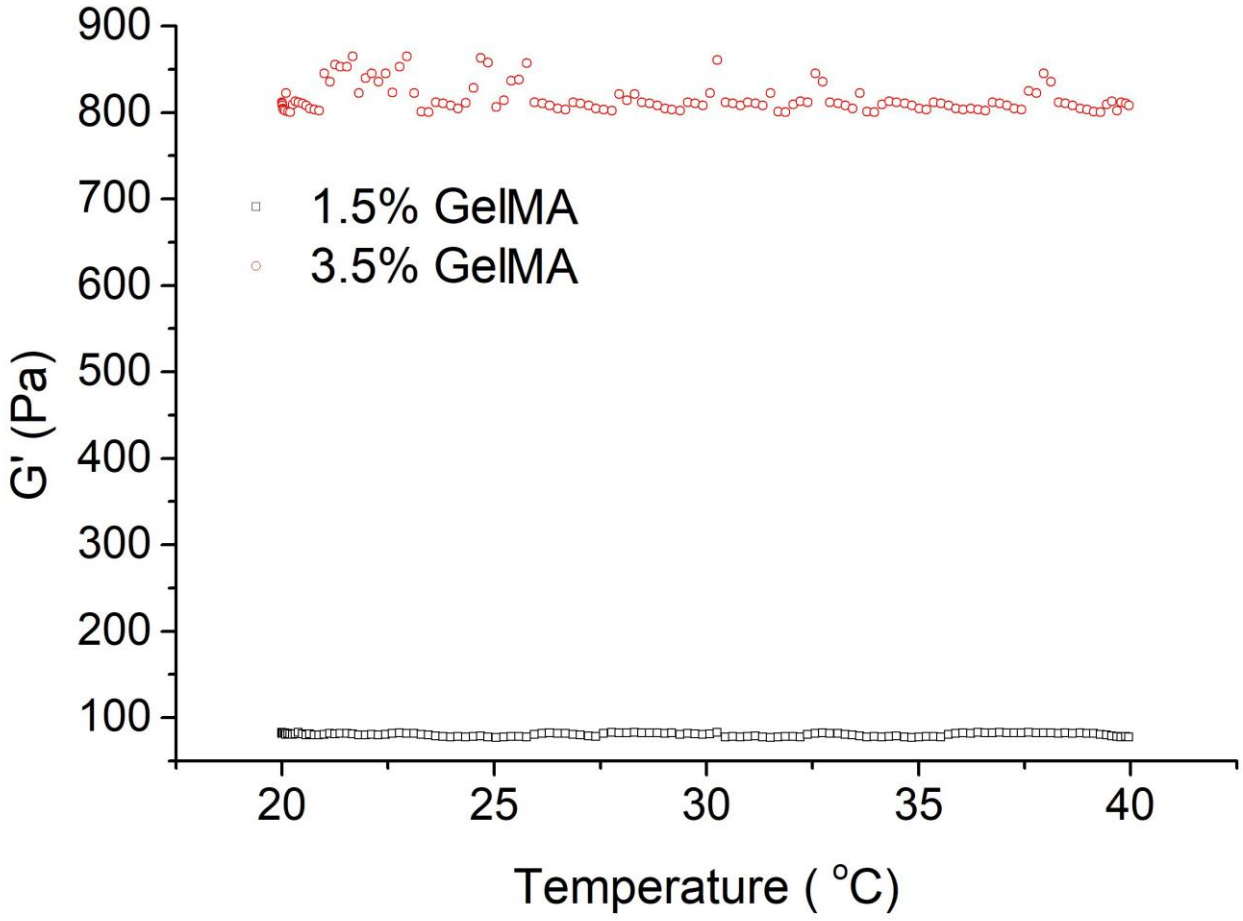

Figure S3. Storage modulus (G′) as a function of temperature for pure 1.5% and 3.5% GelMA from 20 to 40 °C, respectively (1 Hz, 0.1% strain).

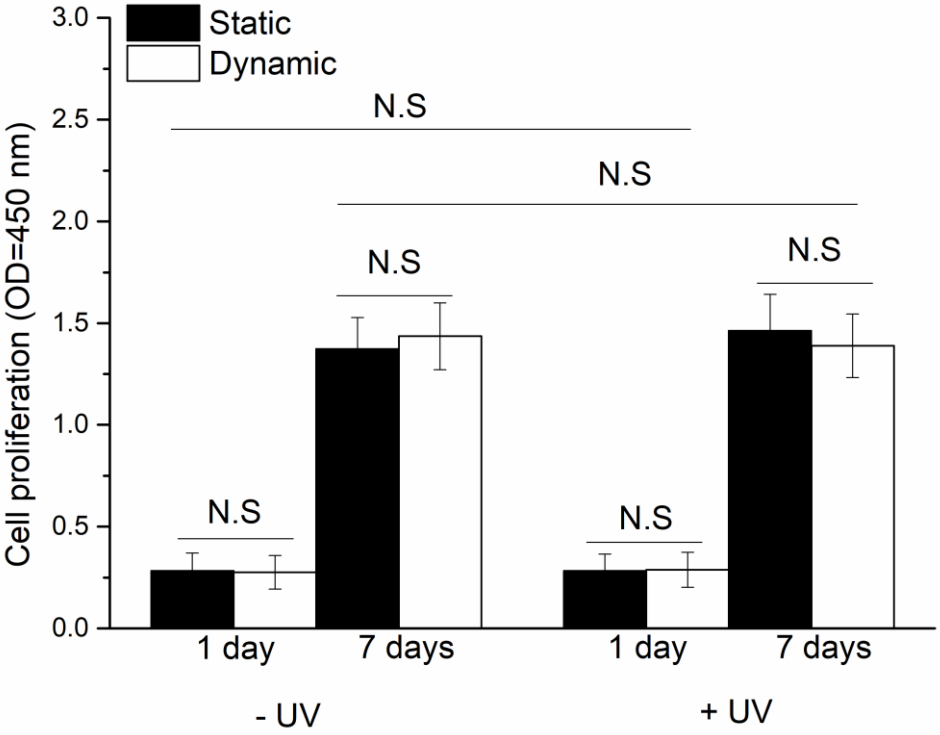

Figure S4. hMSCs proliferation on TCPS were quantified 1 day and 7 days after light treatment under the static and dynamic culture conditions, respectively. All data were expressed as the means ± standard deviations (s.d) with independent experiments (n = 3). N.S, not significant.

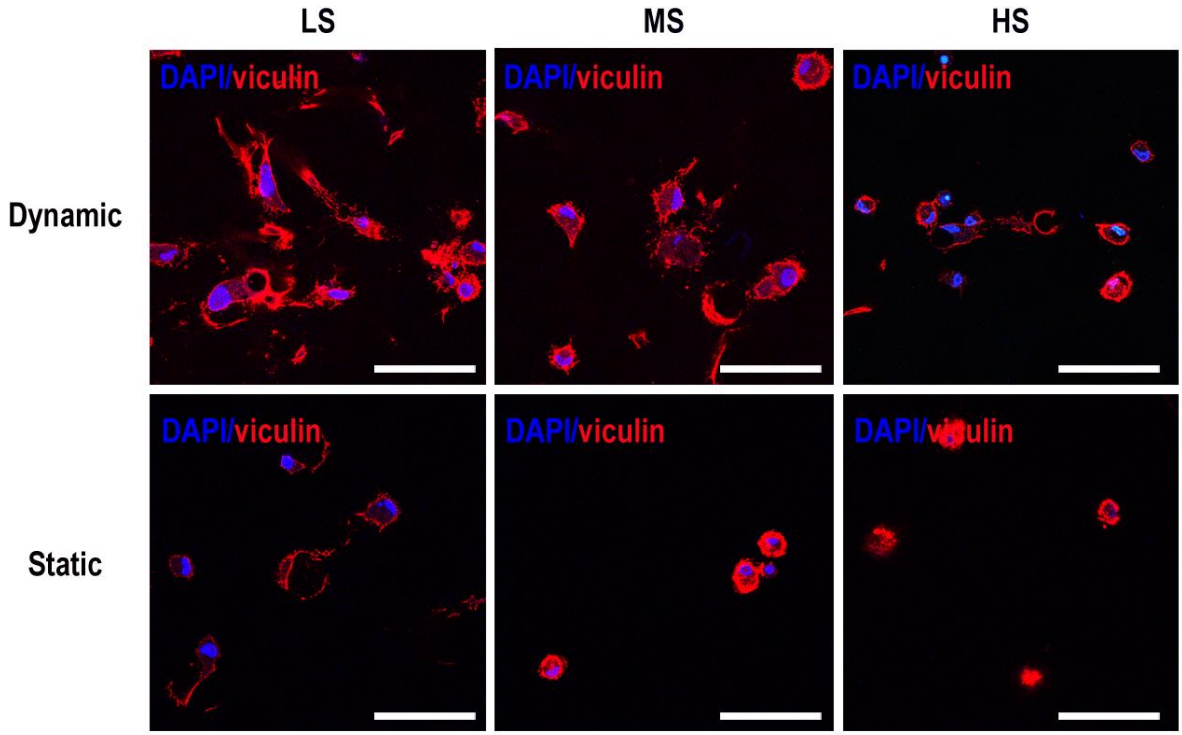

Figure S5. Representative immunofluorescence images of the hMSC spheroids DAPI (blue), vinculin (red) under the static and dynamic culture conditions for 3 days, respectively. Scale bar: 50 μm.

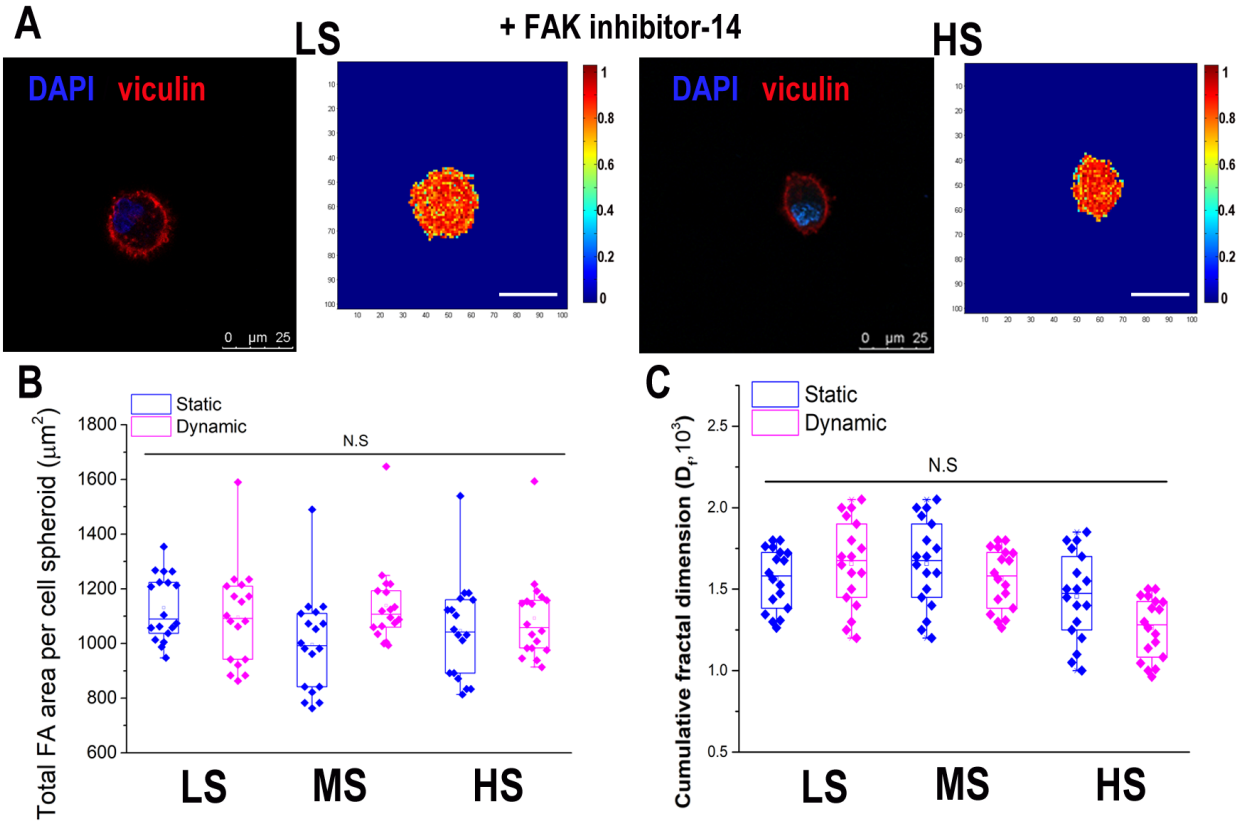

Figure S6. Representative immunofluorescence images of the hMSC spheroids DAPI (blue), vinculin (red) and the results of corresponding 2D fractal dimension (D_f) under dynamic culture conditions with daily FAK inhibition treatment (50μM) for 3 days within LS and HS hydrogels, respectively. Scale bar: 25 μm. (B and C) Quantitative analysis of the total FA area per cell spheroids and Df value in each spheroid region of interest (n = 20 spheroids per each condition from 3 independent experiments). N.S, not significant.

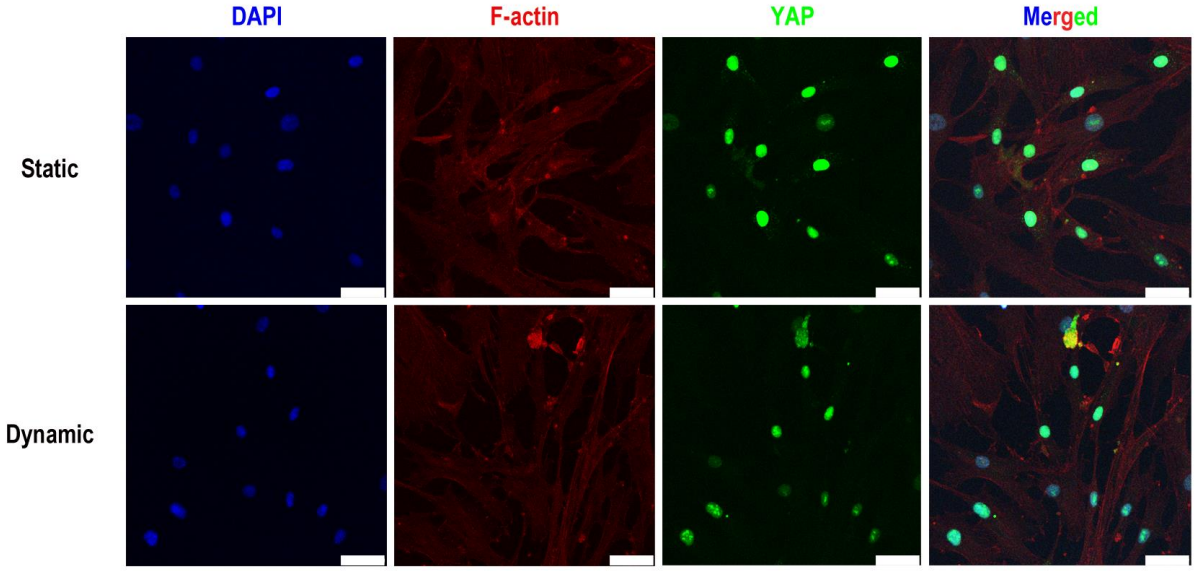

Figure S7. YAP was located in the nuclei of the hMSCs on the TCPS for 20 cycles under the static and dynamic culture conditions. Scale bars: 50 μm.

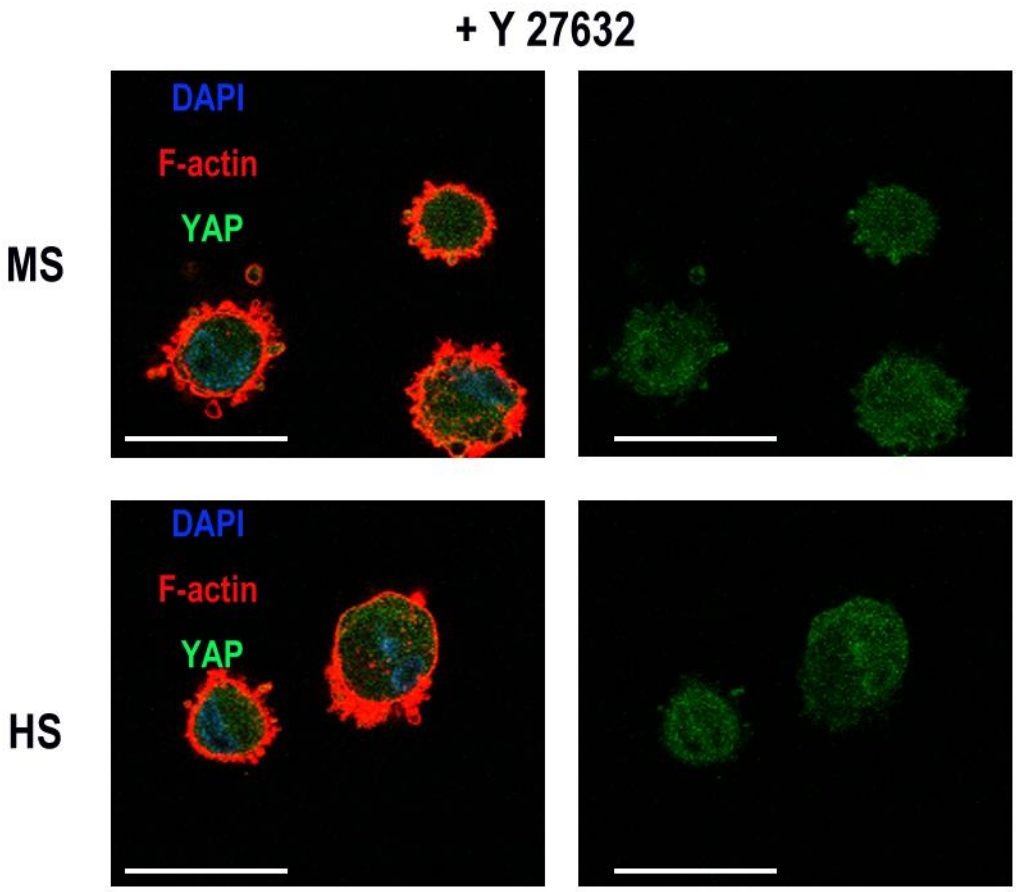

Figure S8. Immunostaining of hMSC spheroids for F-actin (red), YAP (green) and cell nucleus (DAPI, blue) within MS and HS hydrogels following 20 cycles dynamic culture in growth media with 10 μM Y27632 treatment, respectively. Scale bars: 25 μm.

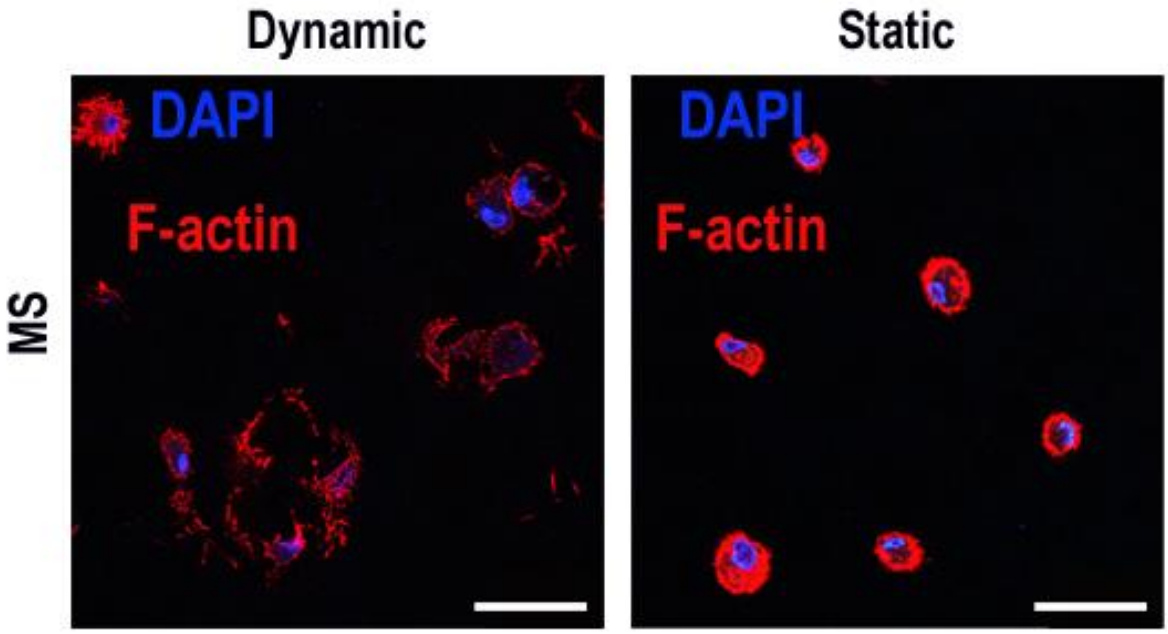

Figure S9. Immunostaining and quantitative analysis of hMSC spheroids per cell spreading area within MS hydrogels following 4 d growth-media under the static and dynamic incubation. F-actin, red; DAPI, blue. Scale bars: 50 µm.

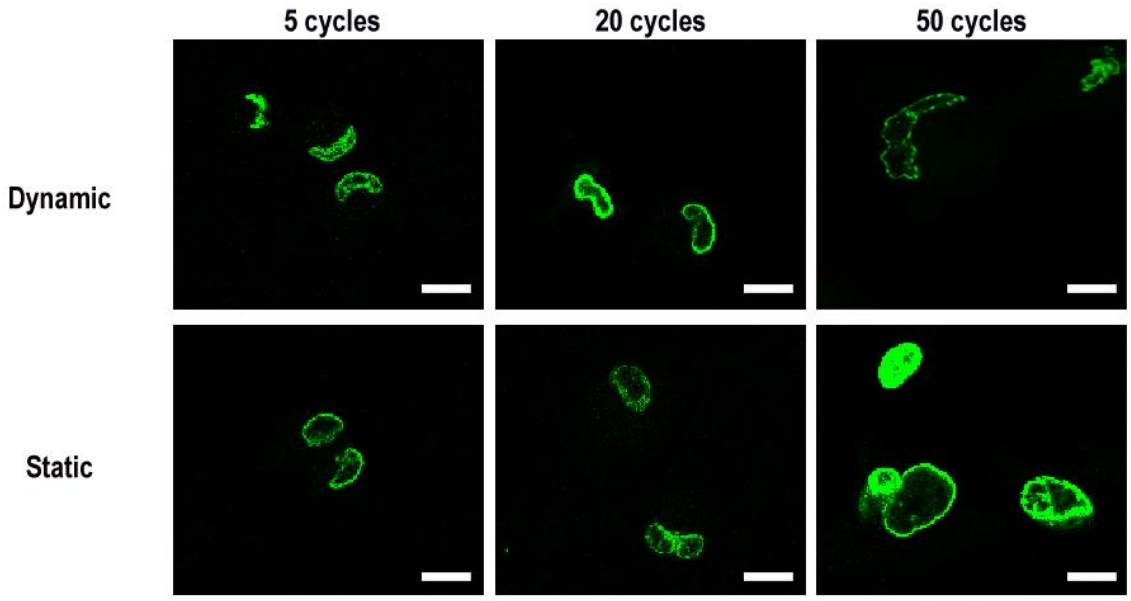

Figure S10. Lamin A/C-dependent differential formation of nuclear deformation in response to cyclic mechanical loading on stem-cell spheroids in LS hydrogels after 5, 20, 50 cycles under the static and dynamic culture conditions, respectively. Lamin A/C (green); F-actin (red); nucleus (blue). Scale bars: 5 μm.

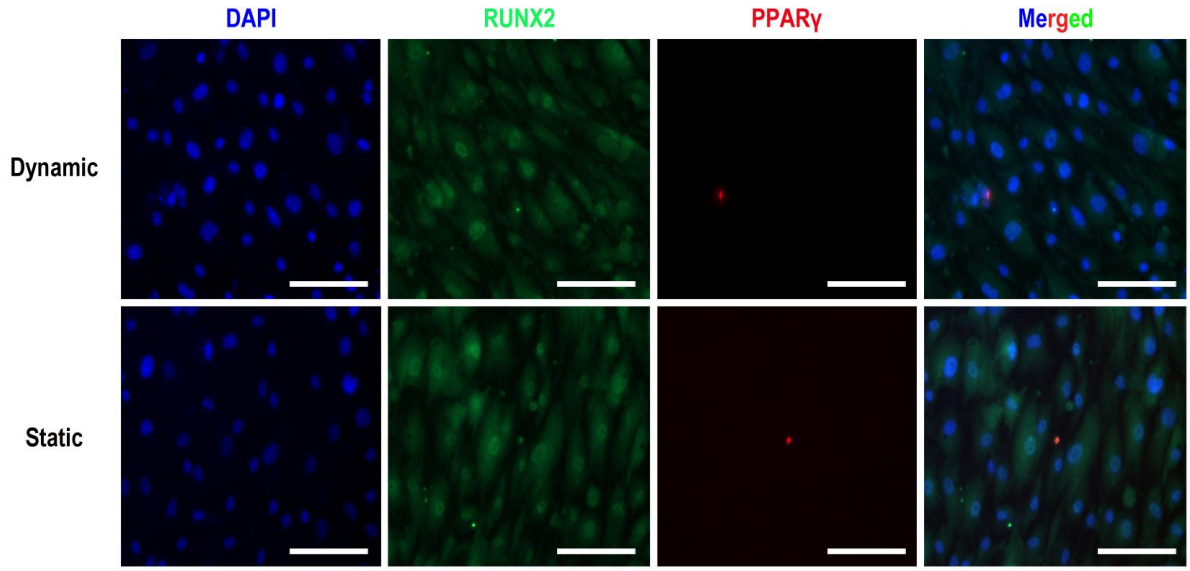

Figure S11. Immunocytochemistry of the hMSCs on the TCPS for 7 days under the static and dynamic culture conditions for co-induction differentiation. Osteogenesis biomarker RUNX2 (green) and adipogenic biomarker PPARɣ (red); DAPI, blue. Scale bars: 50 μm.

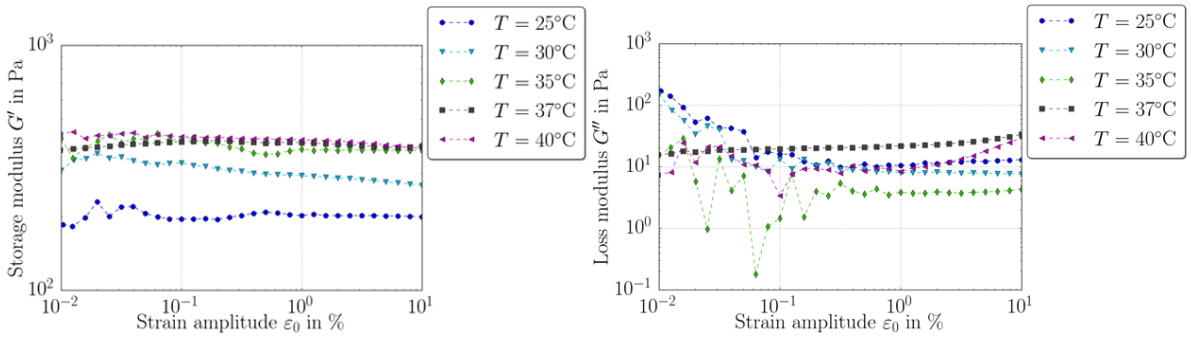

Figure S12. The G' and G" were measured from 0.01% to 10% strain amplitude at different temperature with frequency at 1 Hz and the data is presented on a log-log scale.

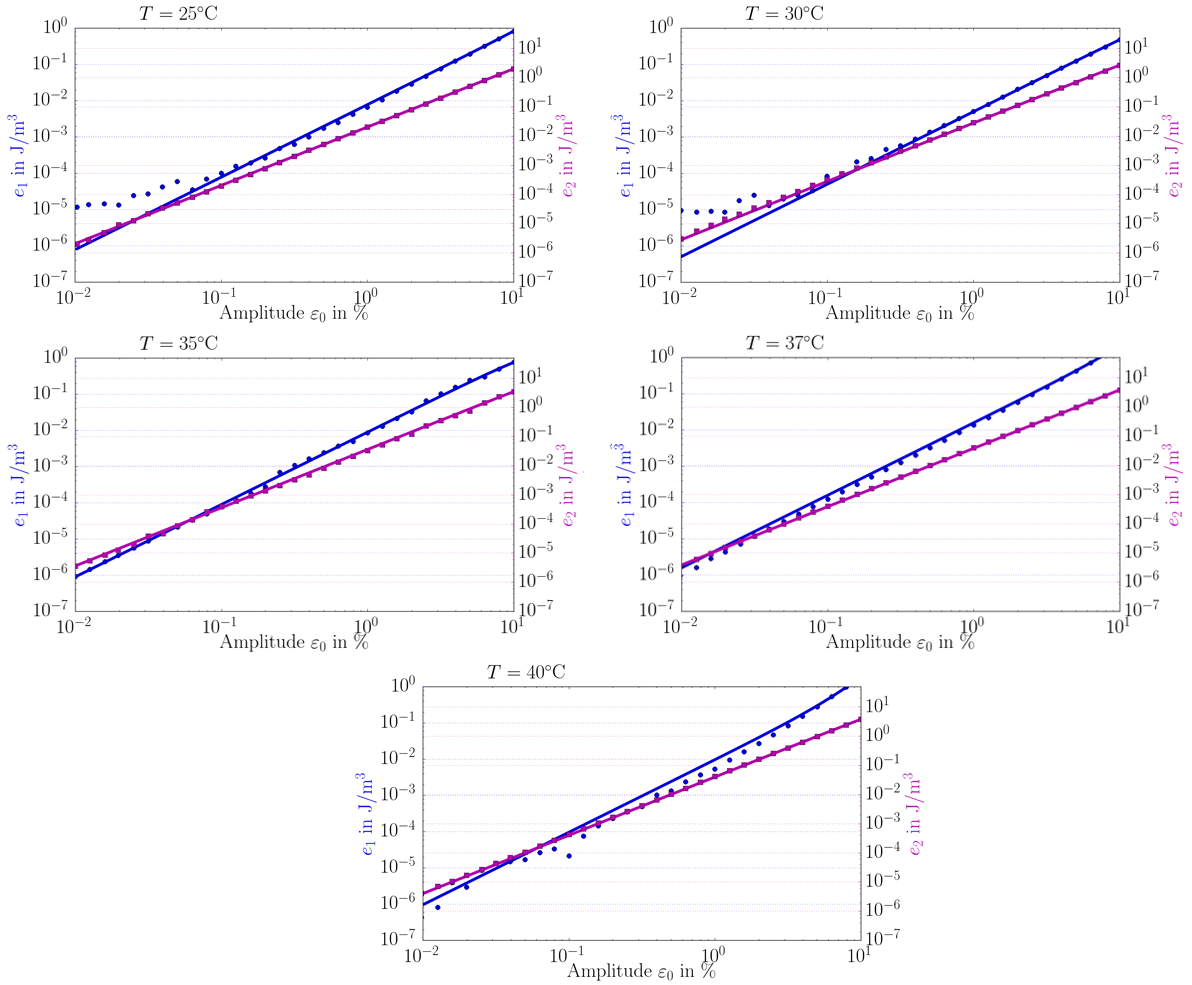

Figure S13. The result of the inverse analysis, continuous lines obtained from the proposed material model and dots were supplied by measurements on a log-log scale.

Supporting Videos

Video S1. Dynamic rheological characterization from 20 to 40 ºC with 1 cycle.

Video S2. hMSC spheroids (stained with cell trace™ CFSE) were encapsulated in the soft Microniches with controlled temperature from 25 to 37 °C.

REFERENCES

1. Sun, X. M.; Lang, Q.; Zhang, H. B.; Cheng, L. Y.; Zhang, Y.; Pan, G. Q.; Zhao, X.; Yang, H. L.; Zhang, Y. G.; Santos, H. A.; Cui, W. G., Electrospun Photocrosslinkable Hydrogel Fibrous Scaffolds for Rapid In Vivo Vascularized Skin Flap Regeneration. *Adv. Funct. Mater.* **2017,** *27* (2), 1604617.

2. Fairbanks, B. D.; Schwartz, M. P.; Bowman, C. N.; Anseth, K. S., Photoinitiated polymerization of PEG-diacrylate with lithium phenyl-2,4,6-trimethylbenzoylphosphinate: polymerization rate and cytocompatibility. *Biomaterials* **2009,** *30* (35), 6702-6707.

4. Conclusions and Future Perspectives

Control of biochemical (e.g., integrin bioligands, growth factors, and drugs) and biophysical (e.g., stiffness, porosity, and geometry) properties of scaffolds to modulate dynamic signals influencing cell behavior is crucial for the fundamental understanding of mechanisms in cellular processes, such as regeneration, embryonic development, and tumor invasion. In this thesis, thermo-triggered reversible dynamic microenvironments were investigated mainly based on the thermoresponsive polymer PNIPAM to mimic intricate feedback loops between multi-responsive 3D ECM and cells that exist *in vivo*. Moreover, we also established a cyclic compressive stress of harnessing mechanical stimuli to study the mechanotransductive response, which provided a versatile approach to preclude the era of modern mechanobiology with computational tools.

In the first project, we successfully fabricated a biodegradable PCL scaffold via electrospinning, which can achieve the dynamic adhesion of endothelial cells. The cRGD-functionalized PNIPAM and antifouling linear polyglycerol (LPG) were anchored on the microfiber matrix based on polydopamine-triggered reactions. At low temperature (25 ºC), the human umbilical vein endothelial cells (HUVECs) were quickly attached to the surface via integrin $\alpha_v\beta_3$-cRGD interaction. However, the increase of the temperature to 37 ºC concealed the cRGD-PNIPAM to the LPG surface, which induced the cell release from the surface. (see Section 3.1). Compared with pure hydrophobic and hydrophilic interaction, using thermo-triggered PNIPAM only, cRGD-PNIPAM grafted surface exhibited higher cell attachment and release efficiency, especially under dynamic flow conditions. Moreover, the ratio of the adhesive factor on the surface was related to the attachment efficiency onto the scaffolds. The fiber matrices provided a suitable microenvironment for accelerating targeted endothelial cells spread and growth after primary screening. Therefore, this tunable dynamic system could dynamically modulate targeted cell attachment and detachment, which could be potentially applied for cell recruitment in vascular tissue engineering or cell isolation for downstream detection of diseases.

Furthermore, in order to understand how cells transduce material properties in the nonlinear dynamic microenvironment, we designed a dynamic nonlinear elastic of the fibrillar network to study the cell behavior under the reversible dynamic mechanical stimulation (RD-MS) with computational tools.

In the second project, we utilized a copolymer of acryloyl carbonated polycaprolactone P(CL-*co*-AC)[157] with a responsive copolymer of N-isopropylacrylamide and 2-hydroxyethyl methacrylate P[(NIPAM-*co*-HEMA)] to introduce the fibrous character of native ECM by electrospinning. The synthetic thermally responsive hybrid microfibrous network shrunk at 37 °C and swelled at 25 °C, which allowed hMSCs to assimilate with their surroundings under the

dynamic tuning of the local stiffness and geometric deformation by RD-MS. The nonlinear elastic fibrous networks increased focal adhesion ligand density, cell spreading, and polarization by recruiting fiber assembly under the RD-MS (see Section 3.2). In addition, compared to the hMSCs cultured under normal culture conditions, the tunable mechanics with multiple cycles from 37 to 25 °C highlighted the intimate control of cell-matrix interactions, which promoted nuclear translocation of YAP and osteogenic differentiation. The hMSCs could benefit more from integrating the combination of multiple stimuli under the RD-MS, such as stiffness, swelling behavior, and porosity, which may serve as a dynamic platform to closer mimic the complex natural system *in vivo*.

In the third project, we show that the commitment and differentiation of encapsulating hMSC spheroids in thermosensitive 3D hydrogels were simply altered by an interpenetrating poly (NIPAM-HEMA) nanogel to a gelatin methacryloyl (GelMA) network. This cell-laden hydrogel provided dynamic mechanics with a covalent crosslinking-coordinated with reversible physical network, which could regulate hMSCs *in situ* by dynamically stiffening soft niches via multicyclic changing temperatures from 25 to 37 ºC (see Section 3.3). Notably, the dynamic microenvironment gradually influenced the distribution from the basal to apical side and expression of nuclear lamin A/C and increased the YAP nuclear localization with cycles, which favors hMSCs undergoing osteogenesis (but not adipogenesis) in soft microniches. These findings highlight the central roles of the dynamic relationship between the biomechanical signals and mechanosensitive transcriptional regulators in the cellular mechanosensing.

To mimic natural ECM properties, this dynamic platform has provided a powerful tool to probe the effects of dynamic signals on cell behavior through mechanotransduction in many *in vitro* studies. We have provided a new insight into how cyclically reversible *in situ* changes in matrix mechanics affect cell fate based on thermo-triggered microenvironment in this thesis. However, there remain several challenges that need to be overcome in this field:

1. The temperature-triggered dynamic platform was very easy to operate and controlled cell adhesion, migration, and differentiation *in vitro*. However, it was difficult to integrate into the *in vivo* tissue microenvironment, where the temperature was relatively constant. Therefore, novel strategies for designing new materials can focus on providing *in vivo* spatiotemporal mechanics cues to make progress towards bridging the gap between *in vitro* and *in vivo* studies.

2. Although mechanotransduction has drawn much attention in the past five years, further studies can be focused on the specific mechanosensing mechanisms, such as embryonic

development, vascular microenvironment, and cardiac fibrotic remodeling. Moreover, traction fore microscopy and computational tools can be employed to explain more complicated mechanisms.

Therefore, the development of the dynamic biomaterials for cell-ECM interactions will contribute to the understanding of the role of ECM in cell signaling, stem cell differentiation, and tissue repair.

5. Kurzzusammenfassung

Die Kontrolle der biochemischen (z.B. Integrin-Bioliganden, Wachstumsfaktoren und Medikamente) und biophysikalischen (z.B. Steifigkeit, Porosität und Geometrie) Eigenschaften von Gerüstarchitekturen zur Modulation dynamischer Signale, welche das Zellverhalten beeinflussen, ist entscheidend für das Verständnis grundlegender Mechanismen zellulärer Prozesse wie Regeneration, Embryonalentwicklung und Tumorinvasion. In dieser Arbeit wurden thermo-getriggerte reversibel dynamische *in vitro* Mikroumgebungen untersucht, die auf dem hauptsächlich thermoresponsiven Polymer PNIPAM basieren, um *in vivo* existierende komplizierte Rückkopplungsschleifen zwischen multiresponsive 3D-ECM und Zellen nachzuahmen. Darüber hinaus wurde zyklische Druckbelastung als mechanischer Reiz genutzt, um mechanotransduktive Reaktion zu untersuchen. Diese Methode bietet einen vielseitigen Ansatz zur Einleitung der Ära der modernen Mechanobiologie mit computergestützten Werkzeugen.

Im ersten Projekt haben wir erfolgreich ein biologisch abbaubares, elektrogesponnenes PCL-Fasergerüst entwickelt, um die dynamische Adhäsion von Endothelzellen zu erreichen. Das cRGD-funktionalisierte PNIPAM und das lineare Polyglycerin (LPG) mit Antifouling-Eigenschaften wurden auf einer Mikrofasermatrix verankert durch Polydopamin-getriggerte Michael-Addition bzw. Schiff-Base-Reaktion. Bei niedriger Temperatur (25 ºC) fand eine schnelle Bindung der Endothelzellen an die Oberfläche über Integrin-$\alpha_v\beta_3$-cRGD-Interaktionen statt. Die Temperaturerhöhung auf 37 ºC schirmt das cRGD-PNIPAM auf der LPG-Oberfläche ab (siehe Abschnitt 3.1). Dabei konnte gezeigt werden, dass die funktionalisierten Gerüste die selektive positive Adhäsion von menschlichen Nabelvenenendothelzellen (HUVECs) auf dynamische Weise kontrollieren können. Zudem korreliert das Verhältnis des Adhäsionsfaktors auf der Oberfläche mit der Effizienz der Bindung an die Gerüste. Darüber hinaus boten die Fasermatrizen eine geeignete Mikroumgebung, um die cRGD-vermittelte Ausbreitung und das Wachstum von Endothelzellen zu beschleunigen. Im Vergleich zu reiner hydrophober und hydrophiler Interaktion mittels thermogetriggertem PNIPAM zeigte die cRGD-PNIPAM-Oberflächen eine verbesserte Zellanhaftungs- und Freisetzungseffizienz, insbesondere unter dynamischen Fließbedingungen. Dies zeigt, dass das hier entwickelte einstellbare System die gezielte Zellanhaftung und -ablösung dynamisch modulieren kann und für die Zellrekrutierung im vaskulären Tissue Engineering oder die Zellisolierung zur nachgelagerten Erkennung von Krankheiten genutzt werden könnte.

Um zu verstehen, wie die Zelle Informationen zur Materialbeschaffenheit der nichtlinearen dynamischen Mikroumgebung weiterleitet, haben wir eine dynamische nichtlineare Elastizität des fibrillären Netzwerks entworfen, um das Zellverhalten unter reversible dynamischer mechanischer Stimulation (RD-MS) mit Hilfe von Computer-basierten Berechnungen zu untersuchen. Im

zweiten Projekt verwendeten wir Elektrospinnen sowie ein Copolymer aus acryloylcarbonisiertem Polycaprolacton P(CL-*co*-AC) [158] und ein responsives Copolymer aus N-Isopropylacrylamid und 2-Hydroxyethylmethacrylat P[(NIPAM-*co*-HEMA)], um einen der ECM ähnlichen faserigen Charakter zu erhalten. Das synthetische thermisch responsive hybride mikrofaserige Netzwerk schrumpfte bei 37 °C und schwoll bei 25 °C. Diese Eigenschaft ermöglichte es hMSCs ihre Umgebung durch dynamische Abstimmung der lokalen Steifigkeit und geometrischen Verformung durch RD-MS anzupassen. Die nichtlineare Elastizität von faserigen Netzwerken erhöhte die Dichte der fokalen Adhäsionsliganden, die Zellausbreitung und die Polarisation durch die Rekrutierung von Faseranordnungen unter dem RD-MS (siehe Abschnitt 3.2). Darüber hinaus ermöglichte die abstimmbare Mechanik mit mehreren Zyklen von 37 bis 25 °C im Vergleich zu normalen Kulturbedingungen eine Kontrolle der Zell-Matrix-Interaktionen der hMSCs und förderte die nukleare Translokation von YAP und die osteogene Differenzierung. Dies zeigt, dass hMSCs von der Kombination mehrerer Reize wie Steifigkeit, Schwellverhalten und Porosität durch RD-MS profitieren, welches als dynamische Plattform das komplexe natürliche System *in vivo* besser nachahmt.

Darüber hinaus wurden erste Arbeiten an linearen elastischen 2D-Substraten für mechanobiologische Studien durchgeführt, und erste 3D-verkapselnde weiche Materialien entwickelt. Im dritten Projekt zeigen wir, dass die Differenzierung von hMSC-Sphäroiden in thermosensitiven 3D-Hydrogelen durch ein interpenetrierendes Poly(NIPAM-HEMA)-Nanogel zu Gelatinemethacryloyl(GelMA)-Netzwerk verändert werden können. Dieses zellbeladene Hydrogel liefert der dynamischen Mechanik ein kovalentes, vernetzendes, koordiniertes, reversibles physikalisches Netzwerk, das hMSCs *in situ* durch dynamisch versteifte weiche Nischen über multizyklische Wechseltemperaturen von 25 bis 37 ºC regulieren kann (siehe Abschnitt 3.3). Insbesondere die dynamische Mikroumgebung beeinflusst die Verteilung der basalen zur apikalen Seite sowie die Expression von nuklearem Lamin A/C und erhöhte die YAP-Lokalisation im Nukleus mit jedem Zyklus, was hMSCs begünstigt, die sich einer Osteogenese (aber nicht einer Adipogenese) in weichen Mikronischen unterziehen. Diese Ergebnisse betonen die zentrale Rolle der dynamischen Beziehung zwischen den biomechanischen Signalen und den mechanosensitiven transkriptionellen Regulatoren.

6. References

[1] C. Frantz, K. M. Stewart, V. M. Weaver, *J. Cell Sci.* **2010**, *123*, 4195-4200.

[2] X. Xue, Y. Sun, A. M. Resto-Irizarry, Y. Yuan, K. M. Aw Yong, Y. Zheng, S. Weng, Y. Shao, Y. Chai, L. Studer, J. Fu, *Nat. Mater.* **2018**, *17*, 633-641.

[3] J. Swift, I. L. Ivanovska, A. Buxboim, T. Harada, P. C. Dingal, J. Pinter, J. D. Pajerowski, K. R. Spinler, J. W. Shin, M. Tewari, F. Rehfeldt, D. W. Speicher, D. E. Discher, *Science* **2013**, *341*, 1240104.

[4] H. M. Xia, X. Li, W. W. Gao, X. Fu, R. H. Fang, L. F. Zhang, K. Zhang, *Nat. Rev. Mater.* **2018**, *3*, 174-193.

[5] A. W. Holle, J. L. Young, K. J. Van Vliet, R. D. Kamm, D. Discher, P. Janmey, J. P. Spatz, T. Saif, *Nano Lett.* **2017**, *18*, 1-8.

[6] Y. L. Li, Y. Xiao, C. S. Liu, *Chem. Rev.* **2017**, *117*, 4376-4421.

[7] T. C. von Erlach, S. Bertazzo, M. A. Wozniak, C. M. Horejs, S. A. Maynard, S. Attwood, B. K. Robinson, H. Autefage, C. Kallepitis, A. D. Hernandez, C. S. Chen, S. Goldoni, M. M. Stevens, *Nat. Mater.* **2018**, *17*, 237-242.

[8] J. Y. Shiu, L. Aires, Z. Lin, V. Vogel, *Nat. Cell Biol.* **2018**, *20*, 262-271.

[9] H. M. Poling, D. Wu, N. Brown, M. Baker, T. A. Hausfeld, N. Huynh, S. Chaffron, J. C. Y. Dunn, S. P. Hogan, J. M. Wells, M. A. Helmrath, M. M. Mahe, *Nat. Biomed. Eng.* **2018**, *2*, 429-442.

[10] A. Khademhosseini, R. Langer, *Nat. Protoc.* **2016**, *11*, 1775-1781.

[11] C. Jia, B. Luo, H. Wang, Y. Bian, X. Li, S. Li, H. Wang, *Adv. Mater.* **2017**, *29*, 1701154.

[12] S. W. Crowder, V. Leonardo, T. Whittaker, P. Papathanasiou, M. M. Stevens, *Cell Stem Cell* **2016**, *18*, 39-52

[13] W. L. Murphy, T.C. McDevitt, A. J. Engler, *Nat. Mater.* **2014**, *13*, 547-557.

[14] F. Guilak, D. M. Cohen, B. T. Estes, J. M. Gimble, W. Liedtke, C. S. Chen, *Cell Stem Cell* **2009**, *5*, 17-26.

[15] T. J. Rabelink, B. M. van den Berg, M. Garsen, G. Wang, M. Elkin, J. van der Vlag, *Nat. Rev. Nephrol.* **2017**, *13*, 201-212.

[16] C. Bonnans, J. Chou, Z. Werb, *Nat. Rev. Mol. Cell Biol.* **2014**, *15*, 786-801.

[17] L. Q. Li, J. Eyckmans, C. S. Chen, *Nat. Mater.* **2017**, *16*, 1164-1168.

[18] F. W. Charbonier, M. Zamani, N. F. Huang, *Adv. Biosys.* **2018**, 1800252.

[19] G. Huang, F. Li, X. Zhao, Y. Ma, Y. Li, M. Lin, G. Jin, T. J. Lu, G. M. Genin, F. Xu, *Chem. Rev.* **2017**, *117*, 12764-12850.

[20] Y. Ma, M. Lin, G. Huang, Y. Li, S. Wang, G. Bai, T. J. Lu, F. Xu, *Adv. Mater.* **2018**, 1705911.

[21] J. D. Humphrey, E. R. Dufresne, M. A. Schwartz, *Nat. Rev. Mol. Cell Biol.* **2014**, *15*, 802-812.

[22] Y. Lu, A. A. Aimetti, R. Langer, Z. Gu, *Nat.Rev.Mater.* **2017**, *2*, 16075.

[23] X. Fu, L. Hosta-Rigau, R. Chandrawati, J. W. Cui, *Chem* **2018**, *4*, 2084-2107.

[24] B. S. Gomes, B. Simões, P. M. Mendes, *Nat. Rev. Chem.* **2018**, *2*, 0120.

[25] A. M. Rosales, S. L. Vega, F. W. DelRio, J. A. Burdick, K. S. Anseth, *Angew. Chem., Int. Ed.* **2017**, *56*, 12132-12136.

[26] Y. Wei, X. J. Mo, P. C. Zhang, Y. Y. Li, J. W. Liao, Y. J. Li, J. X. Zhang, C. Y. Ning, S. T. Wang, X. L. Deng, L. Jiang, *ACS Nano* **2017**, *11*, 5915-5924.

[27] Y. C. Yeh, E. A. Corbin, S. R. Caliari, L. Ouyang, S. L. Vega, R. Truitt, L. Han, K. B. Margulies, J. A. Burdick, *Biomaterials* **2017**, *145*, 23-32.

[28] W. Li, Z. Yan, J. Ren, X. Qu, *Chem. Soc. Rev.* **2018**, *47*, 8639-8684.

[29] K. Uto, J. H. Tsui, C. A. DeForest, D. H. Kim, *Prog. Polym. Sci.* **2017**, *65*, 53-82.

[30] M. Wirkner, J. M. Alonso, V. Maus, M. Salierno, T. T. Lee, A. J. García, A. del Campo, *Adv. Mater.* **2011**, *23*, 3907-3910.

[31] M. J. Salierno, A. J. García, A. del Campo, *Adv. Funct. Mater.* **2013**, *23*, 5974-5980.

[32] S. Zhao, W. Fan, X. Guo, L. Xue, B. Berninger, M. J. Salierno, A. del Campo, *Biomaterials* **2018**, *156*, 238-247.

[33] M. J. Salierno, L. García-Fernandez, N. Carabelos, K. Kiefer, A. J. García, A. del Campo, *Biomaterials* **2016**, *82*, 113-123.

[34] S. Weis, T. T. Lee, A. del Campo, A. J. García, *Acta Biomater.* **2013**, *9*, 8059-8066.

[35] T. T. Lee, J. R. García, J. I. Paez, A. Singh, E. A. Phelps, S. Weis, Z. Shafiq, A. Shekaran, A. del Campo, A. J. García, *Nat. Mater.* **2014**, *14*, 352-360.

[36] C. A. DeForest, D. A. Tirrell, *Nat. Mater.* **2015**, *14*, 523-531.

[37] W. Li, J. S. Wang, J. S. Ren, X. G. Qu, *J. Am. Chem. Soc.* **2014**, *136*, 2248-2251.

[38] Z. Yan, H. Qin, J. Ren, X. Qu, *Angew. Chem., Int. Ed.* **2018**, *57*, 11182-11187.

[39] D. Samanta, J. Gemen, Z. L. Chu, Y. Diskin-Posner, L. J. W. Shimon, R. Klajn, *Pro. Natl. Acad. Sci. U. S. A.* **2018**, *115*, 9379-9384.

[40] L. F. Kadem, M. Holz, K. G. Suana, Q. Li, C. Lamprecht, R. Herges, C. Selhuber-Unkel, *Adv. Mater.* **2016**, *28*, 1799-1802.

[41] L. F. Kadem, K. G. Suana, M. Holz, W. Wang, H. Westerhaus, R. Herges, C. Selhuber-Unkel, *Angew. Chem., Int. Ed.* **2017**, *129*, 231-235.

[42] D. Liu, Y. Xie, H. Shao, X. Jiang, *Angew. Chem., Int. Ed.* **2009**, *48*, 4406-4408.

[43] G. Kocer, J. Ter Schiphorst, M. Hendrikx, H. G. Kassa, P. Leclere, A. Schenning, P. Jonkheijm, *Adv. Mater.* **2017**, *29*, 1606407.

[44] L. Yu, C. Schlaich, Y. Hou, J. Zhang, P. L. M. Noeske, R. Haag, *Chem. Eur. J.* **2018**, *24*, 7742-7748.

[45] J. Edahiro, K. Sumaru, Y. Tada, K. Ohi, T. Takagi, M. Kameda, T. Shinbo, T. Kanamori, Y. Yoshimi, *Biomacromolecules* **2005**, *6*, 970-974.

[46] N. Wang, Y. M. Li, Y. Y. Zhang, Y. Liao, W. G. Liu, *Langmuir* **2014**, *30*, 11823-11832.

[47] W. Li, Z. W. Chen, L. Zhou, Z. H. Li, J. S. Ren, X. G. Qu, *J. Am. Chem. Soc.* **2015**, *137*, 8199-8205.

[48] J. Lahann, S. Mitragotri, T. N. Tran, H. Kaido, J. Sundaram, I. S. Choi, S. Hoffer, G. A. Somorjai, R. Langer, *Science* **2003**, *299*, 371-374.

[49] A. M. D. Wan, R. M. Schur, C. K. Ober, C. Fischbach, D. Gourdon, G. G. Malliaras, *Adv. Mater.* **2012**, *24*, 2501-2505.

[50] H. A. Lin, B. Zhu, Y. W. Wu, J. Sekine, A. Nakao, S. C. Luo, Y. Yamashita, H. H. Yu, *Adv. Funct. Mater.* **2018**, *28*, 1703890.

[51] A. Artzy-Schnirman, D. Blat, Y. Talmon, R. Fishler, D. Gertman, R. Oren, R. Wolchinsky, T. Waks, I. Benhar, Z. Eshhar, U. Sivan, Y. Reiter, *Nano Lett.* **2011**, *11*, 4997-5001.

[52] A. Pulsipher, D. Dutta, W. Luo, M. N. Yousaf, *Angew. Chem., Int. Ed.* **2014**, *53*, 9487-9492.

[53] C. C. A. Ng, A. Magenau, S. H. Ngalim, S. Ciampi, M. Chockalingham, J. B. Harper, K. Gaus, J. J. Gooding, *Angew. Chem., Int. Ed.* **2012**, *51*, 7706-7710.

[54] Z. Chen, Y. Li, W. Liu, D. Zhang, Y. Zhao, B. Yuan, X. Jiang, *Angew. Chem., Int. Ed.* **2009**, *121*, 8453-8455.

[55] R. Green, M. R. Abidian, *Adv. Mater.* **2015**, *27*, 7620-7637.

[56] S. Liang, Y. Zhang, H. Wang, Z. Xu, J. Chen, R. Bao, B. Tan, Y. Cui, G. Fan, W. Wang, W. Wang, W. Liu, *Adv. Mater.* **2018**, *30*, 1704235.

[57] K. M. Persson, R. Karlsson, K. Svennersten, S. Loffler, E. W. H. Jager, A. Richter-Dahlfors, P. Konradsson, M. Berggren, *Adv. Mater.* **2011**, *23*, 4403-4408.

[58] J. Liao, Y. Zhu, Z. Zhou, J. Chen, G. Tan, C. Ning, C. Mao, *Angew. Chem., Int. Ed.* **2014**, *126*, 13284-13288.

[59] M. N. Yousaf, B. T. Houseman, M. Mrksich, *Pro. Natl. Acad. Sci. U. S. A.* **2001**, *98*, 5992-5996.

[60] H. Q. Cao, T. Liu, S. Y. Chew, *Adv. Drug Deliver. Rev.* **2009**, *61*, 1055-1064.

[61] C. A. Myers, P. J. Laz, K. B. Shelburne, D. L. Judd, D. N. Huff, J. D. Winters, J. E. Stevens-Lapsley, P. J. Rullkoetter, *Clin. Biomech.* **2018**, *53*, 93-100.

[62] J. C. Rose, M. Camara-Torres, K. Rahimi, J. Kohler, M. Moller, L. De Laporte, *Nano Lett.* **2017**, *17*, 3782-3791.

[63] A. Omidinia-Anarkoli, S. Boesveld, U. Tuvshindorj, J. C. Rose, T. Haraszti, L. De Laporte, *Small* **2017**, *13*. 1702207.

[64] D. S. H. Wong, J. N. Li, X. H. Yan, B. Wang, R. Li, L. Zhang, L. M. Bian, *Nano Lett.* **2017**, *17*, 1685-1695.

[65] H. Kang, H. J. Jung, D. S. H. Wong, S. K. Kim, S. Lin, K. F. Chan, L. Zhang, G. Li, V. P. Dravid, L. Bian, *J. Am. Chem. Soc.* **2018**, *140*, 5909-5913.

[66] D. M. Pardoll, *Nat. Rev. Cancer* **2012**, *12*, 252-264.

[67] Y. W. Choo, M. Kang, H. Y. Kim, J. Han, S. Kang, J.-R. Lee, G.-J. Jeong, S. P. Kwon, S. Y. Song, S. Go, *ACS Nano* **2018**, *12*, 8977-8993.

[68] C. B. Rodell, S. P. Arlauckas, M. F. Cuccarese, C. S. Garris, R. Li, M. S. Ahmed, R. H. Kohler, M. J. Pittet, R. Weissleder, *Nat. Biomed. Eng.* **2018**, *2*, 578-588.

[69] H. Kang, H. J. Jung, S. K. Kim, D. S. H. Wong, S. Lin, G. Li, V. P. Dravid, L. Bian, *ACS Nano* **2018**, *12*, 5978-5994.

[70] V. Du, N. Luciani, S. Richard, G. Mary, C. Gay, F. Mazuel, M. Reffay, P. Menasché, O. Agbulut, C. Wilhelm, *Nat. Commun.* **2017**, *8*, 400.

[71] M. A. Wheeler, C. J. Smith, M. Ottolini, B. S. Barker, A. M. Purohit, R. M. Grippo, R. P. Gaykema, A. J. Spano, M. P. Beenhakker, S. Kucenas, M. K. Patel, C. D. Deppmann, A. D. Guler, *Nat. Neurosci.* **2016**, *19*, 756-761.

[72] B. Coste, B. Xiao, J. S. Santos, R. Syeda, J. Grandl, K. S. Spencer, S. E. Kim, M. Schmidt, J. Mathur, A. E. Dubin, M. Montal, A. Patapoutian, *Nature* **2012**, *483*, 176-181.

[73] R. R. Ji, Z. Z. Xu, Y. J. Gao, *Nat. Rev. Drug Discov.* **2014**, *13*, 533-548.

[74] A. H. Lewis, A. F. Cui, M. F. McDonald, J. Grandl, *Cell Rep.* **2017**, *19*, 2572-2585.

[75] A. Tay, A. Sohrabi, K. Poole, S. Seidlits, D. Di Carlo, *Adv. Mater.* **2018**, *30*, 1800927.

[76] V. V. Khutoryanskiy, T. K. Georgiou, *Temperature-Responsive Polymers: Chemistry, Properties, and Applications*, John Wiley & Sons, **2018**.

[77] T. L. Sun, G. Y. Qing, *Adv. Mater.* **2011**, *23*, H57-H77.

[78] N. Matsuda, T. Shimizu, M. Yamato, T. Okano, *Adv. Mater.* **2007**, *19*, 3089-3099.

[79] G. Q. Pan, Q. P. Guo, Y. Ma, H. L. Yang, B. Li, *Angew. Chem., Int. Ed.* **2013**, *52*, 6907-6911.

[80] M. Ebara, M. Yamato, T. Aoyagi, A. Kikuchi, K. Sakai, T. Okano, *Biomacromolecules* **2004**, *5*, 505-510.

[81] A. Jiao, N. E. Trosper, H. S. Yang, J. Kim, J. H. Tsui, S. D. Frankel, C. E. Murry, D.-H. Kim, *ACS Nano* **2014**, *8*, 4430-4439.

[82] S. Heinen, S. Rackow, J. L. Cuellar-Camacho, I. S. Donskyi, W. E. S. Unger, M. Weinhart, *J. Mater. Chem. B* **2018**, *6*, 1489-1500.

[83] D. D. Stöbener, J. Scholz, U. Schedler, M. J. B. Weinhart, *Biomacromolecules* **2018**, *19*, 4207-4218.

[84] H. L. Liu, X. L. Liu, J. X. Meng, P. C. Zhang, G. Yang, B. Su, K. Sun, L. Chen, D. Han, S. T. Wang, L. Jiang, *Adv. Mater.* **2013**, *25*, 922-927.

[85] Z. Ke, M. Lin, J.-F. Chen, J.-s. Choi, Y. Zhang, A. Fong, A.-J. Liang, S.-F. Chen, Q. Li, W. Fang, *ACS Nano* **2014**, *9*, 62-70.

[86] H. J. Yoon, A. Shanker, Y. Wang, M. Kozminsky, Q. Jin, N. Palanisamy, M. L. Burness, E. Azizi, D. M. Simeone, M. S. Wicha, *Adv. Mater.* **2016**, *28*, 4891-4897.

[87] Y. J. Kim, M. Ebara, T. Aoyagi, *Angew. Chem., Int. Ed.* **2012**, *51*, 10537-10541.

[88] W. Li, J. Wang, J. Ren, X. Qu, *Adv. Mater.* **2013**, *25*, 6737-6743.

[89] A. Sutton, T. Shirman, J. V. Timonen, G. T. England, P. Kim, M. Kolle, T. Ferrante, L. D. Zarzar, E. Strong, J. Aizenberg, *Nat. Commun.* **2017**, *8*, 14700.

[90] S.-W. Lv, Y. Liu, M. Xie, J. Wang, X.-W. Yan, Z. Li, W.-G. Dong, W.-H. Huang, *ACS Nano* **2016**, *10*, 6201-6210.

[91] E. Reategui, N. Aceto, E. J. Lim, J. P. Sullivan, A. E. Jensen, M. Zeinali, J. M. Martel, A. J. Aranyosi, W. Li, S. Castleberry, A. Bardia, L. V. Sequist, D. A. Haber, S. Maheswaran, P. T. Hammond, M. Toner, S. L. Stott, *Adv. Mater.* **2015**, *27*, 1593-1599.

[92] M. Ebara, K. Uto, N. Idota, J. M. Hoffman, T. Aoyagi, *Adv. Mater.* **2012**, *24*, 273-278.

[93] K. Uto, T. Aoyagi, C. A. DeForest, A. S. Hoffman, M. Ebara, *Adv. Healthcare Mater.* **2017**, *6*, 1601439.

[94] D. M. Le, K. Kulangara, A. F. Adler, K. W. Leong, V. S. Ashby, *Adv. Mater.* **2011**, *23*, 3278-3283.

[95] M. Darnell, D. J. Mooney, *Nat. Mater.* **2017**, *16*, 1178-1185.

[96] K. H. Vining, D. J. Mooney, *Nat. Rev. Mol. Cell Biol.* **2017**, *18*, 728.

[97] A. J. Engler, S. Sen, H. L. Sweeney, D. E. Discher, *Cell* **2006**, *126*, 677-689.

[98] A. M. Rosales, K. S. Anseth, *Nat.Rev.Mater.* **2016**, *1*, 15012.

[99] Y. Ma, M. Lin, G. Huang, Y. Li, S. Wang, G. Bai, T. J. Lu, F. Xu, *Adv. Mater.* **2018**, *30*, 1705911.

[100] A. M. Kloxin, A. M. Kasko, C. N. Salinas, K. S. Anseth, *Science* **2009**, *324*, 59-63.

[101] C. Yang, M. W. Tibbitt, L. Basta, K. S. Anseth, *Nat. Mater.* **2014**, *13*, 645-652.

[102] C. Yang, F. W. DelRio, H. Ma, A. R. Killaars, L. P. Basta, K. A. Kyburz, K. S. Anseth, *Pro. Natl. Acad. Sci. U. S. A.* **2016**, *113*, E4439-4445.

[103] S. Khetan, M. Guvendiren, W. R. Legant, D. M. Cohen, C. S. Chen, J. A. Burdick, *Nat. Mater.* **2013**, *12*, 458-465.

[104] S. R. Caliari, S. L. Vega, M. Kwon, E. M. Soulas, J. A. Burdick, *Biomaterials* **2016**, *103*, 314-323.

[105] N. Huebsch, E. Lippens, K. Lee, M. Mehta, Sandeep T. Koshy, Max C. Darnell, R. M. Desai, Christopher M. Madl, M. Xu, X. Zhao, O. Chaudhuri, C. Verbeke, Woo S. Kim, K. Alim, A. Mammoto, Donald E. Ingber, Georg N. Duda, David J. Mooney, *Nat. Mater.* **2015**, *14*, 1269-1277.

[106] K. Uto, M. Ebara, T. Aoyagi, *Int. J. Mol. Sci.* **2014**, *15*, 1511-1524.

[107] D. Mosqueira, S. Pagliari, K. Uto, M. Ebara, S. Romanazzo, C. Escobedo-Lucea, J. Nakanishi, A. Taniguchi, O. Franzese, P. Di Nardo, *ACS Nano* **2014**, *8*, 2033-2047.

[108] K. R. Levental, H. M. Yu, L. Kass, J. N. Lakins, M. Egeblad, J. T. Erler, S. F. T. Fong, K. Csiszar, A. Giaccia, W. Weninger, M. Yamauchi, D. L. Gasser, V. M. Weaver, *Cell* **2009**, *139*, 891-906.

[109] M. J. Bissell, W. C. Hines, *Nat. Med.* **2011**, *17*, 320-329.

[110] I. Acerbi, L. Cassereau, I. Dean, Q. Shi, A. Au, C. Park, Y. Y. Chen, J. Liphardt, E. S. Hwang, V. M. Weaver, *Integr. Biol.* **2015**, *7*, 1120-1134.

[111] K. A. Jansen, R. G. Bacabac, I. K. Piechocka, G. H. Koenderink, *Biophys. J.* **2013**, *105*, 2240-2251.

[112] M. Guvendiren, J. A. Burdick, *Nat. Commun.* **2012**, *3*, 792.

[113] Y.-C. Yeh, E. A. Corbin, S. R. Caliari, L. Ouyang, S. L. Vega, R. Truitt, L. Han, K. B. Margulies, J. A. Burdick, *Biomaterials* **2017**, *145*, 23-32.

[114] C. A. DeForest, K. S. Anseth, *Nat. Chem.* **2011**, *3*, 925-931.

[115] T. E. Brown, J. S. Silver, B. T. Worrell, I. A. Marozas, F. M. Yavitt, K. A. Günay, C. N. Bowman, K. S. Anseth, *J. Am. Chem. Soc.* **2018**, *140*, 11585-11588.

[116] H. Y. Liu, H. D. Nguyen, C. C. Lin, *Adv. Healthcare Mater.* **2018**, *7*, 1800954.

[117] H.-Y. Liu, M. Korc, C.-C. Lin, *Biomaterials* **2018**, *160*, 24-36.

[118] H.-Y. Liu, T. Greene, T.-Y. Lin, C. S. Dawes, M. Korc, C.-C. Lin, *Acta Biomater.* **2017**, *48*, 258-269.

[119] H. Y. Yoshikawa, F. F. Rossetti, S. Kaufmann, T. Kaindl, J. Madsen, U. Engel, A. L. Lewis, S. P. Armes, M. Tanaka, *J. Am. Chem. Soc.* **2011**, *133*, 1367-1374.

[120] M. L. Previtera, K. L. Trout, D. Verma, U. Chippada, R. S. Schloss, N. A. Langrana, *Ann. Biomed. Eng.* **2012**, *40*, 1061-1072.

[121] H. Shih, C.-C. Lin, *J. Mater. Chem. B* **2016**, *4*, 4969-4974.

[122] R. S. Stowers, S. C. Allen, L. J. Suggs, *Pro. Natl. Acad. Sci. U. S. A.* **2015**, *112*, 1953-1958.

[123] L. Liu, J. A. Shadish, C. K. Arakawa, K. Shi, J. Davis, C. A. DeForest, *Adv. Biosys.* **2018**, 1800240.

[124] L. Peng, M. You, Q. Yuan, C. Wu, D. Han, Y. Chen, Z. Zhong, J. Xue, W. Tan, *J. Am. Chem. Soc.* **2012**, *134*, 12302-12307.

[125] A. M. Rosales, K. M. Mabry, E. M. Nehls, K. S. Anseth, *Biomacromolecules* **2015**, *16*, 798-806.

[126] B. M. Gillette, J. A. Jensen, M. Wang, J. Tchao, S. K. Sia, *Adv. Mater.* **2010**, *22*, 686-691.

[127] J. K. Yoon, M. Misra, S. J. Yu, H. Y. Kim, S. H. Bhang, S. Y. Song, J. R. Lee, S. Ryu, Y. W. Choo, G. J. Jeong, *Adv. Funct. Mater.* **2017**, *27*, 1703853.

[128] R. Kaunas, P. Nguyen, S. Usami, S. Chien, *Pro. Natl. Acad. Sci. U. S. A.* **2005**, *102*, 15895-15900.

[129] M. Tewary, P. W. Zandstra, *Nat. Mater.* **2018**, *17*, 571-572.

[130] J. K. Kim, A. Louhghalam, G. Lee, B. W. Schafer, D. Wirtz, D. H. Kim, *Nat. Commun.* **2017**, *8*, 2123.

[131] I. Levental, P. C. Georges, P. A. Janmey, *Soft Matter* **2007**, *3*, 299-306.

[132] Z. Liu, L. Bilston, *Biorheology* **2000**, *37*, 191-201.

[133] M. Geerligs, G. W. M. Peters, P. A. J. Ackermans, C. W. J. Oomens, F. P. T. Baaijens, *Biorheology* **2008**, *45*, 677-688.

[134] S. J. McDonald, P. C. Dooley, A. C. McDonald, J. A. Schuijers, A. R. Ward, B. L. Grills, *J. Orthop. Res.* **2009**, *27*, 1508-1513.

[135] O. Chaudhuri, L. Gu, M. Darnell, D. Klumpers, S. A. Bencherif, J. C. Weaver, N. Huebsch, D. J. Mooney, *Nat. Commun.* **2015**, *6*, 6364.

[136] O. Chaudhuri, S. T. Koshy, C. B. da Cunha, J. W. Shin, C. S. Verbeke, K. H. Allison, D. J. Mooney, *Nat. Mater.* **2014**, *13*, 970-978.

[137] O. Chaudhuri, L. Gu, D. Klumpers, M. Darnell, S. A. Bencherif, J. C. Weaver, N. Huebsch, H. P. Lee, E. Lippens, G. N. Duda, D. J. Mooney, *Nat. Mater.* **2016**, *15*, 326-334.

[138] D. D. McKinnon, D. W. Domaille, J. N. Cha, K. S. Anseth, *Chem. Mater.* **2014**, *26*, 2382-2387.

[139] J. Z. Lou, F. Liu, C. D. Lindsay, O. Chaudhuri, S. C. Heilshorn, Y. Xia, *Adv. Mater.* **2018**, *30*, 1705215.

[140] D. D. McKinnon, D. W. Domaille, J. N. Cha, K. S. Anseth, *Adv. Mater.* **2014**, *26*, 865-872.

[141] H. M. Seifert, K. Ramirez Trejo, E. V. Anslyn, *J. Am. Chem. Soc.* **2016**, *138*, 10916-10924.

[142] V. Yesilyurt, M. J. Webber, E. A. Appel, C. Godwin, R. Langer, D. G. Anderson, *Adv. Mater.* **2016**, *28*, 86-91.

[143] C. J. Kloxin, T. F. Scott, C. N. Bowman, *Macromolecules* **2009**, *42*, 2551-2556.

[144] T. E. Brown, B. J. Carberry, B. T. Worrell, O. Y. Dudaryeva, M. K. McBride, C. N. Bowman, K. S. Anseth, *Biomaterials* **2018**, *178*, 496-503.

[145] T. E. Brown, I. A. Marozas, K. S. Anseth, *Adv. Mater.* **2017**, *29*, 1605001.

[146] S. Tang, H. Ma, H. C. Tu, H. R. Wang, P. C. Lin, K. S. Anseth, *Adv. Sci.* **2018**, *5*, 1800638.

[147] Y. L. Dorland, S. Huveneers, *Cell Mol. Life Sci.* **2017**, *74*, 279-292.

[148] R. J. Petrie, N. Gavara, R. S. Chadwick, K. M. Yamada, *J. Cell Biol.* **2012**, *197*, 439-455.

[149] R. J. Petrie, K. M. Yamada, *J. Cell Sci.* **2012**, *125*, 5917-5926.

[150] R. K. Das, V. Gocheva, R. Hammink, O. F. Zouani, A. E. Rowan, *Nat. Mater.* **2016**, *15*, 318-325.

[151] J. P. Winer, S. Oake, P. A. Janmey, *Plos One* **2009**, *4*, e6382.

[152] L. Rossetti, L. Kuntz, E. Kunold, J. Schock, K. Müller, H. Grabmayr, J. Stolberg-Stolberg, F. Pfeiffer, S. Sieber, R. Burgkart, *Nat. Mater.* **2017**, *16*, 664-670.

[153] J. H. Wen, L. G. Vincent, A. Fuhrmann, Y. S. Choi, K. C. Hribar, H. Taylor-Weiner, S. C. Chen, A. J. Engler, *Nat. Mater.* **2014**, *13*, 979-987.

[154] B. Trappmann, J. E. Gautrot, J. T. Connelly, D. G. T. Strange, Y. Li, M. L. Oyen, M. A. C. Stuart, H. Boehm, B. J. Li, V. Vogel, J. P. Spatz, F. M. Watt, W. T. S. Huck, *Nat. Mater.* **2012**, *11*, 642-649.

[155] K. Mandal, D. R.-B. Aroush, Z. T. Graber, B. Wu, C. Y. Park, J. J. Fredberg, W. Guo, T. Baumgart, P. A. Janmey, *ACS Nano* **2018**, *13*, 203-214.

[156] T. Razafiarison, C. N. Holenstein, T. Stauber, M. Jovic, E. Vertudes, M. Loparic, M. Kawecki, L. Bernard, U. Silvan, J. G. Snedeker, *Pro. Natl. Acad. Sci. U. S. A.* **2018**, *115*, 4631-4636.

[157] W. Chen, H. Yang, R. Wang, R. Cheng, F. Meng, W. Wei, Z. Zhong, *Macromolecules* **2009**, *43*, 201-207.

7. Abbreviations

ECM	extracellular matrix
DMNPB	3-(4,5-dimethoxy-2-nitrophenyl)-2-butyl ester
UV	ultraviolet light
NIR	near-infrared
UCNPs	upconverting nanoparticles
hMSCs	human mesenchymal stem cells
LCNs	liquid crystal polymer networks
SAM	self-assembled monolayer
PEDOT	poly (3,4-ethylene dioxythiophene)
PPy	polypyrrole
MNPs	magnetic nanoparticles
Anisogel	anisotropic gel
SPIONs	superparamagnetic iron oxide nanoparticles
SCI	spinal cord injury
DRG	dorsal root ganglia
PEG	poly (ethylene glycol)
PD-L1	programmed death-ligand 1
ECSs	embryonic stem cells
HA	hyaluronic acid
MNC	magnetic nanocage
AuNP	gold nanoparticle

7 Abbreviations

PNIPAM	poly (N-isopropylacrylamide)
PCL	poly (ε-caprolactone)
LCST	lower critical solution temperature
CTCs	circulating tumor cells
BSA	bovine serum albumin
AuNRs	gold nanorods
PDMS	polydimethylsiloxane
LBL	layer-by-layer
YAP	yes-associated protein
TAZ	PDZ-binding domain
RUNX2	runt-related transcription factor 2
MMP	matrix metalloproteinase
DTT	dithiothreitol
SPAAC	azide-alkyne cycloaddition
DOPA	dihydroxyphenylalanine
ECs	endothelial cells

8. Appendix

8.1 List of Publications from this Thesis

1. **J Zhang**, C Cheng, JL Cuellar-Camacho, M Li, Y Xia, W Li, R Haag. Thermally Responsive Microfibers Mediated Stem Cell Fate via Reversibly Dynamic Mechanical Stimulation. *Advanced Functional Materials*, **2018**, (47), 1804773.

2. **J Zhang**, W Chen, L Yu, M Li, F Neumann, W Li, R Haag. Selective Endothelial Cell Adhesion via Mussel-Inspired Hybrid Microfibrous Scaffold. *ACS Applied Nano Materials*, **2018**, 1 (4), 1513-1521.

3. **J Zhang,** H Yang, BE Abali, M Li, Y Xia, and R Haag. Dynamic Mechanics-modulated Hydrogels to Regulate the Differentiation of Stem-cell Spheroids in Soft Microniches and Modeling of the Nonlinear Behavior. Small, **2019**, 1901920.

4. C Cheng, **J Zhang**, S Li, Y Xia, C Nie, Z Shi, JL Cuellar‐Camacho, N Ma, R Haag. A Water‐Processable and Bioactive Multivalent Graphene Nanoink for Highly Flexible Bioelectronic Films and Nanofibers. *Advanced Materials*, **2018**, 30 (5), 1705452.

8.2 Curriculum vitae

The CV is not included for privacy reasons.